PLANETARY WAVES IN THE UPPER ATMOSPHERE

A THESIS

Presented to

The Faculty of the Division of Graduate Studies

By

Murry Lewis Salby

In Partial Fulfillment

of the Requirements for the Degree

Doctor of Philosophy

in the School of Aerospace Engineering

Georgia Institute of Technology

March 1978

Planetary Waves in the Upper Atmosphere

by

Murry L. Salby

APPROVED:

Chairman

Date Approved by Chairman: 2/27/79

ACKNOWLEDGMENTS

I am most grateful to Dr. R. G. Roper for suggesting this thesis topic, for his patience, understanding, and advice in the endeavor, and more importantly, for giving me the opportunity to pursue this line of study. I also wish to thank the other members of the reading committee, Dr. C. G. Justus and Dr. W. C. Strahle for their helpful comments and willingness to discuss some of the more difficult questions that arose, Dr. G. H. Meyer for his patience in examining several of the mathematical difficulties and suggesting possible means of solution. A particular note of thanks goes to Dr. Alan D. Pierce for his undying patience, support, illuminating discussions and suggestions.

To all of those that have given of themselves for the sake of my advancement, Doctors Walker, Stallybrass, Ho and Demko of the Mathematics Department, to Professor W. E. Woolf of the Physics Department for inspiring me in this direction, and all of the others too numerous to mention for sharing their wisdom and knowledge, I owe my deepest gratitude. I would like to thank Mrs. Ann Dillon for her patience and fortitude in putting up with me, Dr. Elizabeth Evens for her support and motivation for attaining quality and particularly, my aunt, Mrs. Paula Abrams and friend Barry Zipperman for looking after me when perhaps I was too involved to look after myself.

Most of all I wish to thank my dear father and his wife for their continued support, wisdom, and encouragement during these years, whose guidance and comfort I could not have done without. Finally, I

can only make a feeble acknowledgment of the important influence my late mother had upon me; her unfaltering demand for excellence and perfection remains unequalled.

TABLE OF CONTENTS

TABLE OF CONTENTS (Continued)

LIST OF TABLES

LIST OF ILLUSTRATIONS

LIST OF ILLUSTRATIONS

LIST OF ILLUSTRATIONS (Continued)

LIST OF ILLUSTRATIONS (Continued)

LIST OF ILLUSTRATIONS (Continued)

LIST OF SYMBOLS

a	radius of earth
A	local angular velocity of atmosphere
c_G	group velocity
$c^2 = \gamma RT$	sound speed squared
c	phase speed
d_i	ith direction cosine
e	complex error in surface boundary condition
f	coriolis parameter
E_1, E_2	kinetic energy density in 1st, 2nd velocity components.
$E = E_1 + E_2$	total kinetic energy density
$\vec{e}_L$	line of sight unit vector
g	gravity
h	equivalent depth
$\bar{H}$	mean scale height
H	scale height
h_λ, h_ϕ, h_z	scale factors for curvilinear coordinates
$<I_z>$	vertical energy flux
J	operator defined by (2.56.2)
k	magnitude of wavenumber vector
LTE's	Laplace Tidal Equation
LS	least squares
ℓ_j	jth basis function

LIST OF SYMBOLS (Continued)

L, $\hat{M}$	operators defined by (2.58)
m	zonal wavenumber
n	meridional index
N	Brunt - Väisälä
N_j	jth B-spline
ODE	ordinary differential equation
p	pressure
P	potential energy density
$\underline{P}$	pressure amplitude
PDE	partial differential equation
r	radius
R	specific gas constant
Ro	disturbance Rossby number
$S_{\|u\|^2}$	power spectrum of u
S_{uv}	cross spectrum of u and v
s_{mn}	parameter related to relaxation time (see eq. 2.103)
T	temperature
$\overline{T}$	mean signal time
u,v,w	zonal, meridional and vertical velocities
U_c	Rossby critical velocity
$U(\mu)$	Hough Function, latitude dependence
$\hat{U},\hat{V}$	latitude dependence of zonal and meridional velocities
US76	1976 US Standard Atmosphere
$\vec{V}$	velocity

LIST OF SYMBOLS (Continued)

$\vec{V}_L$	line of sight velocity
$\vec{v}_r$	reference frame velocity
W	vertical velocity amplitude
$\tilde{y}$	velocity divergence
z	height
Z	vertical dependence of $\tilde{y}$
Z_j	jth approximate
$Z, \hat{Z}$	least squares approximate matrices
α	separation parameter
$\beta = \frac{\partial f}{\partial y}$	latitudinal rate of change of f; inverse normalized error in boundary condition
$\gamma = c_p/c_v$	ratio of specific heats; surface lapse rate; effective Lamb's parameter
Γ	adiabatic lapse rate; WKB error parameter
$\delta = \frac{(2\hat{\Omega})^2 a}{g}$	nondimensional parameter
$\varepsilon = \bar{H}/a$	shallowness; error
$\eta = \delta/\varepsilon$	Lamb's parameter
$\kappa = \frac{\gamma-1}{\gamma}$	
λ	longitude
ϕ	latitude
ϕ_c	critical latitude
θ	potential temperature
τ_{mn}^k	relaxation time of (m,n,k)th mode
ρ	density

LIST OF SYMBOLS (Continued)

ν_k	kth frequency
ν_{mn}^k	ratio of PE to total energy for solution of LTE
$\sum_{mn}^k$	ratio of PE to KE
$\mu = \sin \phi$	
Ω	angular velocity of the earth
$\hat{\Omega} = \Omega + A$	total angular velocity
$\xi = \int_o^z \frac{dz'}{H}$	nondimensional pressure height
ζ	nondimensional height
ω	intrinsic angular frequency
σ	angular frequency
σ^2	variance
π, Π	one and two dimensional partitions
ψ_k, χ_k	integrals defined by (2.100)

SUMMARY

The possible existence of planetary normal modes in a realistic atmosphere is investigated. Simplified systems of equations for a generally baroclinic background state are developed for three frequency regimes via dynamic similarity. The problem is pursued for the general frequency range for a barotropic atmosphere in uniform rotation. It is demonstrated that only two vertical modes exist, one being a perturbation of the Lamb mode and the other attaining large amplitudes in the stratosphere and mesosphere. The dynamic character of these is presented along with the discrete set of associated eigenfrequencies and horizontal modes. Relaxation times and signal time lags between different levels of the atmosphere are calculated for each of the vertical modes.

A spectrally unbiased technique for decomposing radio meteor wind data into the velocity component functions is developed. This scheme is demonstrated on known input, and it is shown that it is limited in resolution by only the data.

Meteor wind and rawinsonde data are analyzed for possible spectral content from planetary waves, in particular from the discrete normal modes found earlier. The emperical and theoretical results compare favorably, and suggest that this low frequency regime is composed of essentially discrete spectral content. This discrete nature is present throughout the year in the mesosphere and is most pronounced during winter. The most consistent features that could be resolved in this region were the two and five day waves.

PREFACE

> "The dominant feature of the upper-air (troposphere) flow in mid-latitudes is a strong westerly current circling the globe, but meandering slightly. The meanders include waves with lengths so long that there are only two or three waves around the entire hemisphere. These are often called planetary waves" (Dutton, 1976, p. 351).

The following is an investigation of long-period travelling waves in the earth's upper atmosphere. It is an attempt to document their existence and illuminate the mechanisms involved. Observations of upper atmospheric winds are obtained via the radio meteor technique and are compared with theoretical developments and observations from the lower atmosphere.

This work is divided into three parts. The first part (Chapters I and II) includes a historical sketch and recent developments in the field. A simplified system of equations for global scale disturbances is developed for a generally baroclinic atmosphere on a spherical earth. This system follows from a similarity procedure which makes no a priori assumptions on the unknown disturbance and without invoking the traditional approximation. Three frequency regimes are delineated, each having a different character and simplified set of governing equations. The problem for the general range of frequency is pursued, subject to the restrictions of a barotropic atmosphere in uniform zonal motion. The possible existence of free modes of oscillation of such a system under different mechanical and thermodynamic

configurations is investigated. This type of endeavor seems to be most applicable to an observational analysis, for if such normal modes are found to exist, the data may be searched for the regular appearance of the associated frequencies. We should clarify a point of nomenclature at this time. The terms "free" and "normal" modes will be used interchangeably in this study, the latter being perhaps a misnomer, for it corresponds to orthogonality in the mathematical sense, which may not be the case here. In classical studies the two have become synonymous and therefore should not lead to undue confusion. The second part (Chapter III) links the first and last parts. Because of certain inherent difficulties in the radio meteor technique, the resulting data is not readily amenable to standard analyses. Therefore, Chapter III is devoted to the development of a technique for reducing radio meteor wind data into the true velocity components. The final part (Chapters IV and V), consists of the analysis of these observations and comparison with the theoretical development. Recommendations for future work are also listed.

CHAPTER I

INTRODUCTION

1.1 Historical Sketch

Wave motions in a rotating fluid and their relation to atmospheric and oceanic dynamics have been studied for nearly 200 years. It has been noted (Dikii, 1965; Golitsyn and Dikii, 1966) that the coriolis reaction due to rotation augments the medium with an additional degree of stiffness. This "gyroscopic rigidity" creates the possibility for rotational waves which are not found in fluids resting in an inertial reference frame. Although these waves have been named after C. G. Rossby who examined them in a geophysical context (Rossby, 1939), their character was probably first documented by Hough (1897, 1898) in his study of the solutions of Laplace's Tidal Equation. As a matter of definition, the term " planetary wave," will be taken to mean these gyroscopic or rotational waves which vanish as the rotational speed of the medium goes to zero.

Perhaps the earliest comprehensive study of oscillations of a thin fluid covering a rotating globe was performed by Laplace (1775, 1776) in his investigations of tidal oscillations of the earth's oceans. As a particular case, free oscillations were examined. The resulting differential equation, later coined "Laplace's Tidal Equation (LTE), is a second order, linear ordinary differential equation (ODE), involving the frequency of free oscillation and the ocean depth as parameters.

Laplace's studies, incomplete, were later picked up by Kelvin (1875), Margules (1883) and Hough (1897, 1898). Margules and Hough recognized that the solutions broke down into two categories for small values of Lamb's parameter. "Oscillations of the First Class," are gravity waves propagating zonally in opposite directions with nearly equal and opposite characteristic frequencies. "Oscillations of the Second Class" are Rossby waves and degenerate into the geostrophic modes of motion as the rotational speed goes to zero (Lamb, 1932, p. 350; Greenspan, 1968, p. 87). Laplace's partially unsuccessful attempts were based on a straightforward power series expansion of the solution. Hough later recognized the similarity of LTE to the associated Legendre equation and therefore attempted its solution by an expansion in associated Legendre functions. The result was rapid convergence and determination of the essential features of the solutions; hence, they are named Hough Functions. Love (1913) suggested breaking the solution into an irrotational and a solenoidal component by representing the velocity as the sum of a stream function and a velocity potential.

The mathematical properties of this problem for general domains were examined by Poincare (1910). The name "Poincaré's Problem" refers to the particular boundary value problem (BVP) for these normal modes in a rotating fluid (Greenspan, 1968, p. 51) and also to the general class of BVP's that occur in the theory of PDE's where the tangential derivative appears in the boundary conditions (see Bitsadze, 1968). One of the peculiar features of the former is that the PDE is hyperbolic and, boundary conditions are prescribed completely around the domain. Hence, the general problem cannot be guaranteed a solution. More details on

such "ill-posed" problems may be found in Courent and Hilbert, Vol. 2 (1953, p. 280). Franklin (1972) has developed several existence/uniqueness theorems applicable to this type of problem. Among the solutions of Poincaré's Problem for a rotating fluid are inertial modes, geostrophic modes, and Rossby modes. All of the corresponding characteristic frequencies of these modes are less than the vorticity of the medium in absolute value (Greenspan, 1968, p. 52), and all of the Rossby frequencies are negative. The geostrophic mode is steady and consists of fluid elements moving along lines of constant depth as columns. This is a direct consequence of the Taylor-Proudman Theorem (Greenspan, 1968, p. 37; Charney, 1970, p. 208), and the fluid elements correspond to Taylor-Proudman columns. The inertial modes are in general waves having no mean circulation about the axis of rotation, all of the circulation being carried by the geostrophic and Rossby modes. The Rossby modes take the place and circulation of the geostrophic motion when there exist no closed geostrophic contours; however, they may exist in any configuration where the depth is variable.

One point of controversy in Laplace's investigation was the appearance of certain singular points in LTE, corresponding to "critical latitudes." For over a century it remained unclear whether or not physically plausible, e.g., continuous, solutions existed across the critical latitudes. Brillouin (1932) illuminated the reason for the singularities and demonstrated the existence of continuous solutions at these points. Taylor (1936) indicated that the depth of the ocean appearing in LTE would have an analogue in the atmosphere, an "equivalent depth," corresponding to roughly the scale height.

The analogies between the solutions of LTE and those of Poincaré's Problem are clear, e.g., geostrophic modes and Rossby waves. However, the relation between the inertial and gravity waves is incomplete. Both have similar character, yet, the gravity waves can exist with no rotation while inertial modes cannot. The difference may be due to the fact that the gravitational reaction in Laplace's tidal problem is replaced by a rigid wall reaction in Poincaré's Problem.

Rossby (1939, p. 51) suggested that the earth's atmosphere might respond to a displacement from steady geostrophic equilibrium by radiating waves, much as an atom does when disturbed from or making a transition between stable states. Now since the motions under consideration take place in a rotating reference frame, it is often more illuminating to examine them from a vorticity-torque perspective rather than from the usual velocity-stress equations, e.g., conservation of vorticity, absolute vorticity, and potential absolute vorticity. Rossby considered two dimensional, horizontally divergenceless, and barotropic disturbances from equilibrium on a beta-plane. These motions are governed by the expression of conservation of absolute vorticity. Restricting the disturbance to a transverse velocity perturbation, Rossby found that wave solutions were possible, and they have since been named Rossby waves. These had zonal wave speed c given by

$$c - u_o = -\beta/k^2 \qquad (1.1)$$

where u_o is the zonal background velocity, β is the latitudinal rate

of change of the coriolis parameter, and k is the wave number. Analogous wave speeds are found in Poincaré's Problem. These waves all move westward and are dispersive since their phase velocities depend upon the wavenumber. The effect of the waves is to displace the mean zonal streamlines (Figure 1.1). Simple solutions propagating in an arbitrary horizontal direction are also possible.

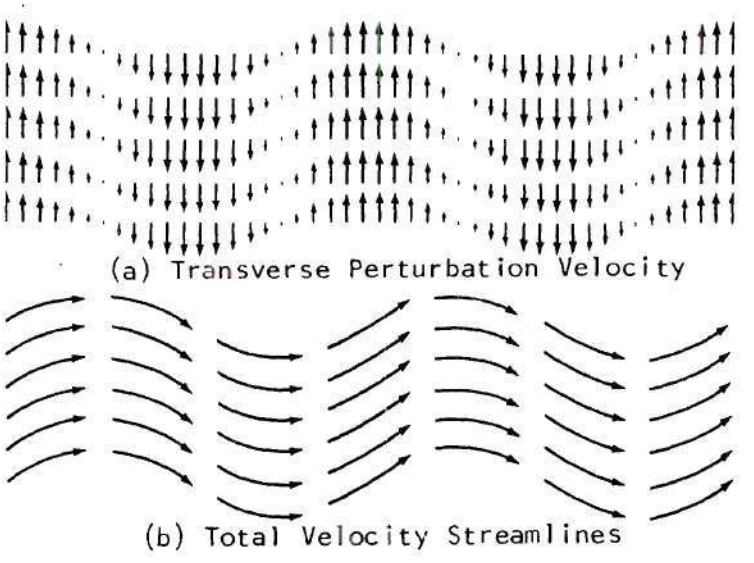

Figure 1.1. Rossby Wave on β-Plane (after Dutton, 1976, p. 353).

Haurwitz (1940, a) generalized Rossby's results by limiting the extent of the beta plane between two vertical walls to simulate the geometrical confinement by the sphere. These additional boundary constraints reduced the continuous spectrum of phase velocities to a discrete set given by

$$c - u_o = \frac{-\beta}{k^2 + (\frac{n\pi}{D})^2} \qquad n = 1,2,... \tag{1.2}$$

D being the width of the channel on the beta-plane. As can be seen, this reduces to the Rossby formula when the channel width tends to infinity. These solutions, called Rossby-Haurwitz waves, consist of closed cells of oscillating polarity superimposed upon the zonal current (Figure 1.2).

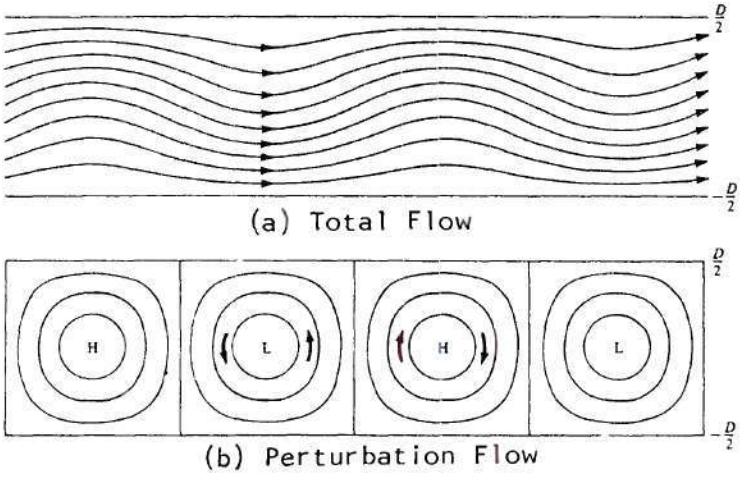

Figure 1.2. Rossby-Haurwitz Waves (after Dutton, 1976, p. 473).

The problem was later solved on the sphere by Haurwitz (1940, b) where the atmosphere was assumed to rotate uniformly with angular velocity α. Again the solutions formed a discrete set of waves with the corresponding zonal "angular" phase velocity, c, given by

$$c - \alpha = \frac{-2\Omega}{n(n+1)} \quad ; \quad n = m, m+1, \ldots \tag{1.3}$$

n and m being the meridional and zonal indices respectively, and Ω the angular velocity of the sphere. For this simple problem, the solutions are spherical harmonics shown in Figure 1.3.

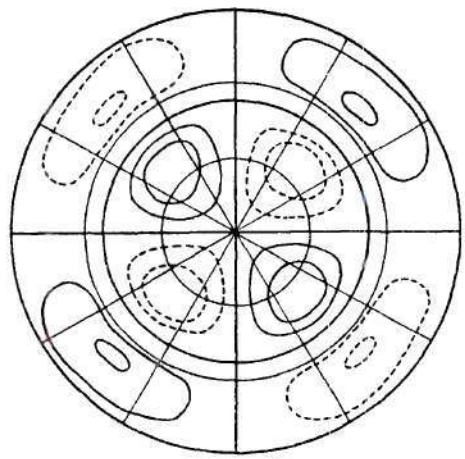

Figure 1.3. Haurwitz Wave m = 2, n = 5; Spherical Harmonic P_{25}.

The reader will notice the similarities between the solutions of these three problems of increasing geometric realism.

1.2 Recent Developments

Much of the recent work that has been done on planetary waves in the atmosphere has been concerned with "stationary waves" whose phase velocity relative to the surface is zero. These are of interest because many of the forcing mechanisms are fixed surface effects, e.g., vertical mass flux from mean flow over topography, horizontal variation of solar insolation. Because this thesis is primarily concerned with travelling waves, which can be observed in the meteor data, further discussion of these fixed waves will be kept to a minimum.

Longuet-Higgens (1964), in a rather illuminating study, linked the solutions of the beta plane to those of the sphere for large values of n. It turns out that the solutions on the sphere are asymptotic

($n \to \infty$) to plane waves with n/a (a is the radius of the sphere) representing the magnitude of the horizontal wavenumber vector. The characteristic velocities on the sphere (equation 1.3) tend to those of the beta-plane (equation 1.2) in this limiting sense. The asymptotic spherical solutions have features which are not predicted by the beta plane. The plane wave solutions propagate obliquely along the sphere between the two critical latitudes, $\pm\phi_c$, where

$$\phi_c = \cos^{-1}\left(\frac{m}{n}\right) , \tag{1.4}$$

and are evanescent along meridians outside this band of latitudes (Figure 1.4).

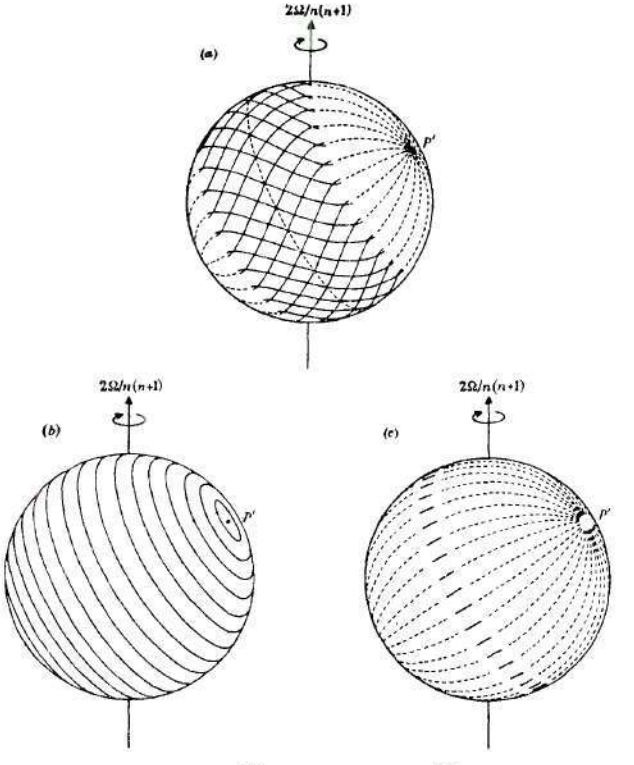

(a) General Case, (b) $\frac{m}{n} \to 0$, (c) $\frac{m}{n} \to 1$

Figure 1.4. Asymptotic Haurwitz Solutions ($n \to \infty$) (after Longuet-Higgens, 1964).

Thus the waves are reflected by these critical latitudes. For those modes such that m/n approaches 0 ($n \to \infty$), the critical latitudes shrink back onto the poles, while for those with m/n tending to 1, the region of meridional propagation is squeezed into the equator (see Figure 1.4, b and c). These results apply to latitude measured from an arbitrary pole on the sphere, drifting with the disturbance, and hence, correspond to a point source anywhere on the sphere. Also these results seem to have relevance to the containment of disturbance energy to the lower and mid latitudes. Finally, it should be pointed out that, inherent in this and virtually all of the previous investigations, is the assumption of linearity. A simple nondimensionalization (Greenspan, 1968, p. 7) reveals that the nonlinear terms and hence the "smallness" required for linearity is proportional to the disturbance Rossby number

$$Ro = \frac{u'}{\Omega\lambda} \tag{1.5}$$

u' being the velocity scale of the disturbance, Ω the inverse time scale, and λ the wavelength. Since λ is proportional to a/n there exists some limiting value of n beyond which the association made by Longuet-Higgens becomes invalid because of violation of the assumptions of linearity.

Longuet-Higgens (1968) also produced one of the more important developments in recent years in his comprehensive study of LTE. The Hough Functions and associated eigenfrequencies were evaluated over a wide range of Lamb's parameter, and asymptotic character was determined for both. Flattery (1968) also presented similar results, most

applicable to tidal theory. Orthogonality of the Hough Functions was demonstrated in this study.

The possibility of planetary wave propagation into the upper atmosphere was first closely studied by Charney and Drazin (1961). Their investigation was prompted by the fact that a large portion of the lower atmosphere's energy is contained in quasi-steady planetary wave motions. If a substantial portion of this energy was allowed to propagate into the upper atmosphere, where dissipative mechanisms predominate and the density is much smaller, very high temperatures would result, forming a corona similar to that of the sun and boiling off the atmosphere. They considered adiabatic, baratropic disturbances on a mid-latitude beta-plane. The mean flow was assumed zonal, varying in the vertical. This investigation indicated that vertical propagation was affected strongly by the character of the zonal flow. For an isothermal atmosphere in uniform motion they found that disturbances would propagate vertically only for the following range of zonal velocities

$$c < u_o < c + U_c \tag{1.6}$$

c being the phase velocity of the disturbance, and the critical velocity U_c is essentially the Rossby wave speed modified by buoyancy effects. Equation 1.6 implies that the mean flow must be westerly (eastward) relative to the disturbance, but less than the critical value U_c. The lower end of this regime corresponds to a zero value of the vertical refractive index or absorption (the disturbance appears motionless relative to the medium). The upper end corresponds to an infinite refractive index, or vertical reflection. Thus according to the Charney

Drazin theory, vertical propagation of slow waves is restricted to regions of weak westerlies, and the smaller horizontal wavelengths are reflected more than the longer wavelengths. A typical value of U_c for mid-latitudes for "stationary waves" is 38 m/sec. This investigation concluded that the stratospheric winter circumpolar cyclone, causing strong westerlies, and the summer circumpolar anticyclone producing easterly motion, would prevent significant penetration of "quasi-stationary waves" into the upper atmosphere. They felt that only possibly during the equinox, when the stratospheric vortex reverses polarity, could appreciable vertical penetration occur. Figure 1.5 shows the vertical refractive index squared for stationary waves in different seasons as computed by Charney and Drazin.

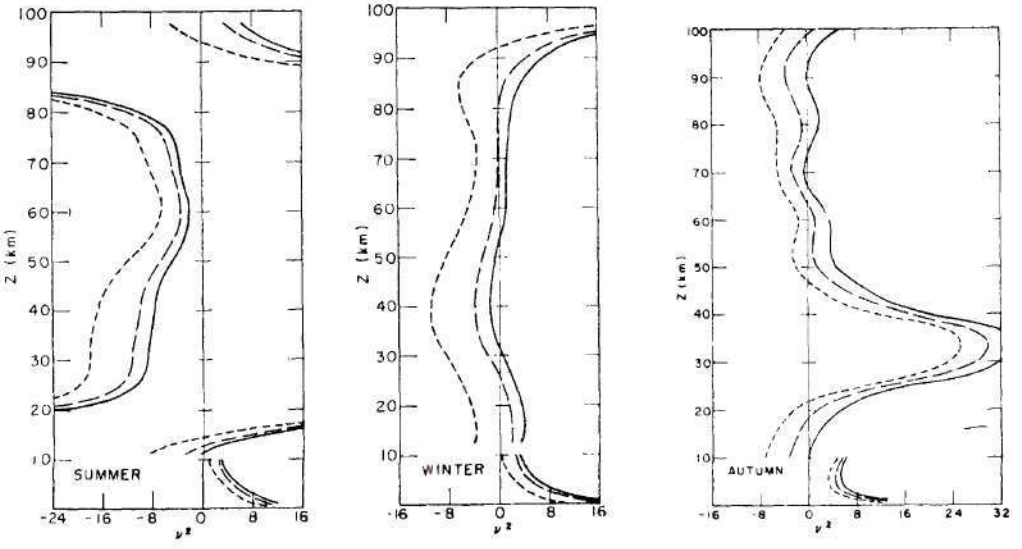

(a) Summer (b) Winter (c) Autumn

Figure 1.5. Refractive Index Squared (after Charney and Drazin, 1961).

According to this the largest horizontal scales have the best chance of vertical penetration. Charney (1970) presented two sequences of isobar charts through the troposphere and the stratosphere to substantiate this. Figure 1.7 shows that for summer, the smaller scale zonal variations are filtered out with increasing height until only the circumpolar anticyclone remains at the 10 mb level. The winter sequence (Figure 1.6) displays similar features, except apparently, the zonal wavenumber 2 remains at the 10 mb level (cf., Figure 1.5, b).

The implication of the Charney Drazin theory to travelling waves is not so explicit, and even the results for stationary waves have not gone unchallenged. Dickinson (1968, a) developed a model on a sphere using an expansion in Hough harmonics valid away from the tropics. This seems to be an appropriate time to mention that this is a consistent limitation with most of the recent studies. Their validity is not global which makes the results for the larger scale disturbances questionable. In contrast to the results of Charney and Drazin, Dickinson found that several stationary wave modes would penetrate westerly winds in excess of 38 m/sec, and two modes were found to penetrate the winter stratospheric jet.

The discrepancy with Charney and Drazin's results was attributed to the invalidity of the beta-plane for the large scale disturbances. Lindzen (1967) found penetration of all wavenumbers on an equatorial beta-plane. In later studies (Lindzen, 1971, 1972), it was indicated that several types of easterly waves, e.g. Rossby waves, Rossby-gravity waves, were capable of penetrating the stratosphere in equatorial latitudes, while the only westerly wave capable was the Kelvin mode.

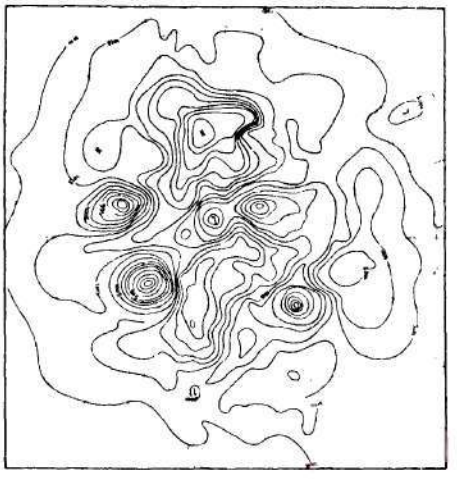

Synoptic weather map. Northern Hemisphere.
January 15, 1959
1230 GMT Sea Level

(a) Sea Level

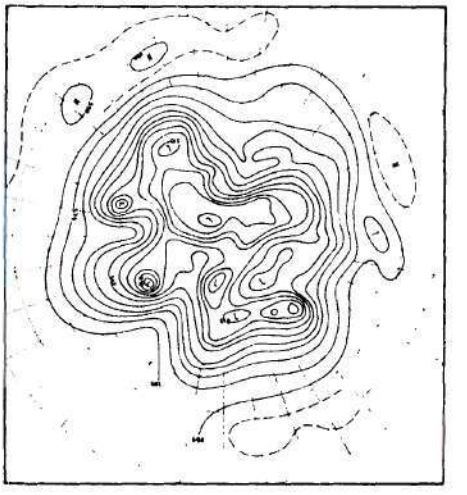

Synoptic Weather Map. Northern Hemisphere
JANUARY 15, 1959
1200 GMT 500 mb

(b) 500 mb.

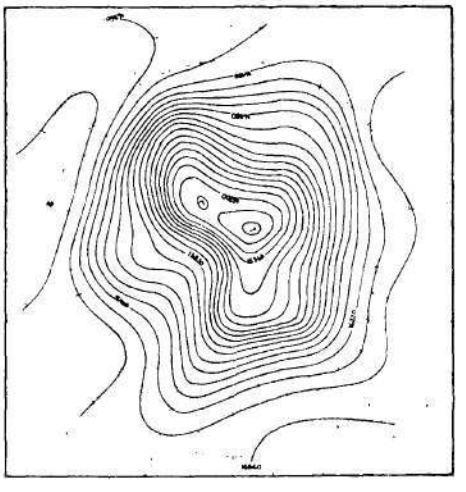

IGC Upper Air Chart Northern Hemisphere
100 mb 1200 GMT JANUARY 15, 1959

(c) 100 mb.

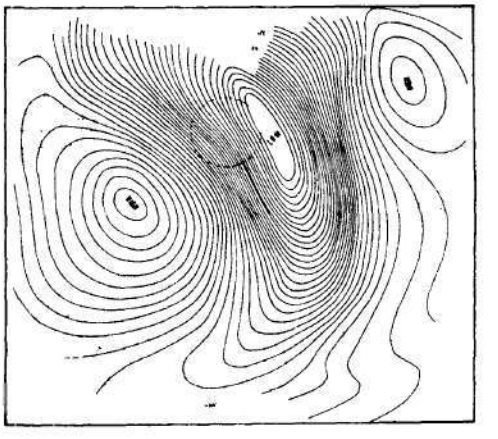

Constant pressure chart 10 mb 1200 GMT
January 15, 1959

(d) 10 mb.

Figure 1.6. Winter Constant Height/Pressure Surfaces.

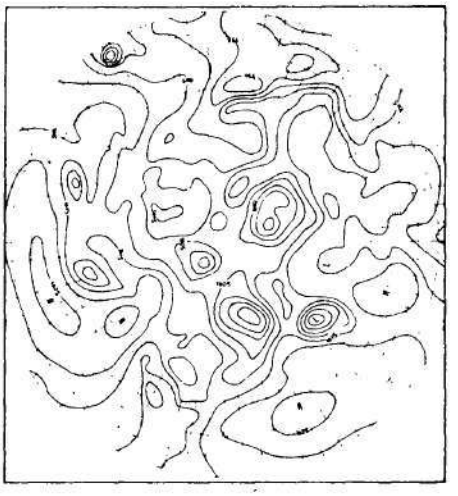

International Geophysical Year world weather maps
Part I - Northern Hemisphere - 15 July, 1958
1200 GMT. Sea Level

(a) Sea Level

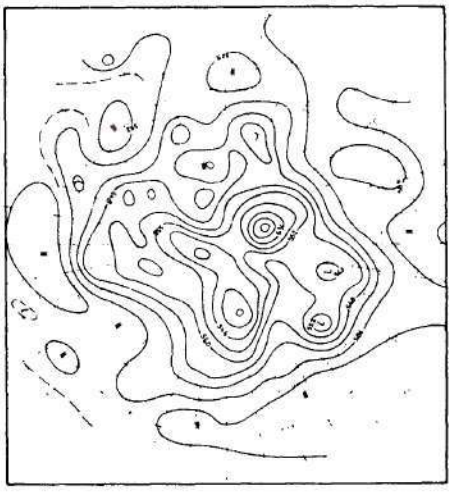

International Geophysical Year World Weather Maps
Part I - Northern Hemisphere - JULY 15, 1958
1200 GMT 500 mb

(b) 500 mb.

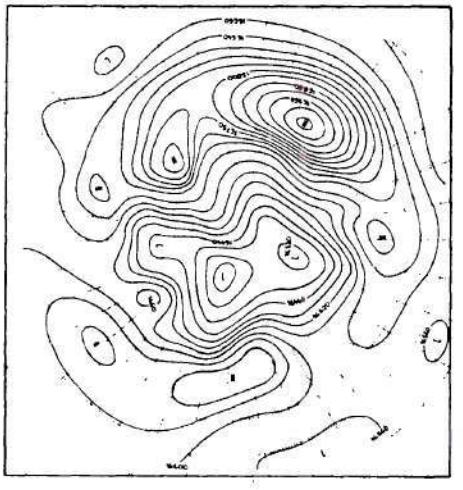

IGY Upper Air Chart Northern Hemisphere
100 mb 1200 GMT JULY 15, 1958

(c) 100 mb.

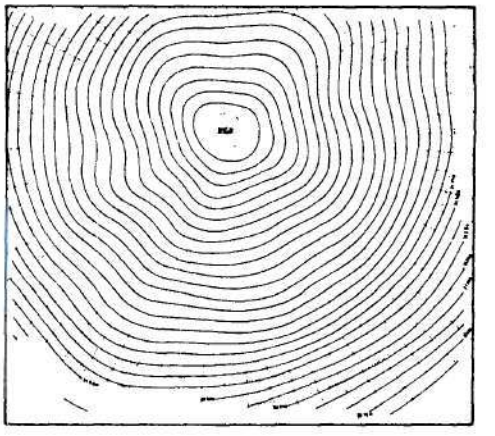

Constant pressure chart 10 mb 1200 GMT
July 15, 1958

(d) 10 mb.

Figure 1.7. Summer Constant Height/Pressure Surfaces.

The results of Dickinson (1968, a) predicted unrealistically large amplitudes in the mesosphere. Later studies investigated possible explanations. Two planetary waveguides were suggested to result from the horizontal variation of mean zonal winds (Dickinson, 1968, b). It was indicated that a polar waveguide would be formed by reflection between the pole and the winter stratospheric jet, and a singular equatorial waveguide would result from reflection from the jet and absorption at the equatorial zero wind line (see Figure 1.8).

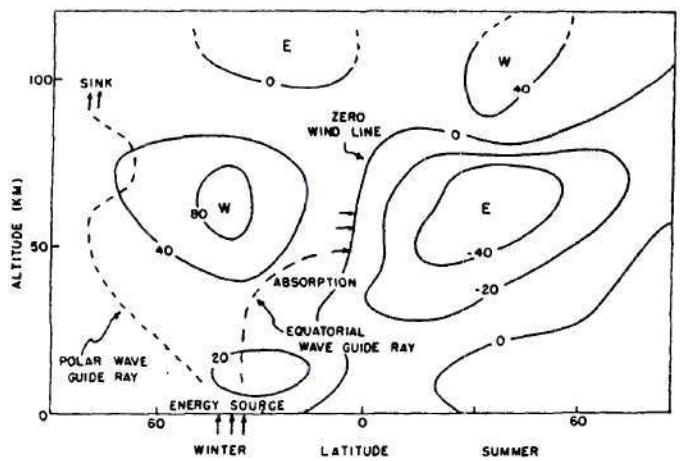

Figure 1.8. Planetary Waveguides Formed by Weak Westerlies (after Dickinson, 1968b).

Some of the features of the polar waveguide have been observed by Matsuno (1970). Damping due to infrared radiation to space by the 15μ CO_2 band in the stratosphere was modeled by Newtonian cooling (Dickinson, 1969). Significant attenuation in the vertical was predicted, which makes the previous results more plausible.

In contrast, Simmons (1974, a) found, on a beta-plane with zonal winds varying both vertically and horizontally, that certain stationary waves were ducted into regions of strong westerlies. These were not attenuated appreciably in the presence of either Newtonian cooling or critical line absorption. Transient responses were examined by Clark (1972). It was found that after switching on a step in vertical velocity at the surface, high frequency planetary waves radiated to infinity, leaving a stationary wave and a travelling barotropic Rossby wave.

Now aside from the stationary forcing at the surface, two mechanisms commonly associated with planetary wave generation are barotropic and baroclinic instability. These allow the background state to interact with, and in essence, "feed" the disturbance. Charney (1970, p. 251) demonstrated a method for obtaining the growth rates for unstable baroclinic waves. Simmons (1974, b) suggested that baroclinic instability might generate planetary wave motions at the stratopause. Baroclinic instability has been examined on the sphere (Simmons and Hoskins, 1976; Warn, 1976), and the results compare favorably with those of the beta-plane, except for the lower wavenumbers. It appears that the spherical curvature plays an important role in these larger disturbances. This was also suggested by Dickinson (1968, a). Duffy (1975) has examined barotropic instability of Rossby waves on a beta-plane.

Lindzen (1967, 1968) has remarked that Rossby wave amplitudes should not grow exponentially in the presence of realistic zonal winds. However, Deland (1970) concluded that this was not the case for the smaller wavenumbers, and these might grow to nonlinear scales in the

upper atmosphere and possibly cause blocking of the zonal flow.

Changes in the vertical energy and momentum fluxes of planetary waves have been linked to sudden stratospheric warmings (Matsuno, 1971; Holton, 1976) and the quasi-biennial oscillation.

Craig (1945) and Neamtan (1946) have shown that at least some of the classical results for planetary waves in simple atmospheres are valid in a nonlinear sense.

Stewartson and Rickard (1969), Stewartson (1971), and Stewartson and Walton (1976) attempted extension of the results of Longuet-Higgens (1968) to a thin but finite spherical annulus by perturbation techniques, where the thickness was taken as the small parameter. The asymptotic expansions failed, apparently because the boundaries are "characteristic" at certain points. Aldridge (1972) remarked that no continuous solutions have been found in which the characteristic surfaces are tangent to the boundary. The solutions pursued in these studies are physically unrealistic; however, it can be shown that the points of singularity are identical with the critical latitudes of LTE. Therefore, this author feels that the possibility of continuous solutions still exists, and they may be related to the singularities in a similar fashion to that shown by Brillouin (1932).

Dikii (1965) has examined the possibility of free modes of oscillation of a barotropic atmosphere on a sphere with "partially" realistic temperature structure. The thermal behavior in the upper thermosphere was taken as growing without bound which forced the upper boundary condition to be one of finiteness rather than the radiation condition. A broad spectrum of wave motions was considered in this

investigation, e.g., acoustic, gravity, gyroscopic. Free modes of each were presented. In another study, Dikii (1961) examined these modes in a baroclinic atmosphere. It appears that in this investigation, an important term, related to vorticity production, was neglected in the linearization process. This may explain why all of the calculated eigenfrequencies were real. These results have been applied to atmospheric motions of other planets (Golitsyn and Dikii, 1966).

External free Rossby modes in realistic vertical shear on a beta-plane were found to exist for a low wavenumber region (Geisler and Dickinson, 1975). These were found to be unstable, whereas an internal mode was neutral. The response of the 5-day external free mode to surface forcing was investigated by Geisler and Dickinson (1976). Using a rigid upper surface, they found that the response was greatest during solstice, and the summer mesosphere appeared resonant to this mode.

Most recently, the eigensolutions of the "balance equations" over a sphere have been obtained by Moura (1976), and most of these correspond closely to those of LTE. The Hough harmonics have been used as a basis set for the spectral method in solving the nonlinear primitive equations over a sphere (Kasahara, 1977).

1.3 Observational and Experimental Studies

Numerous studies have documented the existence of planetary waves in the lower and upper atmosphere. Again, many of these have been concerned with stationary waves, although the existence of travelling

waves has also been reported. The importance of these motions is obvious if one examines the spectral distribution of energy in the lower atmosphere. Figure 1.9 shows that a large portion of this energy is associated with periods between several days and a month.

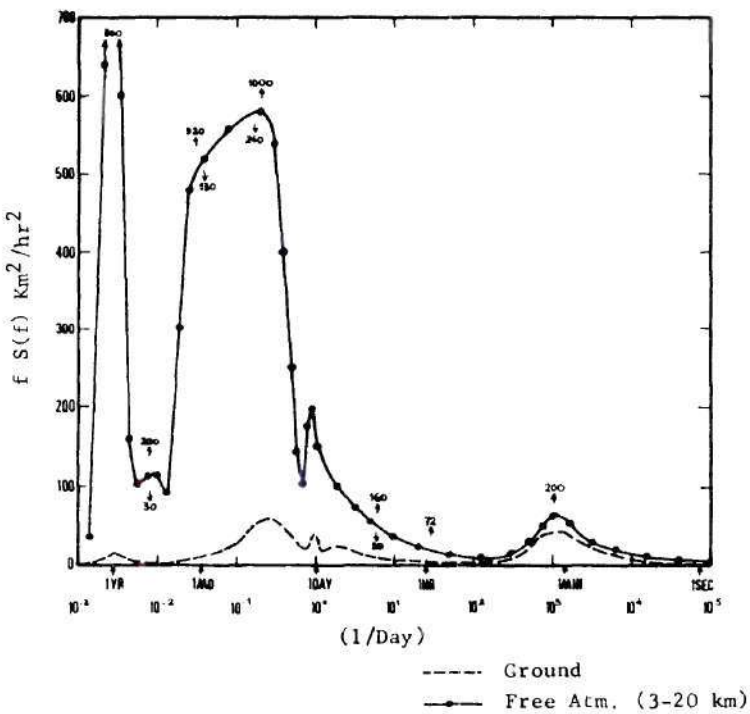

Figure 1.9. Mean Kinetic Energy Density of Zonal Wind Component (after Vinnichenko, 1970 Tellus, 22, 158-166).

Finger et al. (1966) found that the Aleutian high penetrated to at least the stratopause and superimposed on it were large scale travelling waves in autumn and early winter. These waves had periods ranging from 10 to 15 days. Large amplitude temperature oscillations in the 70 to 90 km region during winter were observed by Theon et al. (1967). They found the magnitude to decrease with latitude as called for by Dickinson's (1968, b) results. Also in contrast to the conclusions of

Charney and Drazin, were the results of Deland and Johnson (1968), which indicated that the zonal modes 1 and 2 were present at the 10 mb level throughout the year. The corresponding amplitudes were found to increase with height during winter. The westward tilt with height of the travelling waves was observed to be smaller than that of the stationary waves. It was suggested that this implied an insensitivity to surface forcing. Muench (1968) found travelling waves of zonal wavenumber 1 and 2 in the summer stratosphere, moving westward at 10 to 90 degrees per day, and increasing in amplitude with height. Small temporal variation of amplitude indicated that they were not unstable baroclinic waves. Hirota and Sato (1969) analyzed the data of five winters and also found definite energy communication between the troposphere and stratosphere. Power spectra for zonal wavenumbers 1 and 2 were highly concentrated about a 16-day period. Large scale oscillations in the ionosphere were found to be highly correlated with propagating disturbances in the troposphere and stratosphere, with little or no phase lag (Deland and Friedman, 1972). This indicates evanescence or a large vertical wavelength. Only wavenumber 1 showed true consistency for the samples examined in this study. McNulty (1976) found that although the energy flux of stationary waves into the stratosphere had strong seasonal character, being greatest during winter, the travelling waves were fairly insensitive to the time of year. In agreement with one of Charney and Drazin's results, the largest vertical fluxes were associated with the smallest horizontal wavenumbers. In summer, when the stationary disturbance of wavenumber 2 did not penetrate the

stratosphere significantly, it was found that the corresponding travelling modes did.

There has been repeated evidence for an evanescent 5-day wave which has been observed throughout the year, particularly in summer (Madden and Julian, 1973, Geisler and Dickinson, 1976, Burpee, 1976, Rodgers, 1976). Figure 1.10 shows a spectral peak corresponding to a wavenumber 1 disturbance of period roughly 6.2 days obtained from infrared radiance data from Nimbus 5. A similar mode has also been detected in the NCAR general circulation model (Tsay, 1974). Geisler and Dickinson (1976) have indicated that this may be a free oscillation of the Haurwitz type and might be excited by the unsteady character of the troposphere.

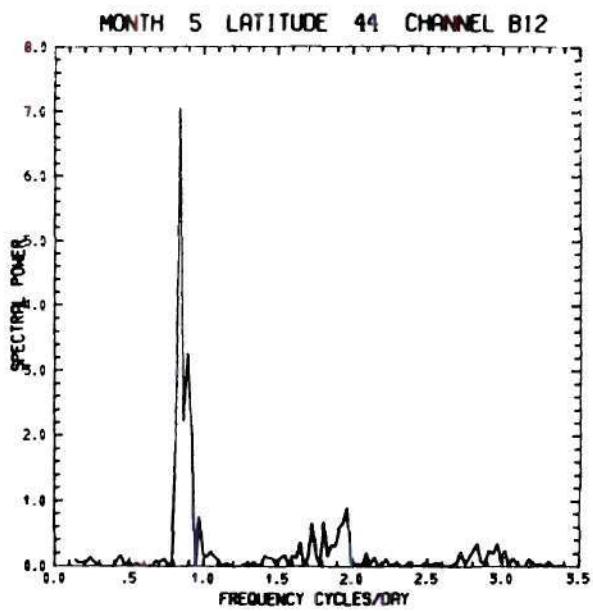

Figure 1.10. Nimbus 5 Radiance Spectrum. Peak Corresponds to 6.2 Day Period (after Rodgers, 1976)

This section will be concluded by very briefly mentioning some of the laboratory investigations of planetary waves that have appeared. Cylindrical geometry has been used for the most part. Baroclinic effects have been studied by incorporating temperature gradients along boundary surfaces. Fultz and Murty (1968) have investigated the relation between variability in depth for inertial and Rossby modes. Rao and Ketchum (1976) have examined baroclinic waves in a spherical annulus. For further studies the reader is referred to the monograph by Greenspan (1968) or the paper by Phillips (1963).

CHAPTER II

MATHEMATICAL FORMULATION

2.1 The Governing Equations

Global-scale adiabatic, inviscid motions of a stratified compressible atmosphere will be considered. The fluid will be taken as an ideal gas throughout, and magneto-hydrodynamic effects in the uppermost levels will be ignored. As seen in the previous chapter, the existence of these low wavenumber components in the upper atmosphere is well documented. For these global scale phenomena, as has been noted in several studies, the spherical geometry plays an important role. Therefore, in the following investigation, full spherical geometry will be retained. The motions will be assumed small in the sense of the disturbance Rossby number. The existence of free modes of oscillation will be examined.

The Eulerian equations of motion for such a system are

$$\frac{d\vec{v}}{dt} + 2\vec{\Omega} \times \vec{v} = -\frac{1}{\rho}\nabla p + \vec{g} \qquad (2.1)$$

$\frac{d}{dt}$ representing the material derivative, $\frac{\partial}{\partial t} + \vec{v} \cdot \nabla$. An expression for the conservation of absolute vorticity or potential absolute vorticity may be obtained by taking the curl of (2.1). This has the advantage of filtering out unwanted high frequency irrotational

motions, e.g., gravity waves, and has proved useful in simpler studies (Haurwitz, 1940, b; Charney and Drazin, 1961). It also illuminates many of the mechanisms involved in these motions. However, it has the disadvantage of raising the order of each of the equations by one and hence, resulting in a considerably more complicated problem upon their consolidation. For this reason, the equations of motion shall be retained instead.

Although equation 2.1 appears docile enough in vector form, even these become considerably more complicated when expressed as the scalar component equations. In spherical geometry they are

$$\frac{\partial u}{\partial t} + \frac{u}{r \cos \phi} \frac{\partial u}{\partial \lambda} + \frac{v}{r} \frac{\partial u}{\partial \phi} + w \frac{\partial u}{\partial r} - 2\Omega(v \sin \phi - w \cos \phi)$$

$$= - \frac{1}{\rho} \frac{1}{r \cos \phi} \frac{\partial p}{\partial \lambda} + \frac{\tan \phi}{r} uv - \frac{1}{r} uw \qquad (2.2.1)$$

$$\frac{\partial v}{\partial t} + \frac{u}{r \cos \phi} \frac{\partial v}{\partial \lambda} + \frac{v}{r} \frac{\partial v}{\partial \phi} + w \frac{\partial v}{\partial r} + 2\Omega u \sin \phi = - \frac{1}{\rho r} \frac{\partial p}{\partial \phi}$$

$$- \frac{\tan \phi}{r} u^2 - \frac{vw}{r} \qquad (2.2.2)$$

$$\frac{\partial w}{\partial t} + \frac{u}{r \cos \phi} \frac{\partial w}{\partial \lambda} + \frac{v}{r} \frac{\partial w}{\partial \phi} + w \frac{\partial w}{\partial r} - 2\Omega u \cos \phi = - \frac{1}{\rho} \frac{\partial p}{\partial r} - g$$

$$+ \frac{u^2 + w^2}{r} \qquad (2.2.3)$$

where u, v, and w are the zonal, meridional, and radial components of

velocity, λ is the longitude, and ϕ is the latitude. Even the linearized forms of these are nearly intractable. Therefore, several approximations are usually introduced. Aside from one or two exceptions, only modest attempts to justify these have appeared over the years.

2.2 The Shallow Atmosphere and the Traditional Approximation

Inherent in the approximations introduced in virtually all of the previous studies is the fact that the earth's atmosphere occupies an extremely thin region adjacent to the surface. In fact the ratio of the depth of the entire neutral atmosphere to the earth's radius a, is of the order .01. Usually the radial dependence of the coefficients is eliminated by formally replacing r by the approximate value a, and $\frac{\partial}{\partial r}$ by $\frac{\partial}{\partial z}$, where $z = r-a$ is the height above the surface. This is known as the "shallow atmosphere approximation." The new coordinates are (λ,ϕ,z) with the corresponding unit vectors $\vec{i}$, $\vec{j}$, $\vec{k}$. Equations (2.2) become

$$\begin{cases} \dfrac{du}{dt} - 2\Omega(v \sin\phi - w\cos\phi) = -\dfrac{1}{\rho a \cos\phi}\dfrac{\partial p}{\partial \lambda} + \dfrac{uv\tan\phi}{a} - \dfrac{uw}{a} & (2.3.1) \\ \dfrac{dv}{dt} + 2\Omega u \sin\phi = \dfrac{-1}{\rho a}\dfrac{\partial p}{\partial \phi} - \dfrac{u^2\tan\phi}{a} - \dfrac{vw}{a} & (2.3.2) \\ \dfrac{dw}{dt} - 2\Omega u\cos\phi = -\dfrac{1}{\rho}\dfrac{\partial p}{\partial z} - g + \dfrac{u^2 + w^2}{a} & (2.3.3) \end{cases}$$

where

$$\frac{d}{dt} = \frac{\partial}{\partial t} + \frac{u}{a \cos \phi} \frac{\partial}{\partial \lambda} + \frac{v}{a} \frac{\partial}{\partial \phi} + w \frac{\partial}{\partial z} \qquad (2.3.4)$$

Now although replacing $\frac{\partial}{\partial r} \circ$ by $\frac{\partial}{\partial z} \circ$ in the gradient is straightforward, transformation of radial terms in other del operations, e.g., $\frac{1}{r^2} \frac{\partial}{\partial r} (r^2 \circ)$ in the divergence, is not so obvious.

Another approximation, almost always introduced, is the neglect of the coriolis terms involving the cosine of ϕ, which arise from the component of the earth's vorticity tangent to the surface. Echart (1960, p. 95) has coined this the "traditional approximation."

Phillips (1966) attempted to justify the latter approximation by a novel use of the former. His scheme was to make the usual transformation $z = r-a$ and replace the exact set of scale factors for spherical coordinates

$$\begin{cases} h_\lambda = r \cos \phi \\ h_\phi = r \\ h_r = 1 \end{cases} \qquad (2.4.1)$$

by the approximate set

$$\begin{cases} h'_\lambda = a \cos \phi \\ h'_\phi = a \\ h'_z = 1 \ . \end{cases} \qquad (2.4.2)$$

This new set of scale factors in effect defines a pseudo-curvilinear coordinate system. The velocity components are determined from

the definitions

$$\begin{cases} u = h'_\lambda \dfrac{d\lambda}{d} \\ v' = h'_\phi \dfrac{d\phi}{dt} \\ w = h'_z \dfrac{dz}{dt} \end{cases} \tag{2.5}$$

as are the vector operations grad, curl etc. by similar expressions. In particular the curl and divergence reduce to

$$\nabla \times \vec{v} = \left[\frac{1}{a}\frac{\partial w}{\partial \phi} - \frac{\partial v}{\partial z}\right]\vec{i} + \left[\frac{\partial u}{\partial z} - \frac{1}{a\cos\phi}\frac{\partial w}{\partial \lambda}\right]\vec{j}$$

$$+ \frac{1}{a\cos\phi}\left[\frac{\partial v}{\partial \lambda} - \frac{\partial}{\partial \phi}(\cos\phi\, u)\right]\vec{k} \tag{2.6.1}$$

$$\nabla\cdot \vec{v} = \frac{1}{a\cos\phi}\frac{\partial u}{\partial \lambda} + \frac{1}{a\cos\phi}\frac{\partial}{\partial \phi}(\cos\phi\, v) + \frac{\partial w}{\partial z} \tag{2.6.2}$$

The radial derivatives have simplified due to the neglect of the divergence of radial lines in the thin spherical domain. When these are substituted into the vector invarient form of equation (2.1), given by

$$\frac{\partial \vec{v}}{\partial t} = -\frac{1}{\rho}\nabla p + \vec{g} - \nabla\left(\frac{1}{2}|\vec{v}|^2\right) + \vec{v} \times [\nabla \times (\vec{v} + \vec{v}_r)] \tag{2.7}$$

$\vec{v}_r$ being the reference frame velocity of the surface, the following simplified system of equations is obtained

$$\begin{cases} \dfrac{du}{dt} - 2\Omega v \sin\phi = -\dfrac{1}{\rho a \cos\phi}\dfrac{\partial p}{\partial \lambda} + \dfrac{uv \tan\phi}{a} & (2.8.1) \\ \dfrac{dv}{dt} + 2\Omega u \sin\phi = -\dfrac{1}{\rho a}\dfrac{\partial p}{\partial \phi} - \dfrac{u^2 \tan\phi}{a} & (2.8.2) \\ \dfrac{dw}{dt} = -\dfrac{1}{\rho}\dfrac{\partial p}{\partial z} - g & (2.8.3) \end{cases}$$

where

$$\frac{d}{dt} = \frac{\partial}{\partial t} + \frac{u}{a \cos\phi}\frac{\partial}{\partial \lambda} + \frac{v}{a}\frac{\partial}{\partial \phi} + w\frac{\partial}{\partial z} \qquad (2.8.4)$$

Aside from the elimination of the radial dependence of the coefficients as in equations (2.3), the coriolis terms involving cos ϕ are absent. This is a direct consequence of the fact that in this pseudo-coordinate system, the earth's vorticity, $\nabla \times \vec{v}_r = 2\vec{\Omega}$, reduces to $2\Omega \sin\phi\, \hat{k}$, the radial (vertical) component; see Figure 2.1.

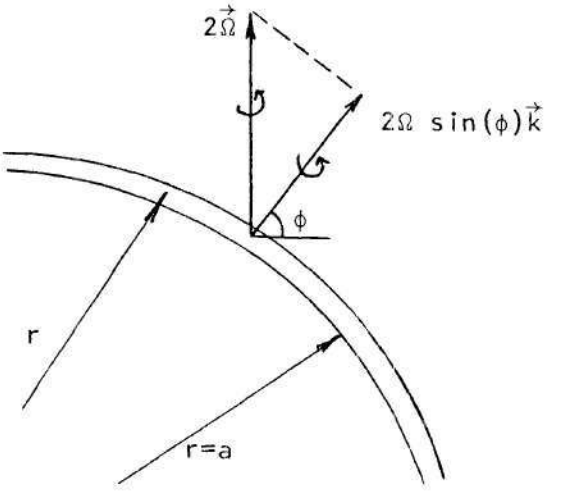

Figure 2.1. The Earth's Vorticity Reduces to the Radial Component Upon Consolidation of the Family of Surfaces r = const.

This should be intuitive to the reader, because in replacing r by a throughout, the family of spherical surfaces r = const. collapses into the one r = a and hence, the rotational motion of the domain reduces to one of surface flow with only a radial component of angular velocity.

Despite the attractiveness of the resulting equations, this feature is disturbing, because at this stage of development, there is little physical justification that the tangential component of the earth's vorticity will not play a significant role in the motions to be described. Veronis (1968) has commented that there is nothing "physical" in Phillips' development, and Phillips (1968) conceded that shallowness of the atmosphere is not justification for the traditional approximation. This appears to lay the entire scheme open to question. Nonetheless, it seems that the "geometric" significance of Phillips suggestion is correct and thus the considerable simplifications obtained by neglecting the divergence of radial lines should hold. It will now be shown that this is indeed the case.

The questionable point in Phillips' derivation is the disappearance of the terms involving cos ϕ corresponding to the tangential component of planetary vorticity. It will be shown that if the actual scale factors (2.4.1) are not replaced by the approximate set (2.4.2) directly, but rather, if they are first expanded in an asymptotic series in the shallowness and then higher order terms neglected, the tangential component remains of the same order as the radial component. In addition, the simplification of the vector operations previously obtained, remains valid.

The vertical coordinate will be nondimensionalized by a suitable quantity, say the mean scale height H. Letting

$$\begin{cases} \varepsilon = H/a & (2.9.1) \\ \zeta = z/a & (2.9.2) \end{cases}$$

we have

$$r = a + z = a(1 + \varepsilon\zeta) \tag{2.10}$$

$$\begin{cases} h_\lambda = a(1 + \varepsilon\zeta)\cos\phi \\ h_\phi = a(1 + \varepsilon\zeta) \\ h_r = 1 \end{cases} \tag{2.11}$$

Now $\varepsilon \cong 0.01$ and since the earth's ellipticity, which is on the order of 1/289, (Lamb, 1932, p. 332), has been neglected, to the same degree of approximation, the terms of $0(\varepsilon)$ may be omitted. Using the definition in generalized curvilinear coordinates, the curl becomes

$$\nabla \times \vec{v} = \frac{1}{a}\left[\frac{\partial w}{\partial \phi} - \frac{1}{\varepsilon}\left(\varepsilon v + \frac{\partial v}{\partial \zeta}\right)\right]\vec{i} + \frac{1}{a\cos\phi}\left[\frac{\cos\phi}{\varepsilon}\left(\varepsilon u + \frac{\partial u}{\partial \zeta}\right)\right.$$

$$\left. - \frac{\partial w}{\partial \lambda}\right]\vec{j} + \frac{1}{a\cos\phi}\left[\frac{\partial v}{\partial \lambda} - \frac{\partial}{\partial \phi}(\cos\phi\, u)\right]\vec{k} + 0(\varepsilon) \tag{2.12}$$

Now for motions where H is an appropriate vertical scale, $\frac{\partial v_i}{\partial \zeta} = 0(1)$ and hence, εv_i may be neglected relative to these terms. Thus (2.12) becomes

$$\nabla \times \vec{v} \sim \left[\frac{1}{a}\frac{\partial w}{\partial \phi} - \frac{\partial v}{\partial z}\right]\vec{i} + \left[\frac{\partial u}{\partial z} - \frac{1}{a\cos\phi}\frac{\partial w}{\partial \lambda}\right]\vec{j}$$

$$+ \frac{1}{a\cos\phi}\left[\frac{\partial v}{\partial \lambda} - \frac{\partial}{\partial \phi}(\cos\phi\, u)\right]\vec{k} \qquad (2.13)$$

which is equivalent to (2.6.1) obtained by Phillips. Similarly,

$$\nabla \cdot \vec{v} = \frac{1}{a\cos\phi}\frac{\partial u}{\partial \lambda} + \frac{1}{a\cos\phi}\frac{\partial}{\partial \phi}(\cos\phi\, v) + \frac{1}{\varepsilon a}\left[2\varepsilon w + \frac{\partial w}{\partial \zeta}\right] + 0(\varepsilon)$$

or

$$\nabla \cdot \vec{v} \sim \frac{1}{a\cos\phi}\frac{\partial u}{\partial \lambda} + \frac{1}{a\cos\phi}\frac{\partial}{\partial \phi}(\cos\phi\, v) + \frac{\partial w}{\partial z} \qquad (2.14)$$

(cf., 2.6.2).

Now concerning the questionable point of Phillips' results, the term generating the coriolis acceleration is $\nabla \times \vec{v}_r$ and

$$\vec{v}_r = u_r\vec{i} = a(1 + \varepsilon\zeta)\cos\phi\,\Omega\,\vec{i} \qquad (2.15)$$

However, for this velocity, H is not an appropriate vertical scale; a is, and hence, equation (2.12) must be used to determine the earth's vorticity. This becomes

$$\nabla \times \vec{v}_r = \frac{1}{\varepsilon a}\left[\varepsilon a\cos\phi\Omega + a\varepsilon\cos\phi\Omega\right]\vec{j} + \frac{1}{a\cos\phi}\left[2\cos\phi\sin\phi\, a\Omega\right]\vec{k} + 0(\varepsilon)$$

or

$$\nabla \times \vec{v}_r = 2\Omega\cos\phi\,\vec{j} + 2\Omega\sin\phi\,\vec{k} + 0(\varepsilon). \qquad (2.16)$$

The tangential and radial components of planetary vorticity are of the same order.

Thus Phillips' pseudo-coordinate system may be viewed as the zeroeth order problem in an asymptotic expansion in ε. If performed carefully, it does not imply the traditional approximation, yet it does justify simplification of the radial terms. The appropriate equations of motion are then

$$\begin{cases} \dfrac{du}{dt} - 2\Omega(v \sin\phi - w\cos\phi) = -\dfrac{1}{\rho a \cos\phi}\dfrac{\partial p}{\partial \lambda} + \dfrac{uv\tan\phi}{a} - \dfrac{uw}{a} & (2.17.1) \\ \dfrac{dv}{dt} + 2\Omega u \sin\phi = -\dfrac{1}{\rho a}\dfrac{\partial p}{\partial \phi} - \dfrac{u^2\tan\phi}{a} - \dfrac{vw}{a} & (2.17.2) \\ \dfrac{dw}{dt} - 2\Omega u\cos\phi = -\dfrac{1}{\rho}\dfrac{\partial p}{\partial z} - g + \dfrac{u^2 + w^2}{a} & (2.17.3) \end{cases}$$

where

$$\frac{d}{dt} = \frac{\partial}{\partial t} + \frac{u}{a\cos\phi}\frac{\partial}{\partial \lambda} + \frac{v}{a}\frac{\partial}{\partial \phi} + w\frac{\partial}{\partial z} \qquad (2.17.4)$$

As a final note, vertical differentiation, $\frac{\partial}{\partial z}$, may still lead to results that are not geometrically consistent. If a term involving a, and hence r before approximation, is to be differentiated, it should be taken as involving $(a+z)$, differentiated, and then evaluated at $z = 0$. This is equivalent to differentiating with respect to ζ and neglecting term of $O(\varepsilon)$.

2.3 The Linearized Equations and Dynamic Similarity

Linearized equations will be developed for isentropic motions in a hydrostatic atmosphere in zonal motion, i.e., $\vec{v}_o = u_o(\phi, z)\vec{i}$. In what follows, primes will indicate perturbation quantities, and zero subscripts background state variables. Also all background state

variables will be assumed independent of λ.

Expanding to first order in perturbation quantities, (2.17.1) becomes

$$\frac{\partial u'}{\partial t} + \frac{u_o}{a \cos \phi} \frac{\partial u'}{\partial \lambda} + \frac{v'}{a} \frac{\partial u_o}{\partial \phi} + w' \frac{\partial u_o}{\partial z} - 2\Omega(v' \sin \phi - w' \cos \phi)$$

$$= - \frac{1}{\rho_o a \cos \phi} \frac{\partial p'}{\partial \lambda} + \frac{u_o v' \tan \phi}{a} - \frac{u_o w'}{a} \qquad (2.18)$$

We may define the local angular velocity of the background state atmosphere as

$$A(\phi, z) = \frac{u_o(\phi, z)}{a \cos \phi} \qquad (2.19)$$

As suggested in the discussion on p. 32, we write

$$u_o(\phi, z) = A(\phi, z)(a + z)\cos \phi \qquad (2.20)$$

in which case

$$\begin{cases} \dfrac{\partial u_o}{\partial \phi} = \dfrac{\partial A}{\partial \phi} a \cos \phi - Aa \sin \phi & (2.21.1) \\ \dfrac{\partial u_o}{\partial z} = \dfrac{\partial A}{\partial z} a \cos \phi + A \cos \phi & (2.21.2) \end{cases}$$

Equation (2.18) becomes

$$\frac{Du'}{Dt} + [-2(\Omega + A)\sin \phi + \frac{\partial A}{\partial \phi} \cos \phi]v' + [2(\Omega + A)\cos \phi + \frac{\partial A}{\partial z} a \cos \phi]w'$$

$$= \frac{-1}{\rho_o a \cos \phi} \frac{\partial p'}{\partial \lambda}$$

where

$$\frac{D}{Dt} + \frac{\partial}{\partial t} + A \frac{\partial}{\partial \lambda} \tag{2.22}$$

or finally

$$\frac{Du'}{Dt} - 2(\Omega + A)[\sin \phi\, v' - \cos \phi\, w'] + [\frac{\partial A}{\partial \phi} v' + a \frac{\partial A}{\partial z} w']\cos \phi$$

$$= - \frac{1}{\rho_o a \cos \phi} \frac{\partial p'}{\partial \lambda} \tag{2.23.1}$$

Similarly, equations (2.17.2) and (2.17.3) become

$$\frac{Dv'}{Dt} + 2(\Omega + A)\sin \phi\, u' = \frac{-1}{\rho_o a} \frac{\partial p'}{\partial \phi} + \frac{1}{a\rho_o^2} \frac{\partial p_o}{\partial \phi} \rho' \tag{2.23.2}$$

$$\frac{Dw'}{Dt} - 2(\Omega + A)\cos \phi\, u' = - \frac{1}{\rho_o} \frac{\partial p'}{\partial z} + \frac{1}{a\rho_o^2} \frac{\partial p_o}{\partial \phi} \rho' \tag{2.23.3}$$

The continuity and energy equations become

$$\frac{D\rho'}{Dt} + \frac{1}{a} \frac{\partial \rho_o}{\partial \phi} v' + \frac{\partial \rho_o}{\partial z} w' + \rho_o \nabla \cdot \vec{v}' = 0 \tag{2.23.4}$$

$$\frac{Dp'}{Dt} + \frac{1}{a} \frac{\partial p_o}{\partial \phi} v' + \frac{\partial p_o}{\partial z} w' = c^2 \left\{ \frac{D\rho'}{Dt} + \frac{1}{a} \frac{\partial \rho_o}{\partial \phi} v' + \frac{\partial \rho_o}{\partial z} w' \right\} \tag{2.23.5}$$

where

$$c^2 = \gamma R T_o \tag{2.24.1}$$

is the local background sound speed, γ is the ratio of specific heats, R is the specific gas constant, and

$$\nabla \cdot \vec{v}' = \frac{1}{a \cos \phi} \frac{\partial u'}{\partial \lambda} + \frac{1}{a \cos \phi} \frac{\partial}{\partial \phi} (\cos \phi \, v') + \frac{\partial w'}{\partial z}. \qquad (2.24.2)$$

Now the background state is assumed hydrostatic; therefore, using the relations

$$\begin{cases} \frac{\partial p_o}{\partial z} = -\rho_o g & (2.25.1) \\ p_o = \rho_o R T_o & (2.25.2) \end{cases}$$

and defining the local pressure scale height

$$H(\phi, z) = \frac{R T_o(\phi, z)}{g} = \frac{p_o}{\rho_o g} \qquad (2.26)$$

it is easily verified that

$$c^2 = \gamma g H \qquad (2.27)$$

$$p_o(z, \phi) = p_o(0, \phi) \; e^{-\xi(z, \phi)} \qquad (2.28.1)$$

where

$$\xi(z, \phi) = \int_o^z \frac{dz'}{H(z', \phi)} \qquad (2.28.2)$$

Using these relations and assuming a uniform surface pressure, the background state density may be eliminated in favor of p_o and H, and equations (2.23) become

$$\left\{\begin{aligned}
&\frac{Du'}{Dt} - 2(\Omega + A)[\sin\phi\, v' - \cos\phi\, w'] + [\frac{\partial A}{\partial \phi} v' + a \frac{\partial A}{\partial z} w']\cos\phi \\
&\qquad = \frac{-gH}{p_o a \cos\phi} \frac{\partial p'}{\partial \lambda} \qquad (2.29.1)\\
&\frac{Dv'}{Dt} + 2(\Omega + A)\sin\phi\, u' = -\frac{gH}{ap_o}\frac{\partial p'}{\partial \phi} - \frac{g^2H^2}{ap_o}\frac{\partial \xi}{\partial \phi}\rho' \qquad (2.29.2)\\
&\frac{Dw'}{Dt} - 2(\Omega + A)\cos\phi\, u' = -\frac{gH}{p_o}\frac{\partial p'}{\partial z} - \frac{g^2H}{p_o}\rho' \qquad (2.29.3)\\
&\frac{D\rho'}{Dt} - \frac{p_o}{agH^2}[H\frac{\partial \xi}{\partial \phi} + \frac{\partial H}{\partial \phi}]v' - \frac{p_o}{gH^2}[1 + \frac{\partial H}{\partial z}]w' + \frac{p_o}{gH}\nabla\cdot\vec{v}' = 0 \qquad (2.29.4)\\
&\frac{Dp'}{Dt} + \frac{p_o}{a}[\frac{\gamma}{H}\frac{\partial H}{\partial \phi} + (\gamma - 1)\frac{\partial \xi}{\partial \phi}]v' + \frac{p_o}{H}[\gamma\frac{\partial H}{\partial z} + (\gamma - 1)]w' = \gamma gH\frac{D\rho'}{Dt} \qquad (2.29.5)
\end{aligned}\right.$$

Now, the zero order motion of the atmosphere is one of pure rotation, essentially sticking to the globe, the earth's velocity at the equator being roughly 400 m/sec, and typical mean zonal velocities being tens of m/sec. Thus the meridional and vertical variations of A appear as perturbations on this uniform motion. For the sake of simplification, in what follows, only the zero order motion will be considered. The total angular velocity is then

$$\hat{\Omega} = \Omega + A = \text{const.} \qquad (2.30)$$

It is interesting to note that if the traditional approximation had been invoked at an earlier stage, as in previous studies, the advection terms due to the component of zonal motion in pure rotation would not have consolidated as they have here to illuminate the total angular

velocity $\hat{\Omega}$. Free oscillations are being sought; therefore, the boundary condition at the surface is that the vertical velocity vanish. The domain is semi-infinite, and hence, either the radiation condition or the finite energy condition must be imposed at the upper extremity.

Equations (2.29) are separable in t and λ, and hence the field variables may be assumed of the form

$$e^{i(m\lambda - \sigma t)}$$

where the zonal wavenumber m is integer by cyclic continuity. Then the Stokes operator becomes

$$\frac{D}{Dt} = -i\sigma + iAm = -i\omega \tag{2.31}$$

where the intrinsic frequency ω, that relative to medium, has been defined. The system then becomes

$$\begin{cases} -i\omega u' - 2\hat{\Omega}[\sin\phi\, v' - \cos\phi\, w'] = -\dfrac{im\,g\,H}{p_o a\cos\phi}\,p' & (2.32.1) \\[2ex] -i\omega v' + 2\hat{\Omega}\sin\phi\, u' = -\dfrac{gH}{ap_o}\dfrac{\partial p'}{\partial\phi} - \dfrac{g^2H^2}{ap_o}\dfrac{\partial\xi}{\partial\phi}\,\rho' & (2.32.2) \\[2ex] -i\omega w' - 2\hat{\Omega}\cos\phi\, u' = -\dfrac{gH}{p_o}\dfrac{\partial p'}{\partial z} - \dfrac{g^2H}{p_o}\,\rho' & (2.32.3) \\[2ex] iw\rho' - \dfrac{p_o}{agH^2}\left[H\dfrac{\partial\xi}{\partial\phi} + \dfrac{\partial H}{\partial\phi}\right]v' - \dfrac{p_o}{gH^2}\left[1 + \dfrac{\partial H}{\partial z}\right]w' + \dfrac{p_o}{gH}\nabla\cdot\vec{v}' = 0 & (2.32.4) \\[2ex] -i\omega p' + \dfrac{p_o}{a}\left[\dfrac{\gamma}{H}\dfrac{\partial H}{\partial\phi} + (\gamma-1)\dfrac{\partial\xi}{\partial\phi}\right]v' + \dfrac{p_o}{H}\left[\gamma\dfrac{\partial H}{\partial z} + (\gamma-1)\right]w' = -i\omega\gamma gH\rho' & (2.32.5) \end{cases}$$

Now these equations contain terms that are of secondary importance for the background state atmosphere and the type of motions that will be considered. In an attempt to expose these terms, all of the field quantities will be nondimensionalized. The appropriate scales for the independent variables are obvious from the known geometry and nature of the background state. Unfortunately this is not true for the dependent variables. Previous studies (Dickinson, 1968, a,c; Phillips, 1963) have used empirical evidence from the lower atmosphere to scale these unknowns. Similarity principles lead one to believe that the appropriate scales for these should follow from geometrical considerations of the domain, dynamical characteristics of the background state, and the governing equations. This line will be pursued with two exceptions.

(i) The velocities will be scaled by an undetermined velocity $\bar{u}$. $\bar{u}$ is of little significance because the problem is linear and homogeneous and hence, if the vector

$$\begin{bmatrix} u' \\ v' \\ w' \\ p' \\ \rho' \end{bmatrix}$$

is a solution, so is the vector

$$c \cdot \begin{bmatrix} u' \\ v' \\ w' \\ p' \\ \rho' \end{bmatrix}$$

for any scalar c. This arbitrariness allows c to be chosen such that at least one of the solution components is O(1). Hence we pick c such that

$$\tilde{u} = u'/\bar{u} = O(1)$$

(ii) Previous considerations of Poincaré's problem lead us to scale ω by $2\hat{\Omega}$, as all of its eigenfrequencies are less than $2\hat{\Omega}$ in absolute value (Greenspan, 1968, p. 52). Also, our definition of planetary waves requires that they vanish with the angular velocity of the medium.

With these established, we start the similarity procedure by defining

$$\begin{cases} \tilde{u} = u'/\bar{u} = O(1) \\ \tilde{v} = v'/\bar{u} = O(1) \\ \tilde{w} = w'/\bar{u} = O(1) \quad \text{or smaller} \\ \tilde{\omega} = \omega/2\hat{\Omega} = O(1) \quad \text{or smaller} \\ \zeta = z/\bar{H} = O(1) \\ \tilde{H} = H/\bar{H} = O(1) \end{cases} \tag{2.33}$$

where $\bar{H} = \langle H \rangle$ is a mean scale height and tildes indicate nondimensional quantities, ζ being exceptional. m and ϕ are already nondimensional and are assumed for this study to be O(1). $\xi(z,\phi)$ becomes

$$\tilde{\xi}(\zeta,\phi) = \int_o^{\zeta} \frac{d\zeta'}{\tilde{H}} \tag{2.34}$$

Now equation (2.32.2) becomes

$$\underbrace{-i\tilde{\omega}\tilde{u}}_{O(1)\text{ or smaller}} - \underbrace{[\sin\phi\,\tilde{u} - \cos\phi\,\tilde{w}]}_{O(1)} = -\frac{img\bar{H}}{2\hat{\Omega}\bar{u}ap_o}\frac{\tilde{H}}{\cos\phi}p'$$

Aside from inertial motions, for which the terms on the left hand side are in balance, the pressure gradient term must balance the largest of the acceleration terms which implies

$$\frac{g\bar{H}}{2\hat{\Omega}\bar{u}ap_o}p' = O(1)$$

Hence we write

$$\tilde{p} = \frac{g\bar{H}}{2\hat{\Omega}a\bar{u}p_o(\zeta,\phi)}p' = O(1) \tag{2.35}$$

The scale for p' depends locally on the background state. In order to determine the appropriate scale for ρ', (2.32.3) is examined. This is

$$\underbrace{-i\tilde{\omega}\tilde{w}}_{O(1)\text{ or smaller}} - \underbrace{\cos\phi\,\tilde{u}}_{O(1)} = -\underbrace{\frac{\tilde{H}}{\varepsilon}\left[\frac{\partial\tilde{p}}{\partial\zeta} - \frac{1}{\tilde{H}}\tilde{p}\right]}_{O(1/\varepsilon)} - \frac{g^2\bar{H}}{2\hat{\Omega}\bar{u}p_o}\tilde{H}\rho'$$

where again the shallowness has been defined as

$$\varepsilon = \bar{H}/a << 1 \tag{2.36}$$

The first term on the right hand side is $O(1/\varepsilon)$ and cannot be balanced by either term on the left hand side. Therefore

$$\frac{g^2\bar{H}}{2\hat{\Omega}\ \bar{u}\ p_o}\ \rho' = O(1/\varepsilon)$$

or

$$\frac{g^2\bar{H}\varepsilon}{2\hat{\Omega}\ \bar{u}\ p_o}\ \rho' = O(1)$$

and we define

$$\tilde{\rho} = \frac{g^2\bar{H}\varepsilon}{2\hat{\Omega}\ \bar{u}\ p_o}\ \rho' = O(1) \tag{2.37}$$

Then the two terms on the left hand side are $O(\varepsilon)$ with respect to the right hand side, and therefore, they will be neglected, leaving

$$0 = -\tilde{H}\ \frac{\partial \tilde{p}}{\partial \zeta} + \tilde{p} - \tilde{H}\ \tilde{\rho} \tag{2.38}$$

for the vertical equation of motion. By defining

$$\delta = \frac{(2\hat{\Omega})^2 a}{g} << 1\ , \tag{2.39}$$

which is on the order of .01 for the earth's atmosphere, and represents the ratio of centripetal to gravitational acceleration at the equator (Lamb, 1932, p. 332) the ratio

$$\eta = \delta/\varepsilon = \frac{(2\hat{\Omega})^2 a^2}{g\bar{H}} = O(10) \tag{2.40}$$

is Lamb's parameter, and equation (2.32.4) becomes

$$\underbrace{-i\eta\tilde{\omega}\,\tilde{\rho}}_{O(\eta)\text{ or smaller}} \quad \underbrace{-\frac{1}{\tilde{H}^2}\left[\tilde{H}\frac{\partial\tilde{\xi}}{\partial\phi} + \frac{\partial\tilde{H}}{\partial\phi}\right]\tilde{v}}_{O(1)} \quad \underbrace{-\frac{1}{\tilde{H}^2}\left[\frac{\partial\tilde{H}}{\partial\zeta} + 1\right]\frac{\tilde{w}}{\varepsilon}}_{O(\tilde{w}/\varepsilon)}$$

$$+\frac{1}{\tilde{H}}\left[\underbrace{\frac{im}{\cos\phi}\tilde{u} + \frac{1}{\cos\phi}\frac{\partial}{\partial\phi}(\cos\phi\,\tilde{v})}_{O(1)} \quad + \underbrace{\frac{1}{\varepsilon}\frac{\partial\tilde{w}}{\partial\zeta}}_{O(\tilde{w}/\varepsilon)}\right] = 0 \tag{2.41}$$

Similarly equation (2.32.5) becomes

$$\underbrace{-i\eta\tilde{\omega}\tilde{\rho}}_{O(\eta)\text{ or smaller}} \quad +\underbrace{\left[\frac{\gamma}{\tilde{H}}\frac{\partial\tilde{H}}{\partial\phi} + (\gamma-1)\frac{\partial\tilde{\xi}}{\partial\phi}\right]\tilde{v}}_{O(1)} \quad + \underbrace{\frac{1}{\tilde{H}}\left[\gamma\frac{\partial\tilde{H}}{\partial\zeta} + (\gamma-1)\right]\frac{\tilde{w}}{\varepsilon}}_{O(\tilde{w}/\varepsilon)}$$

$$= -\underbrace{i\eta\tilde{\omega}\gamma\tilde{H}\tilde{\rho}}_{O(\eta)\text{ or smaller)}} \tag{2.42}$$

The frequency scale must now be specified more precisely (cf., 2.33). Three regimes will be examined.

Regime (i) $\tilde{\omega} = O(1)$. For this class of motions equation (2.41) demands (in order that the first term be balanced) that

$$\tilde{w}/\varepsilon = O(\eta)$$

or

$$\tilde{w}/\delta = O(1)$$

and hence we define

$$\check{w} = \tilde{w}/\delta = w'/\delta\bar{u} \tag{2.43}$$

The implication of (2.43) is that the ratio of the vertical to horizontal velocities for these motions is

$$w'/\bar{u} = O(\delta) \approx 10^{-2}$$

Then the terms involving meridional variation in the background state may be neglected. These terms are associated with baroclinic vorticity production in the vorticity equation, when expanded to linear order, and represent a mechanism for baroclinic interaction with the background state. The horizontal divergence of velocity may also be neglected. Equations (2.41) and (2.42) then reduce to

$$\begin{cases} -i\tilde{\omega}\tilde{\rho} - \frac{1}{\tilde{H}^2}\left[\frac{\partial \tilde{H}}{\partial \zeta} + 1\right]\check{w} + \frac{1}{\tilde{H}}\frac{\partial \check{w}}{\partial \zeta} = 0 & (2.44.1) \\ -i\tilde{\omega}\tilde{p} + \frac{1}{\tilde{H}}\left[\gamma\frac{\partial \tilde{H}}{\partial \zeta} + (\gamma-1)\right]\check{w} = -i\tilde{\omega}\gamma\tilde{H}\tilde{\rho} & (2.44.2) \end{cases}$$

The implications of these equations is that the density of an element changes due to vertical motion against the stratification and the work done is that of the associated isentropic expansion. These are very low frequency gravity waves modified by the rotation of the atmosphere. They are nearly irrotational and hence would not be expected to interact baroclinically with the background state. In addition, the velocity divergence is attributed primarily to motion against the stratification. The relation to the terms neglected is obvious.

Notice that (2.38), (2.44.1) and (2.44.2) form a closed system in $\tilde{p}$, $\tilde{\rho}$, and $\check{w}$, and hence, they have uncoupled from the horizontal equations of motion. Therefore, they may be solved and the solution, $\tilde{p}$,

substituted into the horizontal equations, which are merely linear algebraic in $\tilde{u}$, and $\tilde{v}$. After neglecting terms of $O(\varepsilon)$, these become

$$\begin{cases} -i\tilde{\omega}\tilde{u} - \sin\phi\,\tilde{v} = -\dfrac{im\tilde{H}}{\cos\phi}\,\tilde{p} & (2.44.3) \\ -i\tilde{\omega}\tilde{v} + \sin\phi\,\tilde{u} = -\tilde{H}\dfrac{\partial\tilde{p}}{\partial\phi} + \tilde{H}\dfrac{\partial\tilde{\xi}}{\partial\phi}\,\tilde{p} - \tilde{H}^2\dfrac{\partial\tilde{\xi}}{\partial\phi}\,\tilde{\rho} & (2.44.4) \end{cases}$$

The horizontal components may be solved for directly. Now, none of the equations have any differential dependence on ϕ. Thus the solutions are arbitrary functions of latitude and need not meet any boundary constraints in ϕ. The notion of normal modes for this system is inappropriate, and the frequency, $\tilde{\omega}$, may take on all values in the assumed range.

The physical significance of this is that these disturbances do not "feel" the full spherical nature of the domain and hence, are not restricted by the corresponding geometrical constraints. They resemble waves in free space more than free oscillations in a contained system.

Regime (ii) $\tilde{\omega} = O(1/\eta)$. In order that the third term in (2.42) be balanced it must be no larger than the largest of the others. Hence

$$\tilde{w}/\varepsilon = O(1)$$

and we define

$$\hat{w} = \frac{\tilde{w}}{\varepsilon} = \frac{w'}{\varepsilon\tilde{u}} = O(1) \qquad (2.45)$$

$$\hat{\omega} = \tilde{\omega}/\eta \qquad (2.46)$$

For this class of motions the ratio of the vertical to horizontal velocities is

$$\frac{w'}{\bar{u}} = O(\varepsilon) \approx 10^{-3}$$

and equations (2.41) and (2.42) become

$$\begin{cases} -i\hat{\omega}\tilde{\rho} - \frac{1}{\tilde{H}^2}\left[\tilde{H}\frac{\partial\tilde{\xi}}{\partial\phi} + \frac{\partial\tilde{H}}{\partial\phi}\right]\tilde{v} - \frac{1}{\tilde{H}^2}\left[\frac{\partial\tilde{H}}{\partial\zeta} + 1\right]\hat{w} + \frac{1}{\tilde{H}}\left[\frac{im}{\cos\phi}\tilde{u}\right. \\ \qquad\qquad \left. + \frac{1}{\cos\phi}\frac{\partial}{\partial\phi}(\cos\phi\,\tilde{v}) + \frac{\partial\hat{w}}{\partial\zeta}\right] = 0 \qquad (2.47.1) \\ -i\hat{\omega}\tilde{p} + \left[\frac{\gamma}{\tilde{H}}\frac{\partial\tilde{H}}{\partial\phi} + (\gamma-1)\frac{\partial\tilde{\xi}}{\partial\phi}\right]\tilde{v} + \frac{1}{\tilde{H}}\left[\gamma\frac{\partial\tilde{H}}{\partial\zeta} + (\gamma-1)\right]\hat{w} = -i\hat{\omega}\gamma\tilde{H}\tilde{\rho} \qquad (2.47.2) \end{cases}$$

The terms associated with baroclinic vorticity production and horizontal divergence remain for this case, and the horizontal equations of motion reduce to

$$\begin{cases} -\sin\phi\,\tilde{v} = -\frac{im\tilde{H}}{\cos\phi}\tilde{p} \qquad (2.47.3) \\ \sin\phi\,\tilde{u} = -\tilde{H}\frac{\partial\tilde{p}}{\partial\phi} + \tilde{H}\frac{\partial\tilde{\xi}}{\partial\phi} - \tilde{H}^2\frac{\partial\tilde{\xi}}{\partial\phi}\tilde{\rho} \qquad (2.47.4) \end{cases}$$

The motions described by these equations are Rossby in their horizontal character, and in fact (2.47.3) and (2.47.4) imply that the horizontal motion is geostrophic, something that is often assumed in Rossby wave studies (Dutton, 1976, p. 513). Unlike the motions of regime (i), these must satisfy differential relations on both ϕ and z, and hence the equations and boundary conditions form a linear eigenvalue problem.

We are assuming of course, that the radiation condition and inhomogeneity are sufficient constraints in the vertical.

Regime (iii) $\tilde{\omega} = o(1/\eta)$. These frequencies are sufficiently small so that the time derivative terms in (2.41) and (2.42) may be neglected with respect to those of $0(1)$. The reasoning for choosing the vertical velocity scale is as in the previous case, and (2.41) and (2.42) reduce to

$$\begin{cases} -\frac{1}{\tilde{H}}\left[\tilde{H}\frac{\partial\tilde{\xi}}{\partial\phi}+\frac{\partial\tilde{H}}{\partial\phi}\right]\tilde{v}-\frac{1}{\tilde{H}}\left[\frac{\partial\tilde{H}}{\partial\zeta}+1\right]\hat{w}+\left[\frac{im}{\cos\phi}\tilde{u}+\frac{1}{\cos\phi}\frac{\partial}{\partial\phi}(\cos\phi\,\tilde{v})\right. \\ \qquad\qquad \left.+\frac{\partial\hat{w}}{\partial\zeta}\right]=0 \qquad (2.48.1) \\ \left[\gamma\frac{\partial\tilde{H}}{\partial\phi}+\tilde{H}(\gamma-1)\frac{\partial\tilde{\xi}}{\partial\phi}\right]\tilde{v}+\left[\gamma\frac{\partial\tilde{H}}{\partial\zeta}+(\gamma-1)\right]\hat{w}=0 \qquad (2.48.2) \end{cases}$$

where $\hat{w}$ is given by (2.45). The horizontal equations of motion are the same as (2.47.3) and (2.47.4). These motions are the slowest of the Rossby type and differ from those of regime (ii) by the fact that the compression and expansion work is insensitive to the unsteadiness. Motions of regime (ii) and (iii) appear to be Phillips' geostrophic motions of type II (Phillips, 1963).

The reader will notice that for all of these regimes the one term involving $\cos(\phi)$ that had remained after the shallow atmosphere approximation, was eliminated being $0(\varepsilon)$ or $0(\delta)$ relative to the others. As we have already seen, by not invoking the traditional approximation, it has been possible to consolidate some of the $\cos(\phi)$ terms and identify the total angular velocity $\hat{\Omega}$. The one term remaining was

subsequently found to be $O(\varepsilon)$ or $O(\delta)$ because of the dynamical restrictions placed on the vertical velocity by the background state.

2.4 Development of the Boundary Value Problem

It is apparent from previous studies (Longuet-Higgins, 1968; Lamb, 1932, p. 350) that the highest Rossby frequency is smaller than all of the large scale gravity wave frequencies. However, it is not clear that all of the Rossby frequencies are $O(1/\eta)$ or smaller. Three regimes of $\tilde{\omega}$ have been identified for $m = O(1)$, where the equations may be simplified by neglecting terms of secondary importance. If it is required that the problem be solved for the general range of $\tilde{\omega} < 1$, we must retain all of these terms, even though some may be of negligible importance for particular values of $\tilde{\omega}$.

Therefore the equations we shall consider are

$$\begin{cases} -i\tilde{\omega}\tilde{u} - \sin\phi\,\tilde{v} = -\dfrac{im\tilde{H}}{\cos\phi}\,\tilde{p} & (2.49.1) \\[2ex] -i\tilde{\omega}\tilde{v} + \sin\phi\,\tilde{u} = -\tilde{H}\dfrac{\partial\tilde{p}}{\partial\phi} + \tilde{H}\dfrac{\partial\tilde{\xi}}{\partial\phi}\,\tilde{p} - \tilde{H}^2\dfrac{\partial\tilde{\xi}}{\partial\phi}\,\tilde{\rho} & (2.49.2) \\[2ex] \tilde{\rho} = \dfrac{1}{\tilde{H}}\,\tilde{p} - \dfrac{\partial\tilde{p}}{\partial\zeta} & (2.49.3) \\[2ex] -i\tilde{\omega}\eta\tilde{\rho} - \dfrac{1}{\tilde{H}^2}\left[\dfrac{\partial\tilde{H}}{\partial\phi} + \tilde{H}\dfrac{\partial\tilde{\xi}}{\partial\phi}\right]\tilde{v} - \dfrac{1}{\tilde{H}^2}\left[\dfrac{\partial\tilde{H}}{\partial\zeta} + 1\right]\hat{w} \\ \qquad + \dfrac{im}{\tilde{H}\cos\phi}\,\tilde{u} + \dfrac{1}{\tilde{H}\cos\phi}\dfrac{\partial}{\partial\phi}(\cos\phi\,\tilde{v}) + \dfrac{1}{\tilde{H}}\dfrac{\partial\hat{w}}{\partial\zeta} = 0 & (2.49.4) \\[2ex] -i\tilde{\omega}\eta\tilde{p} + \left[\dfrac{\gamma}{\tilde{H}}\dfrac{\partial\tilde{H}}{\partial\phi} + (\gamma-1)\dfrac{\partial\tilde{\xi}}{\partial\phi}\right]\tilde{v} + \dfrac{1}{\tilde{H}}\left[\gamma\dfrac{\partial\tilde{H}}{\partial\zeta} + (\gamma-1)\right]\hat{w} = -i\tilde{\omega}\eta\gamma\tilde{H}\tilde{\rho} & (2.49.5) \end{cases}$$

where again

$$\hat{w} = \tilde{w}/\varepsilon \tag{2.49.6}$$

and the associated boundary conditions are

$$\begin{cases} \hat{w} = 0 \quad \zeta = 0 \\ \text{radiation/finite energy condition } \zeta \to \infty \end{cases} \tag{2.49.7}$$

Making the standard spherical transformation

$$\mu = \sin \phi \tag{2.50}$$

these become

$$\begin{cases} -i\tilde{\omega}\tilde{u} = \mu\tilde{v} - \dfrac{im\tilde{H}}{\sqrt{1-\mu^2}}\,\tilde{p} & (2.51.1) \\[2ex] -i\tilde{\omega}\tilde{v} = -\mu\tilde{u} - \tilde{H}\sqrt{1-\mu^2}\,\dfrac{\partial\tilde{p}}{\partial\mu} + \tilde{H}\sqrt{1-\mu^2}\,\dfrac{\partial\tilde{\xi}}{\partial\mu}\,\tilde{p} - \tilde{H}^2\sqrt{1-\mu^2}\,\dfrac{\partial\tilde{\xi}}{\partial\mu}\tilde{\rho} & (2.51.2) \\[2ex] \tilde{\rho} = \dfrac{1}{\tilde{H}}\,\tilde{p} - \dfrac{\partial\tilde{p}}{\partial\zeta} & (2.51.3) \\[2ex] -i\tilde{\omega}\tilde{\rho} - \dfrac{\sqrt{1-\mu^2}}{\tilde{H}^2}\left[\dfrac{\partial\tilde{H}}{\partial\mu} + \tilde{H}\,\dfrac{\partial\tilde{\xi}}{\partial\mu}\right] - \dfrac{1}{\tilde{H}^2}\left[\dfrac{\partial\tilde{H}}{\partial\zeta} + 1\right]\hat{w} \\ \quad + \dfrac{im}{\tilde{H}\sqrt{1-\mu^2}}\,\tilde{u} + \dfrac{1}{\tilde{H}}\,\dfrac{\partial}{\partial\mu}(\sqrt{1-\mu^2}\,\tilde{v}) + \dfrac{1}{\tilde{H}}\,\dfrac{\partial\hat{w}}{\partial\zeta} = 0 & (2.51.4) \\[2ex] -i\tilde{\omega}\eta\tilde{p} + \sqrt{1-\mu^2}\left[\dfrac{\gamma}{\tilde{H}}\,\dfrac{\partial\tilde{H}}{\partial\mu} + (\gamma-1)\,\dfrac{\partial\tilde{\xi}}{\partial\mu}\right]\tilde{v} + \dfrac{1}{\tilde{H}}\left[\gamma\,\dfrac{\partial\tilde{H}}{\partial\zeta} + (\gamma-1)\right]\hat{w} \\ \quad = -i\tilde{\omega}\eta\gamma\tilde{H}\tilde{\rho} & (2.51.5) \end{cases}$$

In order to simplify the problem, further discussion will be restricted to a barotropic atmosphere. Hence

$$\tilde{H} = \tilde{H}(\zeta) \ ,$$

and the baroclinic interaction terms vanish. Equations (2.51) reduce to

$$\begin{cases} -i\tilde{\omega}\tilde{u} = \mu\tilde{v} - \dfrac{im\tilde{H}}{\sqrt{1-\mu^2}}\,\tilde{p} & (2.52.1) \\[2ex] -i\tilde{\omega}\tilde{v} = -\mu\tilde{u} - \tilde{H}\sqrt{1-\mu^2}\,\dfrac{\partial\tilde{p}}{\partial\mu} & (2.52.2) \\[2ex] \tilde{\rho} = \dfrac{1}{\tilde{H}}\,\tilde{p} - \dfrac{\partial\tilde{p}}{\partial\zeta} & (2.52.3) \\[2ex] -i\tilde{\omega}\tilde{\rho} - \dfrac{1}{\tilde{H}^2}\left[\dfrac{\partial\tilde{H}}{\partial\zeta} + 1\right]\hat{w} + \dfrac{im}{\tilde{H}\sqrt{1-\mu^2}}\,\tilde{u} + \dfrac{1}{\tilde{H}}\,\dfrac{\partial}{\partial\mu}(\sqrt{1-\mu^2}\,\tilde{v}) + \dfrac{1}{\tilde{H}}\,\dfrac{\partial\hat{w}}{\partial\zeta} = 0 & (2.52.4) \\[2ex] -i\tilde{\omega}\eta\tilde{p} + \dfrac{1}{\tilde{H}}\left[\gamma\,\dfrac{\partial\tilde{H}}{\partial\zeta} + (\gamma-1)\right]\hat{w} = -i\tilde{\omega}\eta\gamma\tilde{H}\tilde{\rho} & (2.52.5) \end{cases}$$

The velocities may be obtained from these in terms of $\tilde{p}$, giving

$$\begin{cases} \tilde{u} = \dfrac{\tilde{H}\sqrt{1-\mu^2}}{\tilde{\omega}^2 - \mu^2}\left\{\mu\,\dfrac{\partial\tilde{p}}{\partial\mu} + \dfrac{\tilde{\omega}m}{1-\mu^2}\,\tilde{p}\right\} & (2.53.1) \\[2ex] \tilde{v} = \dfrac{-i\tilde{H}\sqrt{1-\mu^2}}{\tilde{\omega}^2 - \mu^2}\left\{\tilde{\omega}\,\dfrac{\partial\tilde{p}}{\partial\mu} + \dfrac{m\mu}{1-\mu^2}\,\tilde{p}\right\} & (2.53.2) \\[2ex] \hat{w} = \dfrac{i\tilde{\omega}\eta\tilde{H}}{\left(\dfrac{\partial\tilde{H}}{\partial\zeta} + \kappa\right)}\left\{\tilde{H}\,\dfrac{\partial\tilde{p}}{\partial\zeta} - \kappa\tilde{p}\right\} & (2.53.3) \end{cases}$$

where

$$\kappa = \frac{(\gamma-1)}{\gamma} \tag{2.54}$$

Now, eliminating the density, (2.52.4) may be written as

$$(\frac{\partial}{\partial\zeta} - \frac{1}{\tilde{H}})[i\tilde{\omega}\eta\tilde{p} + \hat{w}/\tilde{H}] + \frac{1}{\tilde{H}}\frac{\partial}{\partial\mu}[\sqrt{1-\mu^2}\,\tilde{v}] + \frac{im}{\tilde{H}\sqrt{1-\mu^2}}\tilde{u} = 0 \tag{2.55}$$

It proves convenient to introduce

$$\tilde{y} = \tilde{p} - \frac{i}{\tilde{\omega}\eta\tilde{H}}\hat{w} \tag{2.56.1}$$

which becomes

$$\tilde{y} = \frac{1}{(\frac{\partial\tilde{H}}{\partial\zeta} + \kappa)}\frac{\partial}{\partial\zeta}(\tilde{H}\tilde{p}) = J[\tilde{p}] \ . \tag{2.56.2}$$

$\tilde{y}$ is $\frac{1}{-i\tilde{\omega}\eta}\frac{d'\tilde{p}}{dt}$, where $\frac{d'}{dt}$ is the linearized version of $\frac{d}{dt}$. Hence as Lindzen and Chapman (1969, p. 114) and Dikii (1965) have pointed out, $\tilde{y}$ is related to the velocity divergence through the energy equation. Equation (2.55) becomes

$$-i\tilde{\omega}\eta(\frac{\partial}{\partial\zeta} - \frac{1}{\tilde{H}})\tilde{y} + \frac{1}{\tilde{H}}\frac{\partial}{\partial\mu}[\sqrt{1-\mu^2}\,\tilde{v}] + \frac{im}{\tilde{H}\sqrt{1-\mu^2}}\tilde{u} = 0, \tag{2.57}$$

or with the use of (2.53) and (2.56.2)

$$J\cdot L[\tilde{y}] = \hat{M}[\tilde{y}] \tag{2.58.1}$$

where we define the linear operators

$$L[\circ] = \left(\frac{\partial}{\partial \zeta} - \frac{1}{\tilde{H}}\right) \circ \tag{2.58.2}$$

$$\hat{M}[\circ] = \frac{1}{\eta}\frac{\partial}{\partial \mu}\left[\frac{1-\mu^2}{\tilde{\omega}^2 - \mu^2}\frac{\partial}{\partial \mu} \circ\right] + \frac{1}{\eta(\tilde{\omega}^2 - \mu^2)}\left[\frac{m}{\tilde{\omega}}\frac{\tilde{\omega}^2+\mu^2}{\tilde{\omega}^2-\mu^2} - \frac{m^2}{1-\mu^2}\right] \circ \tag{2.58.3}$$

Equations similar to (2.58) have been obtained by Lindzen and Chapman (1969, p. 116), Dikii (1965), Schoeberl and Geller (1977) and others in tidal and planetary disturbance studies. The goals of these studies differ but in general they have had to introduce additional assumptions, whereas equations (2.58) have resulted essentially from dynamic similarity.

It should be pointed out that this BVP has an essential feature of Poincoré's Problem. Equation 2.58.1 is hyperbolic for the band of latitudes given by

$$|\mu| < |\omega|$$

and yet, boundary conditions are specified completely around the domain. This unusual characteristic has been absent in other studies, which through additional approximations, have obtained a uniformly elliptic problem (Dickinson, 1968b). The circles of latitude where 2.58.1 changes from hyperbolic to elliptic are just the critical latitudes of LTE and of the spherical annulus studies of Stewartson (1971), Stewartson and Pickard (1969), and Stewartson and Walton (1976) (cf., discussion, p. 17). This feature may also be compared with the nature of the asymptotic spherical solutions determined by Longuet-Higgins

(1964) (cf., Figure 1.4).

Now (2.58.1) is separable, and assuming

$$\tilde{y} = Z(\zeta)\ U\ (\mu)\ , \tag{2.59}$$

the following BVP's result

$$\begin{cases} J \circ L[Z] + \alpha Z = 0 & (2.60.1) \\ \tilde{H}\ Z' + (\alpha\tilde{H} - 1)Z = 0 \quad \zeta = 0 \quad (\alpha \neq 0) & (2.60.2) \\ \text{radiation/finite energy condition } \zeta \to \infty & (2.60.3) \end{cases}$$

$$\begin{cases} \hat{M}[U] + \alpha U = 0 & (2.61.1) \\ U \text{ bounded at } \mu = \pm 1 & (2.61.2) \end{cases}$$

where α is the separation constant. The derivation of the surface boundary condition, (2.60.2), is given in Appendix A. The case $\alpha = 0$ is exceptional, and must be treated separately. It is shown not to be a characteristic value in Appendix B. Equation (2.61.1) is equivalent to LTE if $\frac{(2\Omega)^2 a^2}{gh}$ is replaced by

$$\alpha\eta = \alpha \frac{(2\hat{\Omega})^2 a^2}{g\bar{H}}$$

Thus $\alpha\eta$ is the effective Lamb's parameter and $\frac{\bar{H}}{\alpha}$ is Taylor's (1936) "equivalent depth." An attractive feature of these two problems is that the dependence on the parameters $\tilde{\omega}$ and α is uncoupled. Dikii (1965) examined a similar problem which contained a broader range of motions

e.g., acoustic waves. The price for including these was that the eigenparameters, $\tilde{\omega}$ and α, coupled the two BVP's. The method of solution is enlightening, and the reader is referred to that paper for the details.

2.5 Solution of the Vertical Equation

The problem is to find those values of α which admit (to a degree which will be discussed shortly) nontrivial solutions of (2.60). These are the characteristic values and will be referred to as nearly characteristic if the conditions are approximately satisfied. Flattery (1968) has indicated that for real $\tilde{\omega}$, (2.61) has solutions only for real α. Therefore, at least for this barotropic atmosphere, the search may be restricted to real values of α.

Because the density decays as $e^{-\tilde{\xi}}$, it proves convenient to transform (2.60) by letting

$$Z(\zeta) = e^{\tilde{\xi}/2}\, v(\zeta) \ . \tag{2.62}$$

The vertical BVP then becomes

$$\begin{cases} \tilde{H}v'' + \tilde{H}'\, v' + \{\alpha(\tilde{H}' + \kappa) - \dfrac{1}{4\tilde{H}}\}\, v = 0 & (2.63.1) \\ \tilde{H}v' + (\alpha\tilde{H} - 1/2)v = 0 \quad \zeta = 0 \quad (\alpha \neq 0) & (2.63.2) \\ \text{radiation/finite energy condition} \quad \zeta \to \infty & (2.63.3) \end{cases}$$

(2.63.1) may be reduced to its normal form (cf., Rektorys, 1969, p. 791) by letting

$$v(\zeta) = \frac{1}{\sqrt{\tilde{H}}}\, u(\zeta) \ , \tag{2.64}$$

in which case it becomes

$$u'' + k^2(\zeta;\, \alpha)u = 0 \ , \tag{2.65.1}$$

where

$$k^2(\zeta;\, \alpha) = \frac{1}{\tilde{H}}\left\{\alpha(\tilde{H}' + \kappa) - \frac{\tilde{H}''}{2} + \frac{1}{4\tilde{H}}[(\tilde{H}')^2 - 1]\right\} \tag{2.65.2}$$

plays the role of a local vertical wavenumber or refractive index squared. The problem reduces to a simpler appearance if the dependent variable is changed from geometric height to a pressure height $\tilde{\xi}(\zeta)$. By letting

$$\begin{cases} \hat{Z}(\tilde{\xi}(\zeta)) = Z(\zeta) & (2.66.1) \\ \hat{H}(\tilde{\xi}(\zeta)) = \tilde{H}(\zeta) & (2.66.2) \end{cases}$$

and again transforming the dependent variable

$$\hat{Z}(\tilde{\xi}) = e^{\tilde{\xi}/2}\, \hat{v}(\tilde{\xi}) \ , \tag{2.66.3}$$

the problem becomes

$$\begin{cases} \hat{v}'' + \hat{k}^2(\tilde{\xi};\, \alpha)\hat{v} = 0 & (2.67.1) \\ \hat{v}' + (\alpha\hat{H} - 1/2)\hat{v} = 0 \quad \tilde{\xi} = 0 \ (\alpha \neq 0) & (2.67.2) \\ \text{radiation/finite energy conditions } \tilde{\xi} \to \infty & (2.67.3) \end{cases}$$

where

$$\hat{k}^2(\tilde{\xi};\ \alpha) = \alpha(\hat{H}' + \kappa\hat{H}) - 1/4 \qquad (2.67.4)$$

and primes denote differentiation with respect to $\tilde{\xi}$. Quantities with carets are functions of $\tilde{\xi}$, and those without are functions of ζ. For the most part, it is more convenient to use geometric height; however, it is instructive to examine the character of the problem from (2.67).

First this seems to be an appropriate time to discuss the physical significance of the approximate normal modes that are being sought. Now the system is semi-infinite in the vertical. There are three ways in which a persistent or free oscillation may exist.

(i) The solution is completely evanescent; energy propagates solely in the horizontal and therefore is contained by the spherical geometry. For this type of disturbance, it is required that the energy of the motion be finite (finite energy condition).

(ii) The solution is internal for finite ζ, but evanescent for all ζ above some level. Hence, a disturbance sees an infinite barrier and is completely refected (Morse and Feshbach, 1953, p. 1100). The finite energy condition is also appropriate in this situation.

(iii) The solution is internal, but leaks energy out at a "slow" rate. This is a relaxation of the classical definition of free modes. If driven steadily, it would be expected that the amplitude of such a disturbance would grow to a large value before a steady state situation was realized. Similarly, viewed as an initial value problem, if several disturbances were excited simultaneously, this type should persist the longest, and hence be the most evident. The appropriate upper boundary condition for this type of solution is that energy propagate

away from the region of possible generation (radiation condition).

In cases (ii) and (iii), variability of the refractive index may cause partial reflection of energy. If the index becomes imaginary over a portion of the domain, that region will appear as a barrier, some of the energy being reflected and some transmitted. Thus, although only outward propagation of energy is allowed in (iii) at infinity, this is not the case for finite heights. In order that the homogeneous boundary condition at the surface (physically no surface work) be approached, the phases of the upward and downward propagating waves must combine at the surface so that the vertical velocity is cancelled.

Now (2.53.3) implies that $\tilde{p}$ and $\hat{w}$ have the same μ dependence, and from (2.56.1) this must be $U(\mu)$. Therefore we define

$$\begin{cases} \tilde{p} = \underline{P}(\zeta)\ U(\mu) & (2.68.1) \\ \hat{w} = W(\zeta)\ U(\mu) & (2.68.2) \end{cases}$$

and (2.53.3) becomes

$$\hat{w} = U(\mu)\ \frac{i\tilde{\omega}\eta\tilde{H}}{(\tilde{H}' + \kappa)}\{\tilde{H}\underline{P}' - \kappa\underline{P}\} \qquad (2.69)$$

where $\underline{P}' = \frac{\partial \underline{P}}{\partial \zeta}$.

The time averaged vertical energy flux is

$$\langle I_z \rangle = \langle p'w' \rangle = \frac{1}{2}\,\mathrm{Re}\{p'w'^{*}\}$$

where * denotes complex conjugation. Using (2.69), (2.35), and (2.49.6), this becomes

$$\langle I_z \rangle = -U^2(\mu)\ \frac{\hat{\Omega}\bar{u}^2 \varepsilon a \tilde{\omega} \eta p_o(0) e^{-\tilde{\xi}}}{g\bar{H}} \cdot \frac{\tilde{H}^2}{(\tilde{H}' + \kappa)}\ \mathrm{Im}\{\underline{P}^* \underline{P}'\} \qquad (2.70)$$

With (2.62) and the following relation derived in Appendix A

$$\underline{P} = \frac{1}{\alpha}\left(\frac{1}{\tilde{H}} Z - Z'\right) \qquad (\alpha \neq 0) \qquad (2.71)$$

(2.70) reduces to

$$\langle I_z \rangle = -U^2(\mu)\ \frac{\hat{\Omega}\bar{u}^2 \delta a \tilde{\omega} p_o(0)}{g\bar{H}\alpha} \cdot \tilde{H}\ \mathrm{Im}\{v'v^*\} \qquad (2.72)$$

The kinetic energy density is defined as

$$E = E_1 + E_2 = \frac{1}{2} \rho_o (|u'|^2 + |v'|^2) \qquad (2.73)$$

The contribution from the vertical component is $O(\delta^2)$ or smaller and hence is neglected. By letting

$$\hat{U}(\mu) = \frac{\sqrt{1-\mu^2}}{\tilde{\omega}^2 - \mu^2}\left\{\mu U' + \frac{\tilde{\omega} m}{1-\mu^2} U\right\} \qquad (2.74.1)$$

$$\hat{V}(\mu) = \frac{\sqrt{1-\mu^2}}{\tilde{\omega}^2 - \mu^2}\left\{\tilde{\omega} U' + \frac{m\mu}{1-\mu^2} U\right\}, \qquad (2.74.2)$$

$u' + v'$ become

$$u' = \bar{u}\tilde{H}\,\underline{P}(\zeta)\hat{U}(\mu) \qquad (2.75.1)$$

$$v' = -i\bar{u}\tilde{H}\,\underline{P}(\zeta)\hat{V}(\mu) \qquad (2.75.2)$$

Lindzen and Chapmen (1969, p. 115) have indicated that equations (2.75)

do not imply that u' and v' are 90 degrees out of phase since $\hat{U}$ and $\hat{V}$ are different operators on $U(\mu)$ which is complex. However, $U(\mu)$ turns out to be the eigenfunctions of LTE, and since the associated eigenfrequencies are nondegenerate in general, the Hough functions may be taken as all real (A.D. Pierce, personal communication). Since the operators $\hat{U}$ and $\hat{V}$ are real, it follows that v' should lag u' by 90 degrees.

(2.73) becomes

$$E = (\hat{U}^2 + \hat{V}^2)\,\frac{p_o(0)\bar{u}^2}{2g\bar{H}\,\alpha^2}\cdot\frac{1}{\tilde{H}}\left|\frac{1}{2}v - \tilde{H}v'\right|^2 \qquad (2.76)$$

The radiation condition then requires

$$\langle I_z \rangle \geq 0 \qquad \zeta \to \infty \qquad (2.77.1)$$

and the finite energy condition requires that

$$\int_0^\infty E(\zeta)d\zeta < \infty \qquad (2.77.2)$$

We will very briefly examine the case of an isothermal atmosphere, as it will have application to the more general situation. In this case $\tilde{\xi} = \zeta$, $\tilde{H} = \hat{H} = 1$ and (2.67) reduce to

$$\begin{cases} \hat{v}'' + \hat{k}^2\hat{v} = 0 & (2.78.1) \\ \hat{v}' + (\alpha - 1/2)\hat{v} = 0 \quad \tilde{\xi} = 0 & (2.78.2) \\ \hat{k}^2 = (\alpha\kappa - 1/4) & (2.78.3) \end{cases}$$

where

The general solution is of the form

$$\hat{v} = Ae^{i\hat{k}\tilde{\xi}} + Be^{-i\hat{k}\tilde{\xi}} \quad \hat{k} \neq 0 \tag{2.79}$$

(2.72) then becomes

$$\langle I_z \rangle = \begin{cases} U^2 \dfrac{\hat{\Omega}\bar{u}^{-2} a \delta \tilde{\omega} p_o(0)\hat{k}}{g\bar{H}\alpha} \left(|B|^2 - |A|^2\right) & \alpha > \frac{1}{4\kappa} \\ 0 & \alpha < \frac{1}{4\kappa} \end{cases} \tag{2.80}$$

Thus, the vertical propagation of energy is opposite to that of the phase. If $\alpha < \frac{1}{4\kappa}$, $\hat{k}$ is imaginary and by letting

$$\hat{k} = i\tilde{k} \tag{2.81.1}$$

the energy density becomes

$$E = (\hat{U}^2 + \hat{V}^2) \frac{\bar{u}^{-2} p_o(0)}{2g\bar{H}\alpha^2} \left\{ |A|^2 (\tfrac{1}{2} + \tilde{k})^2 e^{-2\tilde{k}\tilde{\xi}} + 2(\tfrac{1}{4} - \tilde{k}^2)\mathrm{Re}\{AB^*\} + |B|^2 (\tfrac{1}{2} - \tilde{k})^2 e^{2\tilde{k}\tilde{\xi}} \right\} \tag{2.81.2}$$

As is to be expected for this isothermal atmosphere, mechanisms (ii) and (iii) described on p. 55 are inoperative, and only an evanescent solution is capable of satisfying the problem. In fact, it may be verified that the only solution to the problem is the Lamb mode (Siebert, 1961; Wilkes, 1949), where

$$Z(\zeta) = e^{\kappa\zeta} \tag{2.82.1}$$

and

$$\alpha = 1 - \kappa \cong .714 \qquad (2.82.2)$$

It may be seen from (2.53.3) that the vertical velocity is zero throughout.

For the general case, it is instructive to examine equations (2.67). Now $\hat{k}^2(\tilde{\xi}; \alpha)$ given by (2.67.4) defines a family of functions with α as a parameter. This family is represented in Figure 2.2 and corresponds to a typical atmospheric profile.

In general $\hat{k}^2(\tilde{\xi}; \alpha)$ is monotone in α; thus, the larger α is the shorter is the vertical wavelength. For sufficiently large positive α, the index is real throughout similarly for sufficiently large negative values it is imaginary throughout. For intermediate values there may

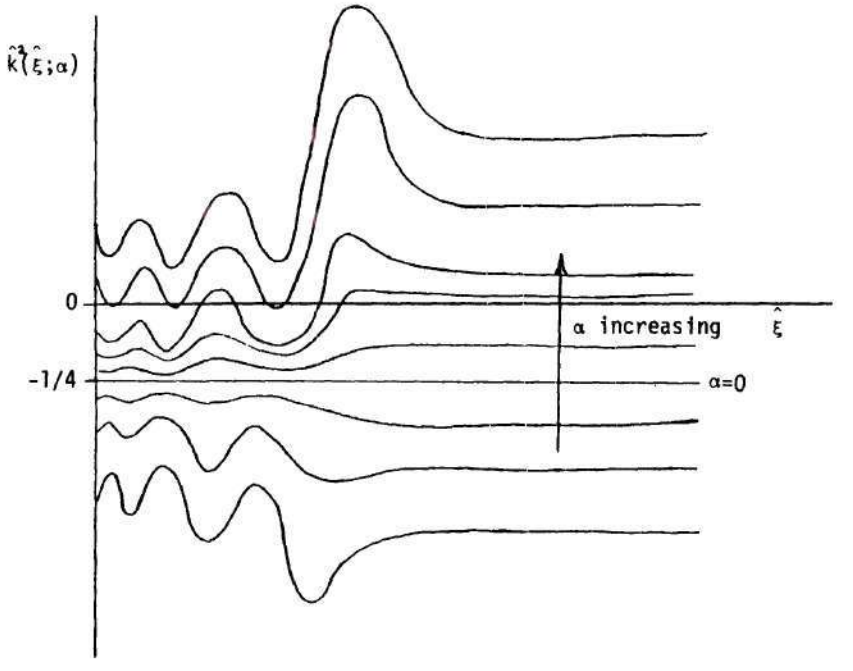

Figure 2.2. Family of Refractive Indices Squared with Parameter α.

exist several barriers to vertical propagation. The atmosphere will be assumed asymptotically isothermal, $\zeta \to \infty$; hence $\hat{k}^2 \to \hat{k}_\infty^2 = \text{const.}$ Mechanism (ii) is then possible only for $\alpha < \frac{1}{4\kappa\tilde{H}_\infty}$ where $\tilde{H}_\infty$ is the limiting scale height, $\zeta \to \infty$.

The solution of (2.67) may be approached with the WKB approximation. This treatment is valid if

$$\hat{\Gamma}(\tilde{\xi};\ \alpha) = \frac{3}{4\hat{k}^4}\left(\frac{\partial \hat{k}}{\partial \tilde{\xi}}\right)^2 - \frac{1}{2\hat{k}^3}\frac{\partial^2 \hat{k}}{\partial \tilde{\xi}^2} << 1 \qquad (2.83)$$

for all $\tilde{\xi}$ of interest (Nayfeh, 1973, p. 324). (2.83 is satisfied if the refractive index varies slowly over a wavelength and $|\hat{k}| >> 0$ – short wavelength approximation). It can be shown that

$$\hat{\Gamma} \sim \frac{b}{\alpha} \quad |\alpha| \to \infty \qquad (2.84)$$

where b is a constant, and therefore the WKB approximation will be valid for sufficiently large positive/negative values of α (cf., Figure 2.2).

For α large positive ($\hat{k}^2 >> 0$), the general solution of (2.67.1) is

$$\hat{v}(\tilde{\xi}) = \frac{1}{\sqrt{\hat{k}(\tilde{\xi})}}\left\{A\, e^{i\int_0^{\tilde{\xi}} \hat{k}d\xi'} + B e^{-i\int_0^{\tilde{\xi}} \hat{k}d\xi'}\right\} \qquad (2.85.1)$$

Since

$$\hat{k} \sim \hat{k}_\infty = \text{const.} \quad \tilde{\xi} \to \infty \qquad (2.85.2)$$

the radiation condition demands that (cf., 2.80)

$$A = 0 \tag{2.85.3}$$

and

$$\hat{v}(\tilde{\xi}) = \frac{B}{\sqrt{\hat{k}(\tilde{\xi})}} e^{-i\int_0^{\tilde{\xi}} \hat{k} d\xi'} \tag{2.85.4}$$

It is shown in Appendix C that this solution does not satisfy the surface boundary condition and hence there are no solutions for this range of α. This should not be surprising, because the physical consequence of (2.83) for $\hat{k}^2 >> 0$ is that the transmission coefficient is 1.0 for all $\tilde{\xi}$ (Morse and Feshbach, 1953, p. 1094); and hence, all of the energy propagating up is transmitted and none reflected.

For α large negative, $\hat{k}^2 = -\tilde{k}^2 << 0$, the general solution is given by

$$\hat{v}(\tilde{\xi}) = \frac{1}{\sqrt{\hat{k}(\tilde{\xi})}} \left\{ A e^{\int_0^{\tilde{\xi}} \tilde{k} d\xi'} + B e^{-\int_0^{\tilde{\xi}} \tilde{k} d\xi'} \right\} \tag{2.86.1}$$

Again, since

$$\tilde{k} \sim \tilde{k}_\infty = \text{const.} \quad \tilde{\xi} \to \infty \tag{2.86.2}$$

the finite energy condition demands that (cf., 2.81.2)

$$A = 0 \tag{2.86.3}$$

and

$$\hat{v}(\tilde{\xi}) = \frac{B}{\sqrt{\hat{k}(\tilde{\xi})}} \, e^{-\int_0^{\tilde{\xi}} \tilde{k} d\xi'} \tag{2.86.4}$$

It is also shown in Appendix C that for realistic atmospheres, this solution also cannot satisfy the surface boundary condition, and hence no solutions exist in this regime of α.

We have now restricted our search to a finite region of α. For this regime, the refractive index may exhibit several barriers to propagation with corresponding turning points. Although the "truly" homogeneous solution to this steady state problem cannot propagate energy across the barriers, if one views this as an initial value problem, or one that is being driven, energy can tunnel across. Thus one may envision a complicated picture of multiple reflection and transmission, the energy being delayed on its eventual route out of the system. The mathematics being equally complicated, a numerical procedure will be employed.

As a matter of convenience, geometric height and system (2.63) will be used. Now this BVP is linear and homogeneous. Therefore, its solution is unique only up to a complex multiplicative constant. Since

$$k^2(\zeta;\alpha) \sim \begin{cases} k_\infty^2 & \alpha \geq \dfrac{1}{4\kappa\tilde{H}_\infty} \\ -\tilde{k}_\infty^2 & \alpha < \dfrac{1}{4\kappa\tilde{H}_\infty} \end{cases} \qquad \zeta \to \infty \tag{2.87.1}$$

where

$$\begin{cases} k_\infty = \dfrac{1}{2\tilde{H}_\infty}\sqrt{4\alpha\kappa\tilde{H}_\infty - 1} & (2.87.2) \\ \tilde{k}_\infty = \dfrac{1}{2\tilde{H}_\infty}\sqrt{1 - 4\alpha\kappa\tilde{H}_\infty}\,, & (2.87.3) \end{cases}$$

the radiation/finite energy conditions imply that

$$v(\zeta) \sim \begin{cases} v_\infty e^{-ik_\infty\zeta} & \alpha > \dfrac{1}{4\kappa\tilde{H}_\infty} \\ v_\infty e^{-k_\infty\zeta} & \alpha < \dfrac{1}{4\kappa\tilde{H}_\infty} \end{cases} \qquad \zeta \to \infty \qquad (2.88)$$

where v_∞ is arbitrary complex.

Thus (2.63) may be solved as an IVP using the known behavior of $v(\zeta)$ in the region, $\zeta \to \infty$, as initial conditions and marching down. Since $v_\infty = |v_\infty|e^{i\theta}$ is arbitrary, the particular location at which the initial conditions are imposed is irrelevant.

A variable step 5th order Runge-Kutta scheme is employed (CDC Math Science Library, 1971, RKINIT). The 1976 US Standard Atmosphere (hereafter denoted US76) is used as the global mean for the background state, and a cubic spline is used to interpolate the scale height (shown in Figure 2.3) for the variable step method. The IVP is solved, scanning the restricted region of α where the WKB approximation is invalid. It is here that the greatest reflection is expected and hence, the greatest likelihood of obtaining a nearly characteristic value of α. The complex error in the surface boundary condition

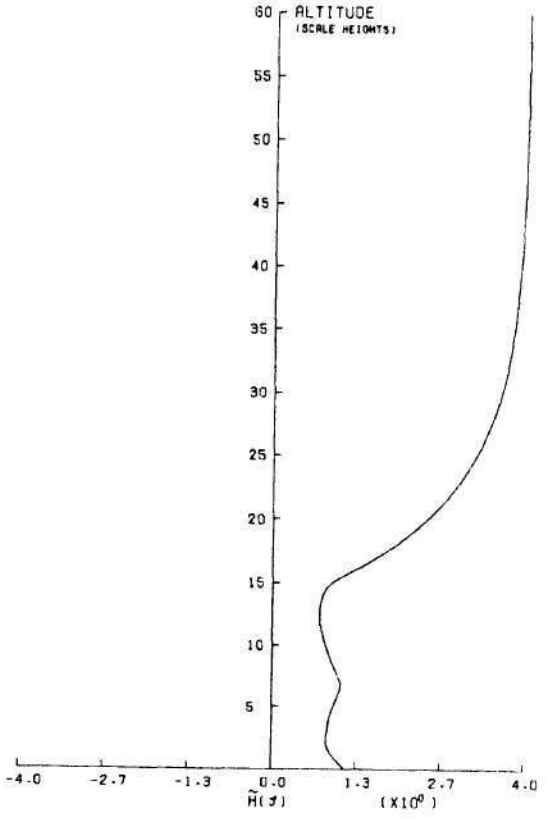

Figure 2.3 Normalized Scale Height for the 1976 US Standard Atmosphere.

$$e = \tilde{H}_o v_o' + (\alpha \tilde{H}_o - 1/2) v_o \tag{2.89}$$

should be small in some normalized sense at a nearly characteristic value of α (zero subscripts denote surface evaluation). Hence, normalizing by the value of the solution at the surface, the inverse of this normalized error

$$\beta(\alpha) = \frac{|v_o(\alpha)|}{|e(\alpha)|} \tag{2.90}$$

should be large at these values (although it may appear that v_o and hence β may vanish at a nontrivial solution to the problem, 2.63.2

rules this out).

Besides the mathematical meaning, β has physical significance too. The quantity e is proportional to the vertical velocity at the surface and hence the work rate there. Using (2.63.2) and (2.72) it can be seen that the surface energy flux (work rate)

$$\langle I_z \rangle_o \propto \frac{1}{\tilde{H}_o} \operatorname{Im}\{e\, v^*\} \tag{2.91.1}$$

Similarly, the surface energy density is

$$E_o \propto \frac{1}{\tilde{H}_o} \left| \alpha \tilde{H}_o v_o - e \right|^2 \tag{2.91.2}$$

Since the disturbance may be considered as being excited at the surface, it seems reasonable to take E_o as a measure of the total energy. Then in this light, the ratio of the disturbance energy to the work rate being done at the surface is

$$\frac{E_o}{\langle I_z \rangle_o} \propto \frac{\left| \alpha \tilde{H}_o v_o - e \right|^2}{\operatorname{Im}(ev^*)} \; ; \quad \langle I_z \rangle_o \neq 0$$

At nearly characteristic values this is approximately

$$\frac{E_o}{\langle I_z \rangle_o} \propto \frac{|v_o|}{|e|} = \beta$$

Since the system is conservative, this must also be proportional to the ratio of energy to leakage.

The parameter which measures the validity of the WKB approximation may be written

$$\Gamma(\zeta;\, \alpha) = \frac{5}{16(k^2)^3} \left[\frac{\partial}{\partial \zeta}(k^2)\right]^2 - \frac{1}{4(k^2)^2} \frac{\partial^2}{\partial \zeta^2} (k^2) \tag{2.92}$$

Several profiles of Γ for different values of α are shown in Figure 2.4. The lack of smoothness has two origins: first the digitizing noise of US76, and second the fact that Γ involves 4th order derivatives and $\tilde{H}$ is represented by a 3rd order spline. Recalling the asymptotic nature of Γ with α, (2.84), it can be seen that the maximum value of Γ collapses to within $\pm.10$ outside the interval (-3.0, 15.0). Several profiles of $k^2(\zeta)$ in this interval are presented in Figure 2.5. The maximum values of Γ near the surface for large $|\alpha|$ may be associated with the small values of k^2 there. It will therefore be assumed that the WKB approximation is valid outside this interval and the investigation will be restricted to the interval (-3.0, 15.0).

The resulting spectrum of β is shown in Figure 2.6. It can be seen that there are two peaks associated with the α values: .7346 and 1.1450, corresponding to $k_\infty^2 > 0$. The associated values of β are 9.8×10^4 and 4.85, the former being much closer to characteristic than the latter. There also appears to be a small peak at $\alpha = .2190$, where $k_\infty^2 = 0$. However, this is really a discontinuity following a general rise in β due to the change from oblique to horizontally propagating waves (see Siebert, 1961; Yanowitch, 1967; Figure 2.5, d). Now $\alpha = .2190$ ($k_\infty^2 = 0$) must be excluded because of the finite energy condition. For $\alpha < .2190$ ($k_\infty^2 < 0$), the solution to the homogeneous problem is evanescent for $\zeta \to \infty$, i.e., the disturbance sees a barrier of infinite extent. Therefore, the energy is completely reflected and there is no leakage. For this range of α, the solutions are real and hence, w' and p' are 90 degrees out of phase throughout (cf., 2.53.3).

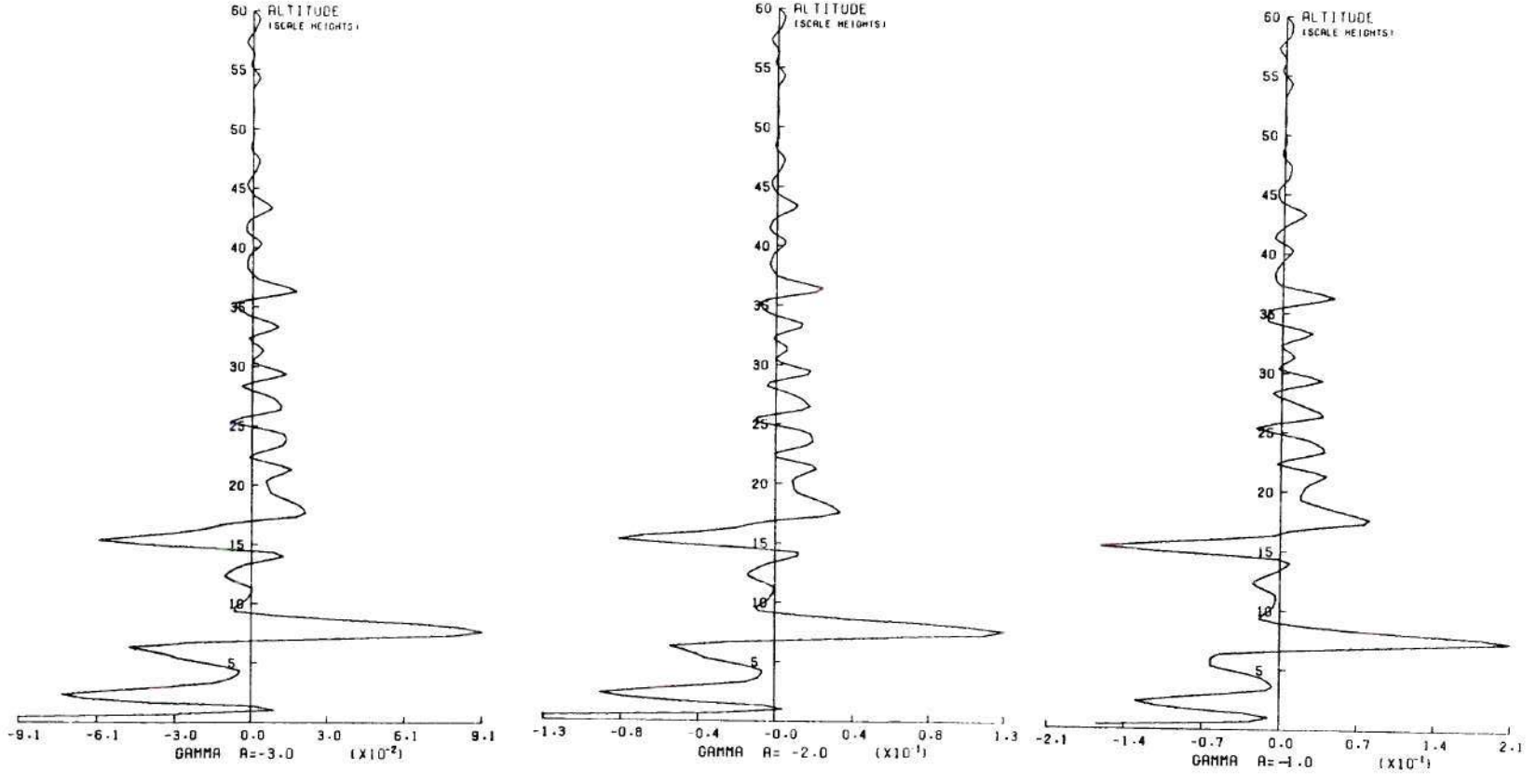

(a) $\alpha = -3.0$ (b) $\alpha = -2.0$ (c) $\alpha = -1.0$

Figure 2.4 WKB Approximation Error Parameter Γ as a Function of Altitude.

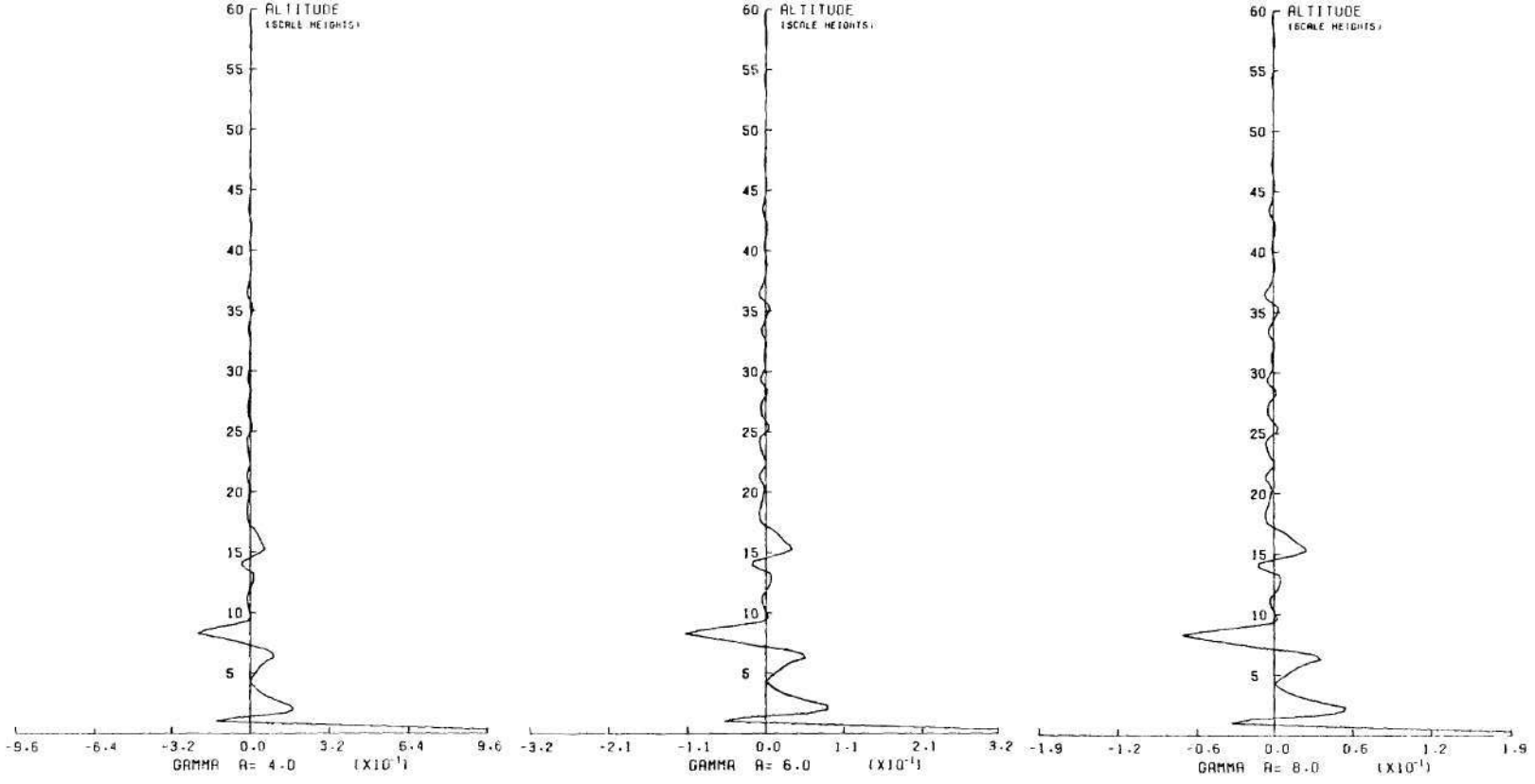

(d) $\alpha = 4.0$ (e) $\alpha = 6.0$ (f) $\alpha = 8.0$

Figure 2.4. (Continued)

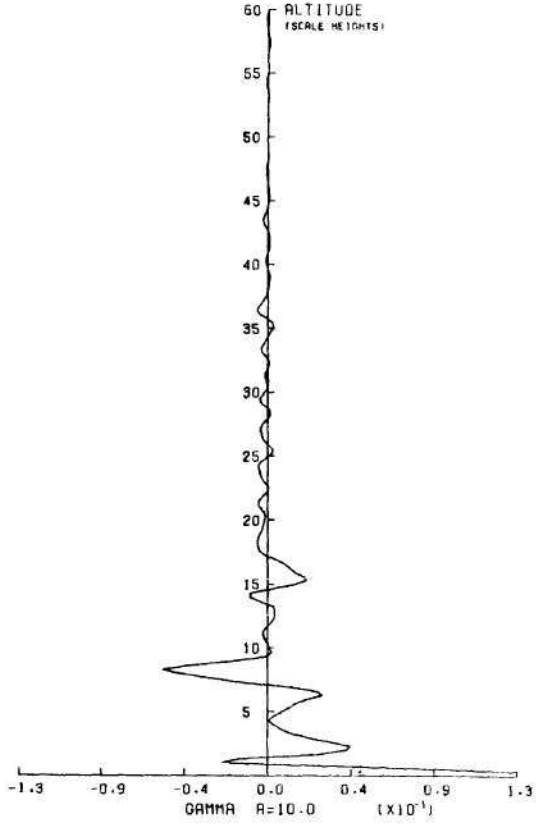

(g) α = 10.0

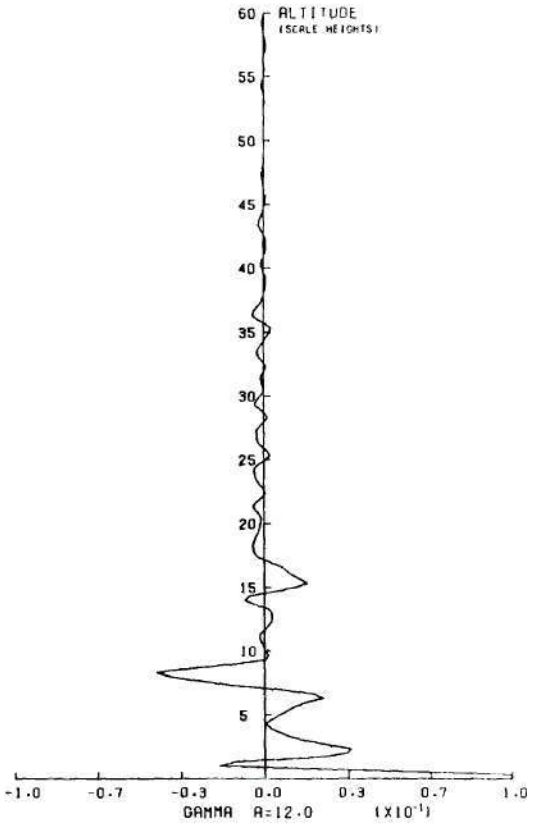

(h) α = 12.0

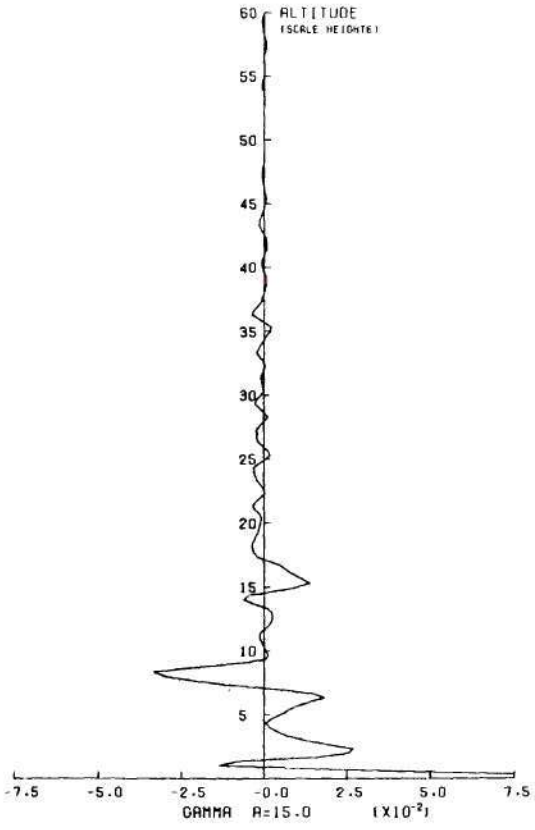

(i) α = 15.0

Figure 2.4. (Continued)

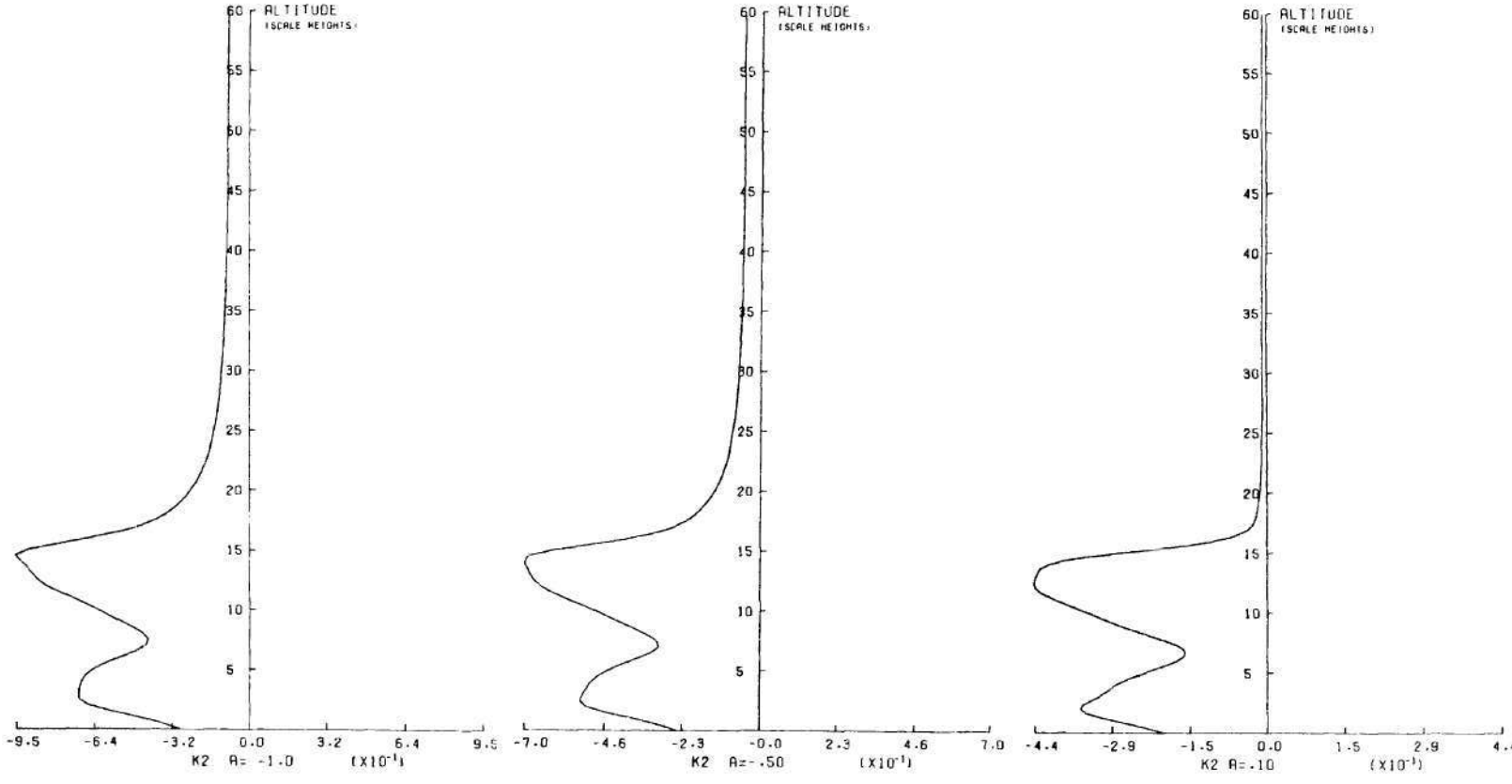

(a) $\alpha = -1.0$ (b) $\alpha = -.50$ (c) $\alpha = .10$

Figure 2.5. Vertical Refractive Index Squared, k^2, as a Function of Altitude.

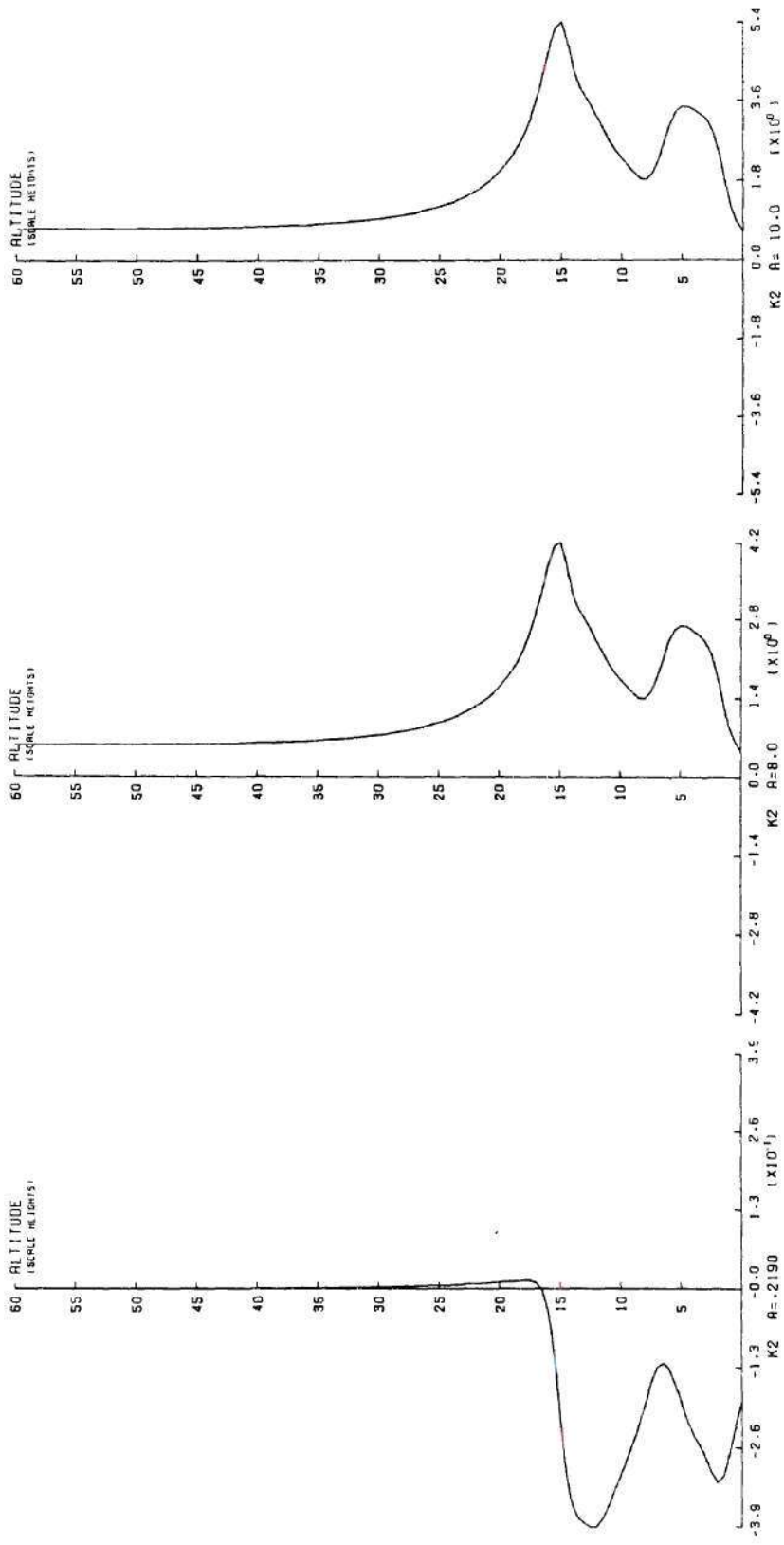

(d) α = .2190 (e) α = 8.0 (f) α = 10.0

Figure 2.5. (Continued)

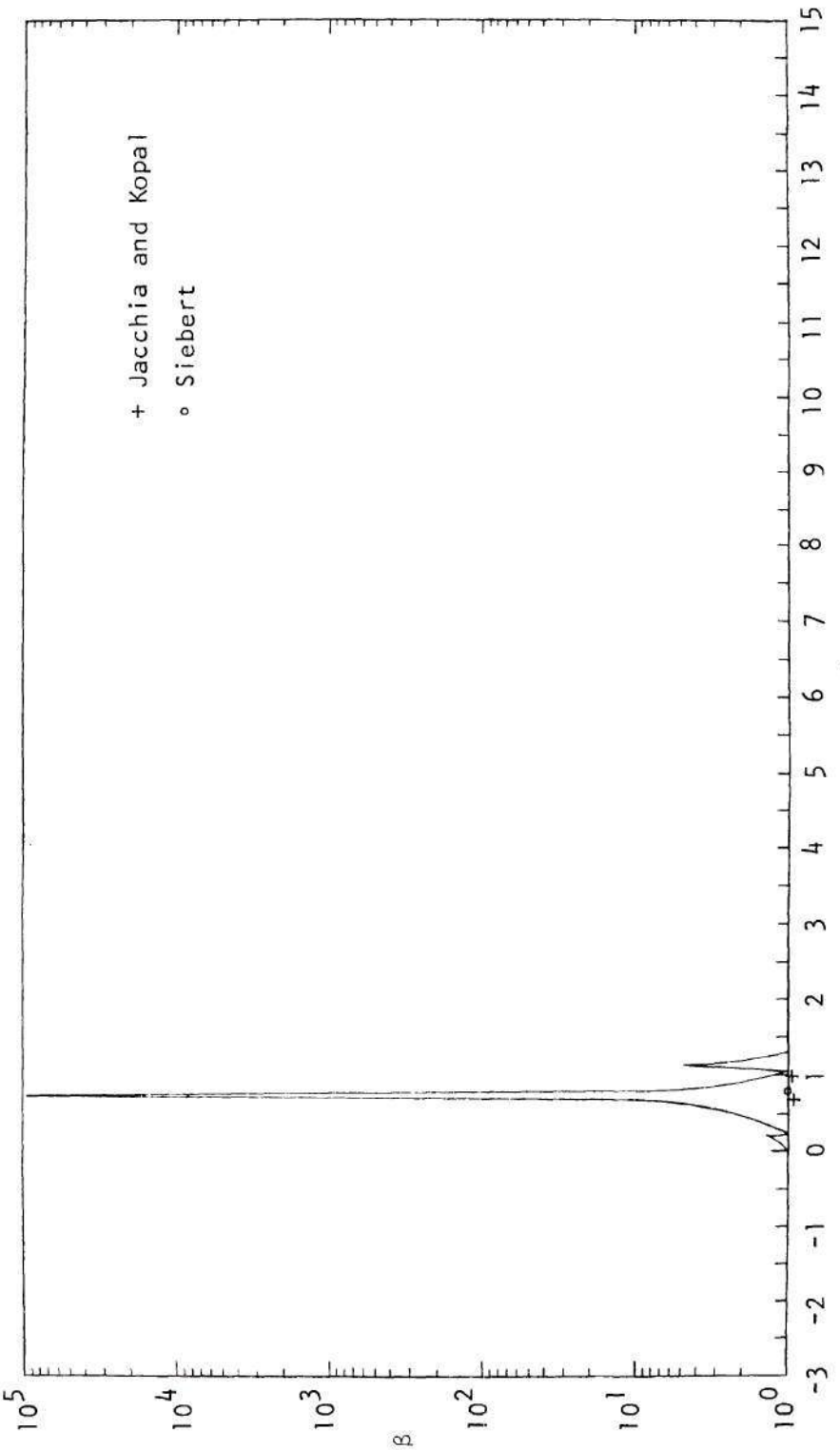

Figure 2.6. Inverse Normalized Surface Error as a Function of α.

Thus the energy flux and work rate at the surface is zero. It will be seen in the next section that if the values $\alpha < .2190$ are taken as free modes, there will exist a continuous spectrum of frequencies. β decreases monotonically with α decreasing from .2190. There is no clear value that may be used as a cutoff. For this reason and because the surface boundary condition is satisfied to a poorer degree than with either of the peaks in β, these values of α will not be considered in future development. From the previous discussion of large $|\alpha|$, it appears that the two remaining peaks correspond to the only vertical normal modes of the system; they will be indexed by k = 1 and 2 respectively.

The refractive index squared, $\mathrm{Re}(v(\zeta))$, normalized magnitude of the velocities, kinetic energy density, vertical energy flux, and vertical divergence of the latter are shown in Figure 2.7 for the first mode. The normalized quantities shown are

$$\frac{|u'|\alpha e^{-\tilde{\xi}/2}}{\bar{u}\hat{U}(\mu)} = \frac{|v'|\alpha e^{-\tilde{\xi}/2}}{\bar{u}\hat{V}(\mu)} = \left|\frac{v}{2} - \tilde{H}v'\right| \qquad (2.93.1)$$

$$\frac{|w'|\alpha}{\bar{u}U(\mu)} e^{-\tilde{\xi}/2} = \tilde{\omega}\delta\left|(\alpha\tilde{H} - 1/2)v + \tilde{H}v'\right| \cong \varepsilon\left|(\alpha\tilde{H} - 1/2)v + \tilde{H}v'\right| \qquad (2.93.2)$$

$$\frac{2E\, g\bar{H}\,\alpha^2}{\bar{u}^2 p_o(0)(\hat{U}^2 + \hat{V}^2)} = \frac{1}{\tilde{H}}\left|\frac{v}{2} - \tilde{H}v'\right|^2 \qquad (2.93.3)$$

$$\frac{\langle I_z\rangle g\bar{H}\alpha}{\hat{\Omega}a\bar{u}^2 p_o(0)\tilde{\omega}\eta U^2(\mu)} = -\varepsilon\tilde{H}\,\mathrm{Im}\{v'v^*\} \qquad (2.93.4)$$

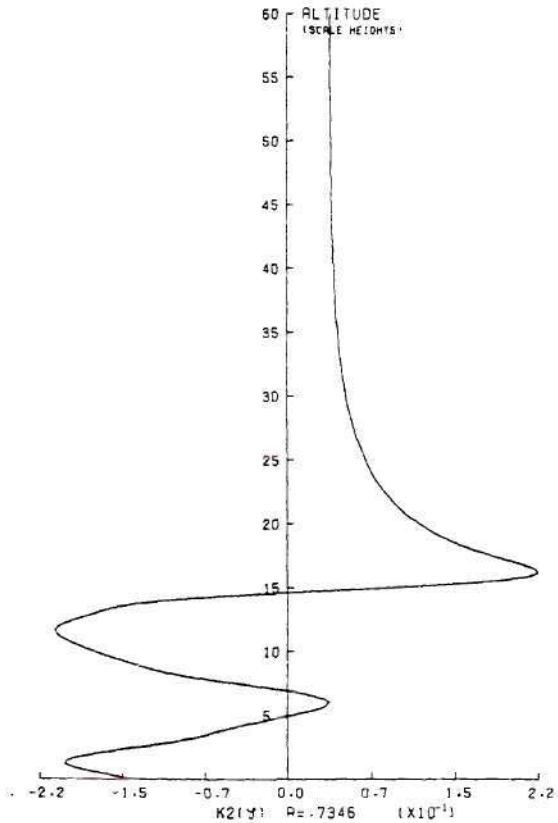

(a) Refractive Index Squared

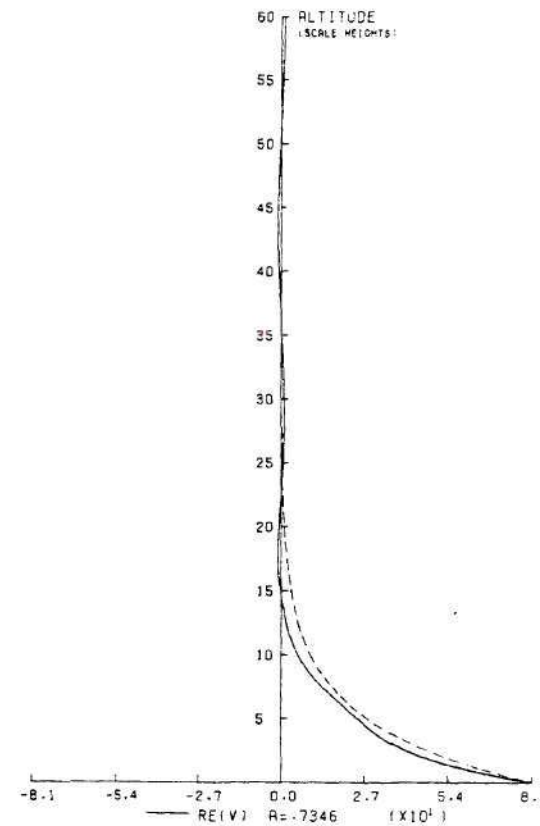

(b) Real Part of Normalized Solution; Dashed Line Indicates Lamb Mode

Figure 2.7. First Vertical Mode (α = .7346).

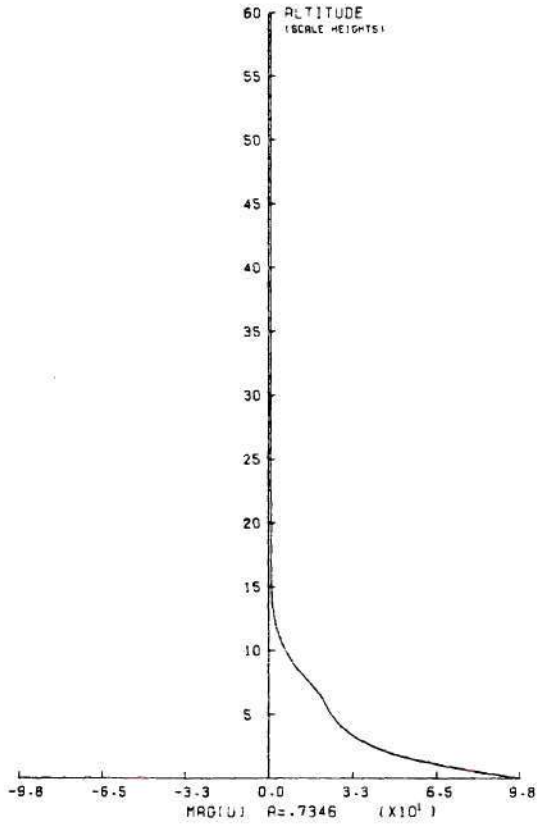

(c) Magnitude of Normalized Horizontal Velocity

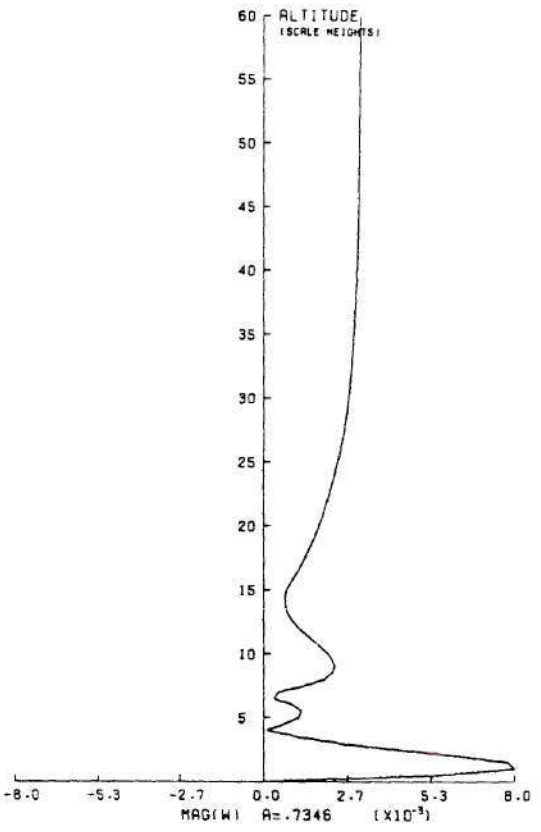

(d) Magnitude of Normalized Vertical Velocity

Figure 2.7. (Continued)

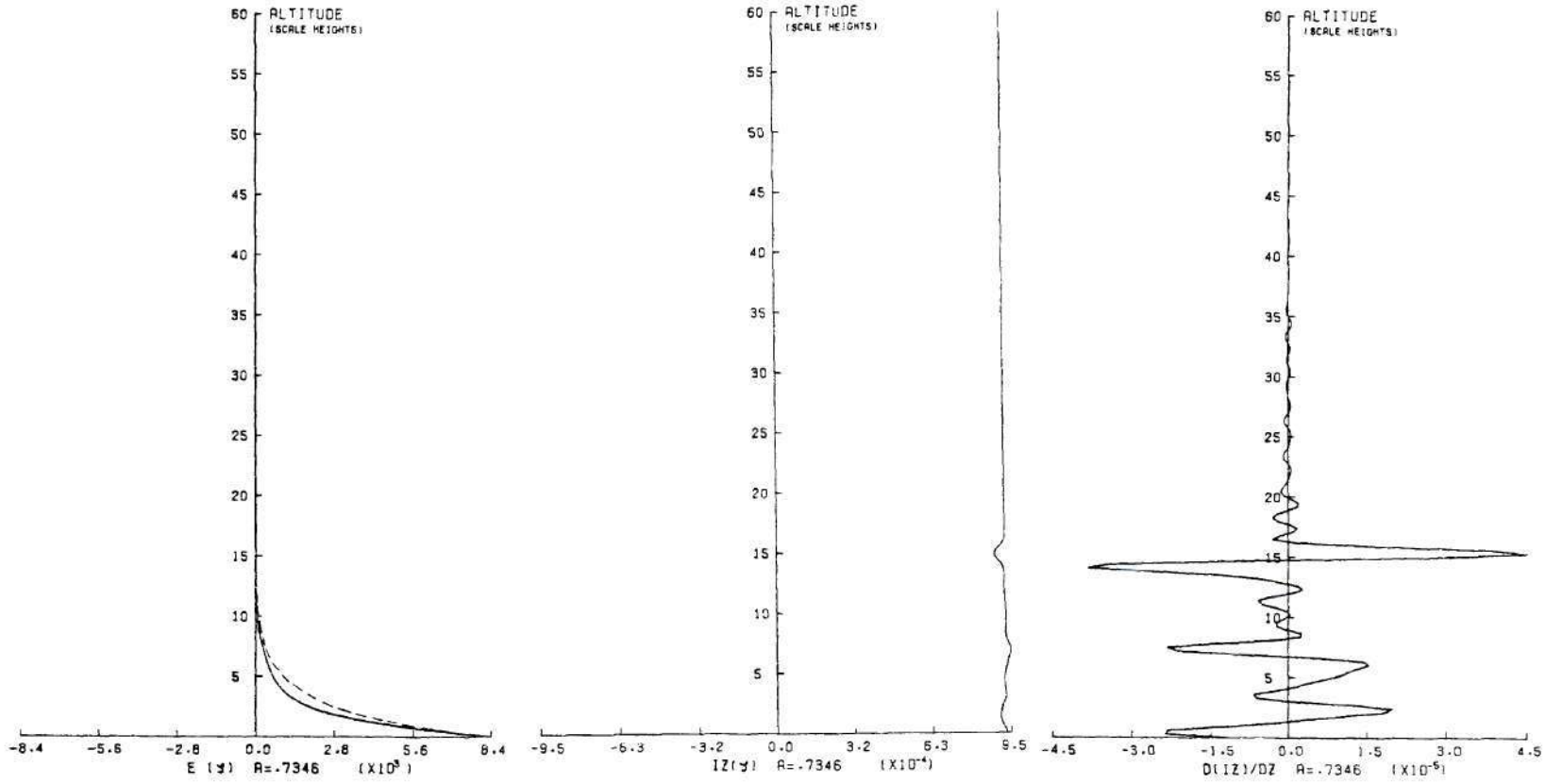

(e) Kinetic Energy Density, Dashed Line Indicates Lamb Mode

(f) Vertical Energy Flux

(g) Divergence of Energy Flux

Figure 2.7. (Continued)

$$\frac{\frac{\partial}{\partial z}\langle I_z\rangle\, g\alpha}{\hat{\Omega}a\bar{u}^{-2}p_o(0)\,\tilde{\omega}\eta U^2(\mu)} = -\varepsilon\frac{d}{d\zeta}\left[\tilde{H}\ \mathrm{Im}\{v'v^*\}\right] \qquad (2.93.5)$$

The index squared for this mode is negative over most of the heights corresponding to the neutral atmosphere except for a thin region in the upper stratosphere. The asymptotic value, k_∞^2, is positive, the last turning point being in the lower thermosphere. Thus, the energy is eventually radiated away. The Re(v) indicates that the solution is composed of a small amplitude internal mode to propagate energy away from the surface, superimposed upon a much larger amplitude evanescent wave. The Lamb mode is also shown for reference. Similar features were found by Geisler and Dickinson (1975) in their study which included realistic zonal winds. They, however, attributed the internal mode to the rigid surface that they imposed near $\zeta = 15$. These results seem to indicate that such a mode would appear even without the unrealistic boundary condition in order to carry off energy input at the surface. Also, it will be discussed later that these are fairly insensitive to changes in $\tilde{H}$ at large ζ. Although the normalized velocity amplitudes shown appear to decay with height, the actual velocities grow exponentially due to the factor $e^{\tilde{\xi}/2}$, as is commonly the case in the linear inviscid theory.

The vertical velocity magnitude seems to exhibit the character of k^2 the most of all the parameters shown. This is evidence that the vertical motion is essentially that of a buoyancy wave. It is also down some four orders of magnitude from the horizontal component and

achieves its maximum value in the troposphere.

The energy density is reminiscent of a classical edge wave, and is concentrated near the surface slightly more than that of the Lamb wave for an isothermal atmosphere. This close resemblance and the small deviation from the Lamb eigenvalue, $\alpha_{Lamb} = .714$, suggests that this is the Lamb mode modified by the vertical temperature structure. In the limit of the variation going to 0, it is expected that this solution would tend to the Lamb wave.

Except for some small perturbations, the vertical energy flux (Figure 2.7, f), is constant, equal to the surface work rate. Although small, these fluctuations apparently are not due to noise in the representation of US76. The associated divergence, $\frac{\partial}{\partial z} \langle I_z \rangle$ (Figure 2.8, g), indicates that energy is being deposited, (either in the disturbance or background state) beneath the tropopause and mesopause, and removed from above them. Similarly, it is being removed from below the stratopause and deposited above it. Because the energy density does not exhibit similar features, the generalization seems to be that a sharp increase in stability results in the atmosphere absorbing disturbance energy flow beneath the increase and emitting it above.

Figure 2.8 shows the same parameters for the second mode. The distinguishing feature of the refractive index relative to that of the first mode is the larger region of positive k^2 near $\zeta = 5$. The corresponding values are four times that of the previous mode in this vicinity. A glance at Figure 2.7, b indicates why this mode is not nearly so characteristic as the first. The amplitude of the internal

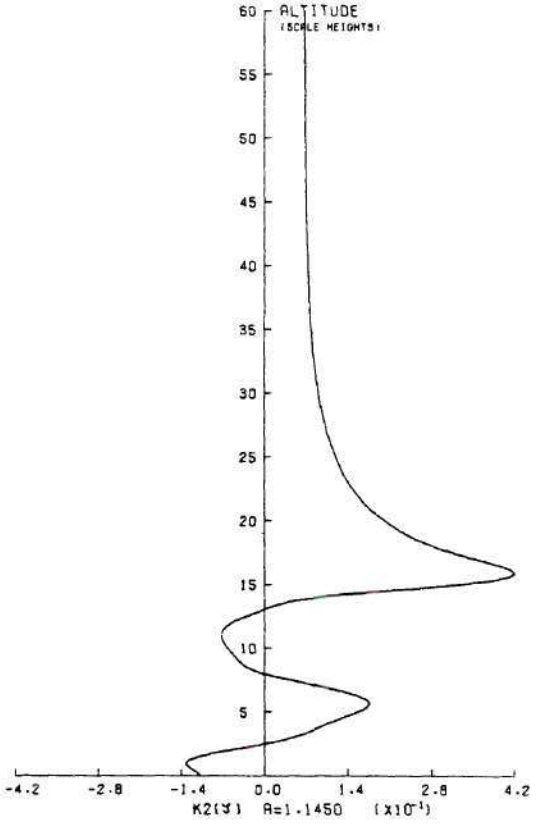

(a) Refractive Index Squared

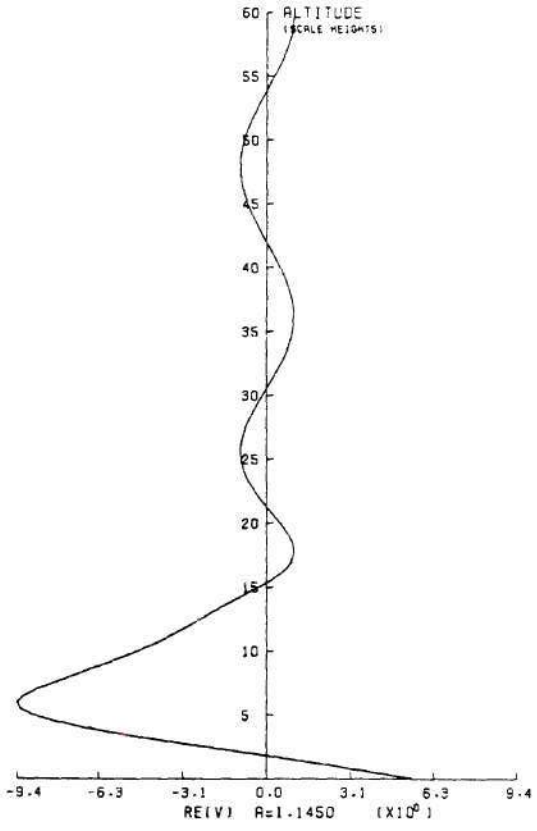

(b) Real Part of Normalized Solution

Figure 2.8. Second Vertical Mode ($\alpha = 1.1450$).

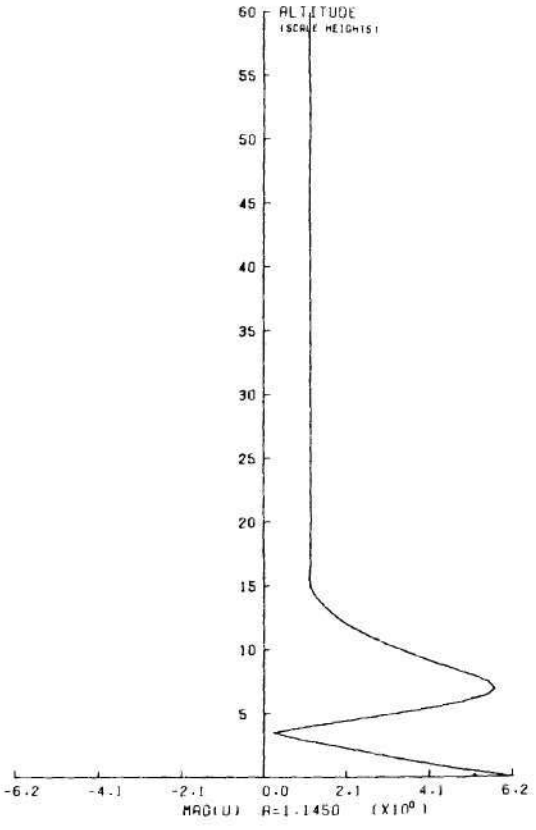

(c) Magnitude of Normalized Horizontal Velocity

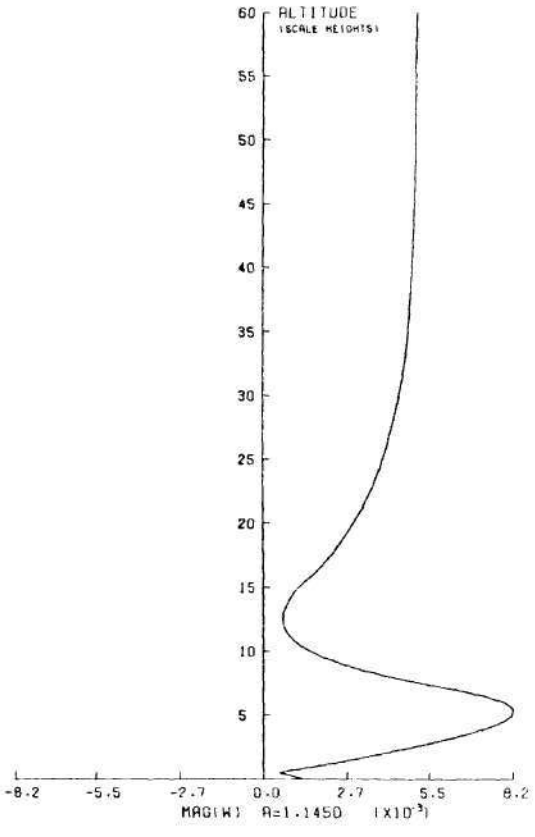

(d) Magnitude of Normalized Vertical Velocity

Figure 2.8. (Continued)

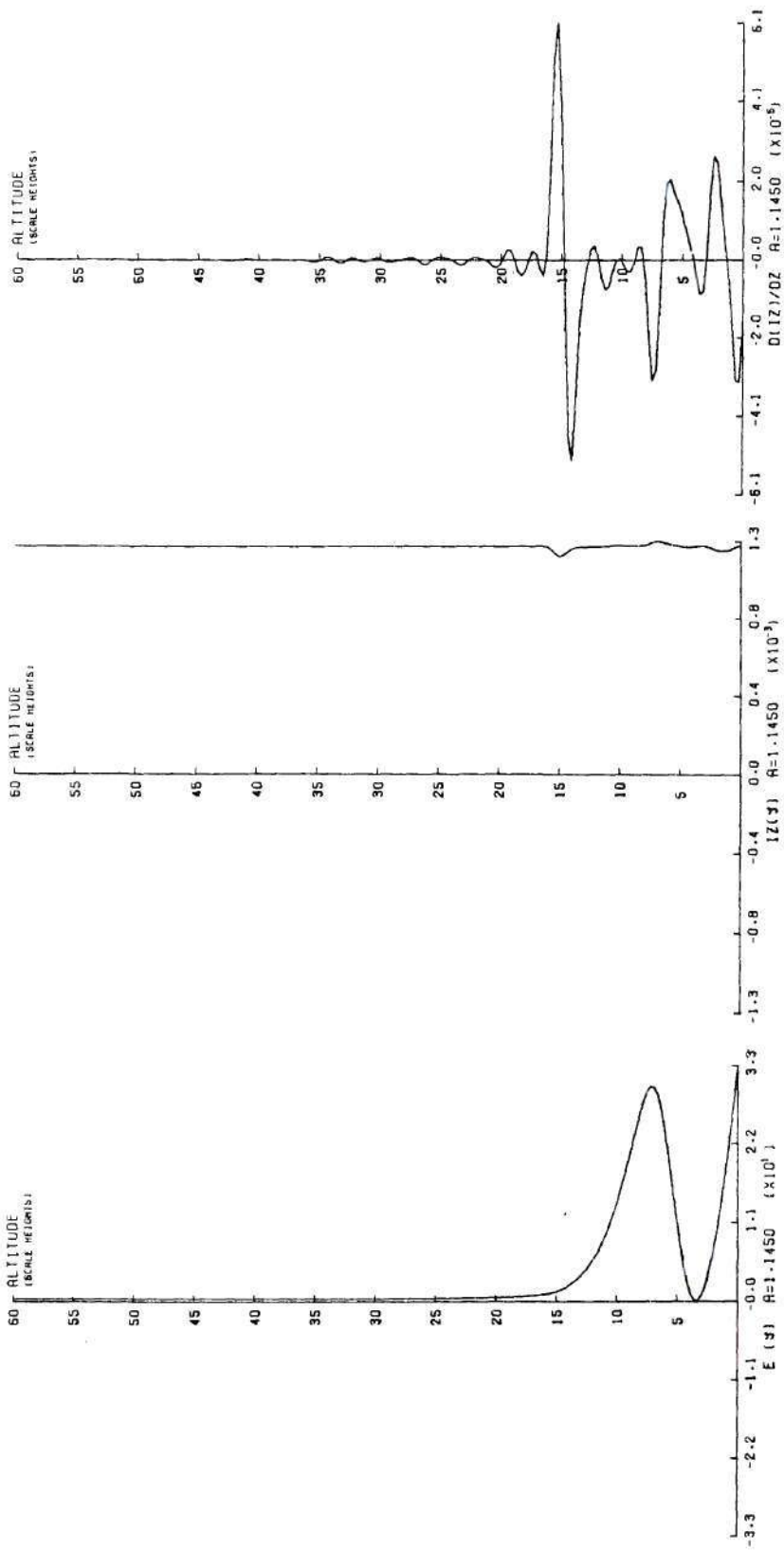

(e) Kinetic Energy Density (f) Vertical Energy Flux (g) Divergence of Energy Flux

Figure 2.8. (Continued)

part of the solution is much larger relative to the solution's overall size. Unlike the previous mode, this solution does not exhibit an overall evanescent character. The normalized horizontal and vertical velocity amplitudes attain maxima near the stratopause.

The energy density for this mode has several interesting features. It is evanescent in the lowest region of $k^2 < 0$ but then increases throughout the region of $k^2 > 0$ until the second barrier is reached, after which it decays to a small value essentially due to the internal component. The distribution of this energy peak gives the appearance of a resonating strato-mesospheric cavity. Geisler and Dickinson (1976) found similar results for the 5-day wave in the presence of realistic zonal winds. The possibly surprising feature is that the energy peak is not contained symmetrically between the two barriers above and below the stratosphere. This may be explained as follows. Energy travelling down the cavity will be partially reflected by the thin region of $k^2 < 0$ followed by complete reflection at the surface. Upward travelling energy, however, will only be partially reflected by the second barrier, followed by essentially free transmission for the penetrating energy to escape. Thus the energy can penetrate more effectively upwards than it can downwards.

The character of the vertical energy flux and hence its derivative, is indistinguishable from that of the previous mode. Its value in relation to the energy of the disturbance is, of course, significantly greater.

2.6 Solution of the Horizontal Equation

The BVP for the horizontal dependence is essentially LTE, which has been studied comprehensively by Longuet-Higgens (1968) and Flattery (1967). The latter investigation has greater relevance to tidal theory. Some of the results of the former that pertain to this investigation will be mentioned. As previously stated, the effective Lamb's parameter is

$$\gamma_k = \alpha_k \eta = \alpha_k \frac{(2\hat{\Omega})^2 a^2}{g\bar{H}} , \qquad (2.94)$$

or the equivalent depth is $\bar{H}/\alpha_k$ $k = 1,2$. Thus for each of the vertical modes there is a corresponding set of horizontal modes and eigenfrequencies. The solutions, $U^k_{mn}(\mu)$, $n = m, m+1, \ldots$ are the Hough Functions and n is the meridional index. These fall into two basic categories: eastward and westward travelling gravity waves (first class, type 1), and westward moving Rossby waves (second class, type 2). As $\gamma \to \infty$ a third category emerges - comprised of Kelvin waves concentrated near the equator. The gravity mode frequencies increase and the Rossby frequencies decrease with increasing $n - m$.

The dependence of the normalized eigenfrequencies, $\tilde{\omega}$, on γ is shown in Figure 2.9. The gravity modes form the upper curves; the Rossby modes correspond to the lower set in Figure 2.9, b and are all negative. Also indicated are the values γ_1 and γ_2. The dependence for different values of m is similar. It is inferred from these results that for $\gamma = \gamma_1, \gamma_2$ all of the gravity mode frequencies are O(1) or

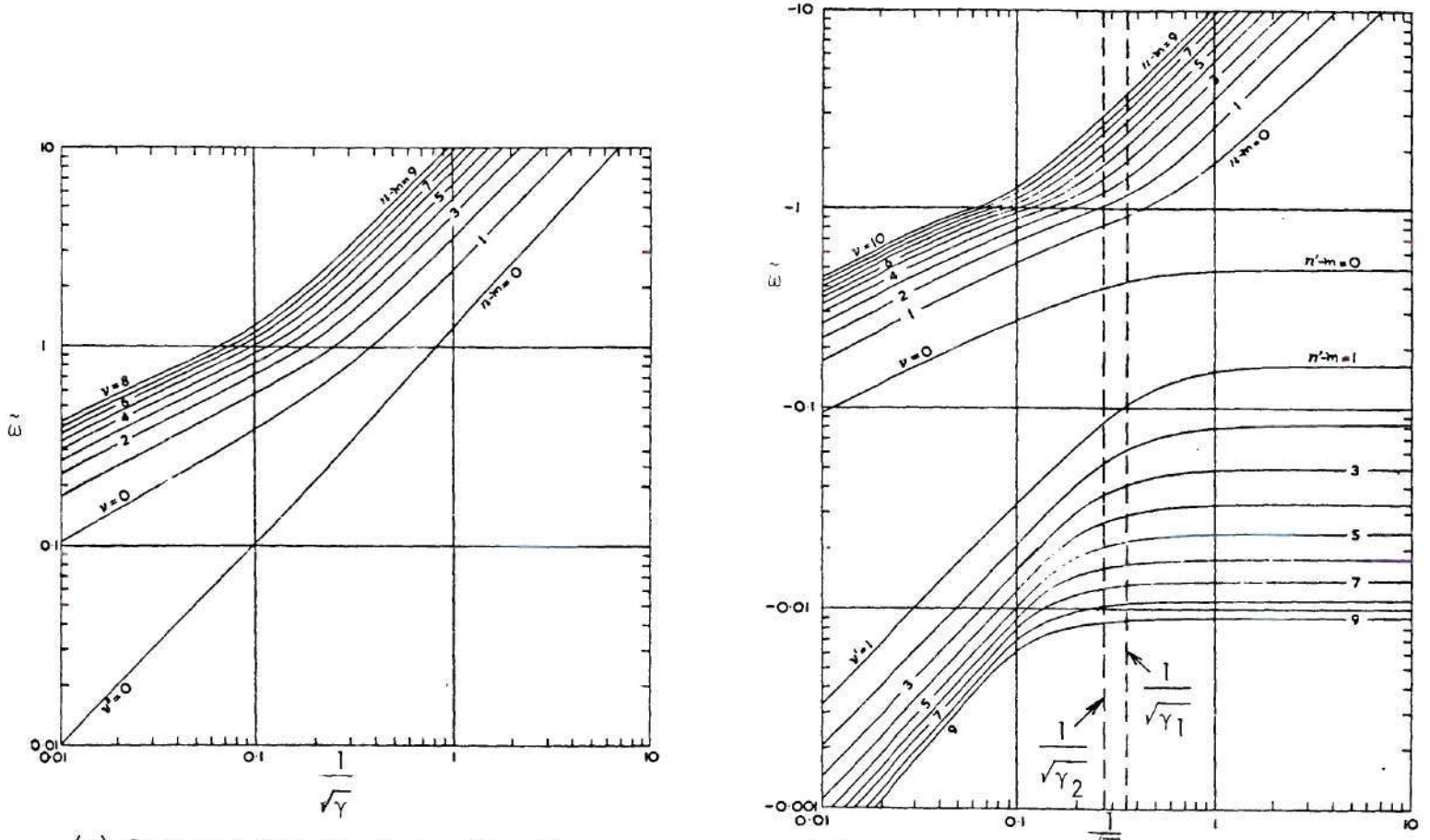

(a) Eastward Gravity Modes ($\tilde{\omega} > 0$)

(b) Westward Gravity (Upper Branch) and Rossby (Lower Branch) Modes ($\tilde{\omega} < 0$)

Figure 2.9. Dependence of Normalized Eigenfrequencies $\tilde{\omega}$ on Effective Lamb's Parameter γ (after Longuet-Higgens, 1968).

larger, and all of the Rossby mode frequencies are $O(1/n)$ or smaller, with the possible exception of the $n = m$ Rossby modes for the first few values of m. Thus it appears that the gravity modes are operative under regime (i) (cf., p. 53) while the Rossby waves are in regimes (ii) and (iii). This suggests that the simplified equations presented in Section 2.3 should be valid. Because of our original definition of planetary waves and our discussion of the insensitivity of the motions of regime (i) to the boundaries, further discussion will be restricted to the Rossby modes.

Now, as is evident from Figure 2.9, these eigenfrequencies and the corresponding solutions exhibit convenient asymptotic behavior for large and small γ. In fact the asymptotic Rossby wave frequency ($\gamma \to 0$) is the same as that obtained by Haurwitz (1940), equation 1.3, using conservation of vorticity. These asymptotic solutions may be expressed in terms of the associated Legendre functions (Dikii, 1965, 1966). Unfortunately, for the earth's atmosphere, $\eta = 12.1$ and

$$\gamma_k = \begin{cases} 8.89 & k = 1 \\ 13.8 & k = 2 \end{cases} \tag{2.95}$$

As can be seen from Figure 2.9, except for large values of $n - m$, these values lie intermediate to the asymptotic regions, and the numerical results must be used. Table 2.1 shows the nondimensional eigenfrequencies and associated frequencies and periods for the first 6 values of n for $m = 1,2,3,4,5$, $k = 1,2$, as determined by iterative interpolation of Longuet-Higgens results.

Table 2.1. Frequencies and Periods for the Two Vertical Modes k = 1,2 For Several Horizontal Modes (m,n)

		K = 1				K = 2	
n	$\tilde{\omega}^1_{mn}$	Frequency ($Days^{-1}$)	Period (Days)		$\tilde{\omega}^2_{mn}$	Frequency ($Days^{-1}$)	Period (Days)
1	.422	.844	1.18		.38	.76	1.31
2	.099	.198	5.05		.082	.164	6.09
3	.06	.12	8.33	m = 1	.052	.104	9.61
4	.04	.08	12.5		.034	.068	14.7
5	.029	.058	17.2		.026	.052	19.2
6	.021	.042	23.8		.020	.040	25.0
2	.308	.616	1.62		.27	.54	1.85
3	.134	.268	3.73		.11	.22	4.54
4	.085	.170	5.88	m = 2	.071	.142	7.04
5	.059	.118	8.47		.05	.10	10.0
6	.043	.086	11.6		.038	.076	13.2
7	.033	.066	15.2		.03	.06	16.7
3	.24	.48	2.08		.23	.46	2.17
4	.14	.28	3.57		.12	.24	4.16
5	.090	.180	5.56	m = 3	.086	.172	5.81
6	.066	.132	7.58		.061	.122	8.19
7	.05	.16	10.0		.048	.096	10.4
8	.04	.08	12.5		.037	.074	13.5
4	.195	.390	2.56		.18	.36	2.77
5	.125	.250	4.00		.12	.24	4.16
6	.089	.178	5.62	m = 4	.082	.164	6.09
7	.068	.136	7.35		.064	.128	7.81
8	.053	.106	9.43		.050	.100	10.0
9	.043	.086	11.6		.040	.080	12.5
5	.164	.328	3.05		.16	.32	3.12
6	.114	.228	4.39		.105	.21	4.76
7	.086	.172	5.81	m = 5	.081	.162	6.17
8	.067	.134	7.46		.066	.132	7.57
9	.054	.108	9.26		.051	.102	9.8
10	.044	.088	11.4		.042	.084	11.9

Flattery (1968) showed that the Hough Functions form an orthogonal set. Aside from having solutions for positive γ, which have obvious physical significance, LTE also exhibits eigensolutions for negative values. Lindzen (1966) suggested that these should be important in forced oscillations, e.g., tides. Longuet-Higgens (1968) has pointed out that the eigenfunctions would not form a "complete" set and hence, not be able to represent an arbitrary forcing potential, unless all of the solutions including those of negative γ were used. A few of the Hough Functions U_{mn} and the corresponding velocity functions $\hat{U}_{mn}$ and $\hat{V}_{mn}$ are shown in Figure 2.10 as functions of latitude. These correspond to the value $\gamma = 10$. For all intents and purposes, the eigenfunctions to the present problem for both γ_1 and γ_2 should be indiscernible from these. The following integral relations also follow from the results of Longuet-Higgens

$$\begin{cases} \frac{1}{a^2} \iint_S U^2 \, dS = 2\pi (1 - \nu_{mn}^k) & (2.96.1) \\ \\ \frac{1}{a^2} \iint_S (\hat{U}^2 + \hat{V}^2) dS = 2\pi \nu_{mn}^k & (2.96.2) \end{cases}$$

where ν_{mn}^k is the ratio of kinetic energy to total energy of the (m,n)th solution of LTE for $\gamma = \gamma_k$.

Table 2.2 lists several values of ν_{mn}^k for $m = 1,2$ as derived from Longuet-Higgens results.

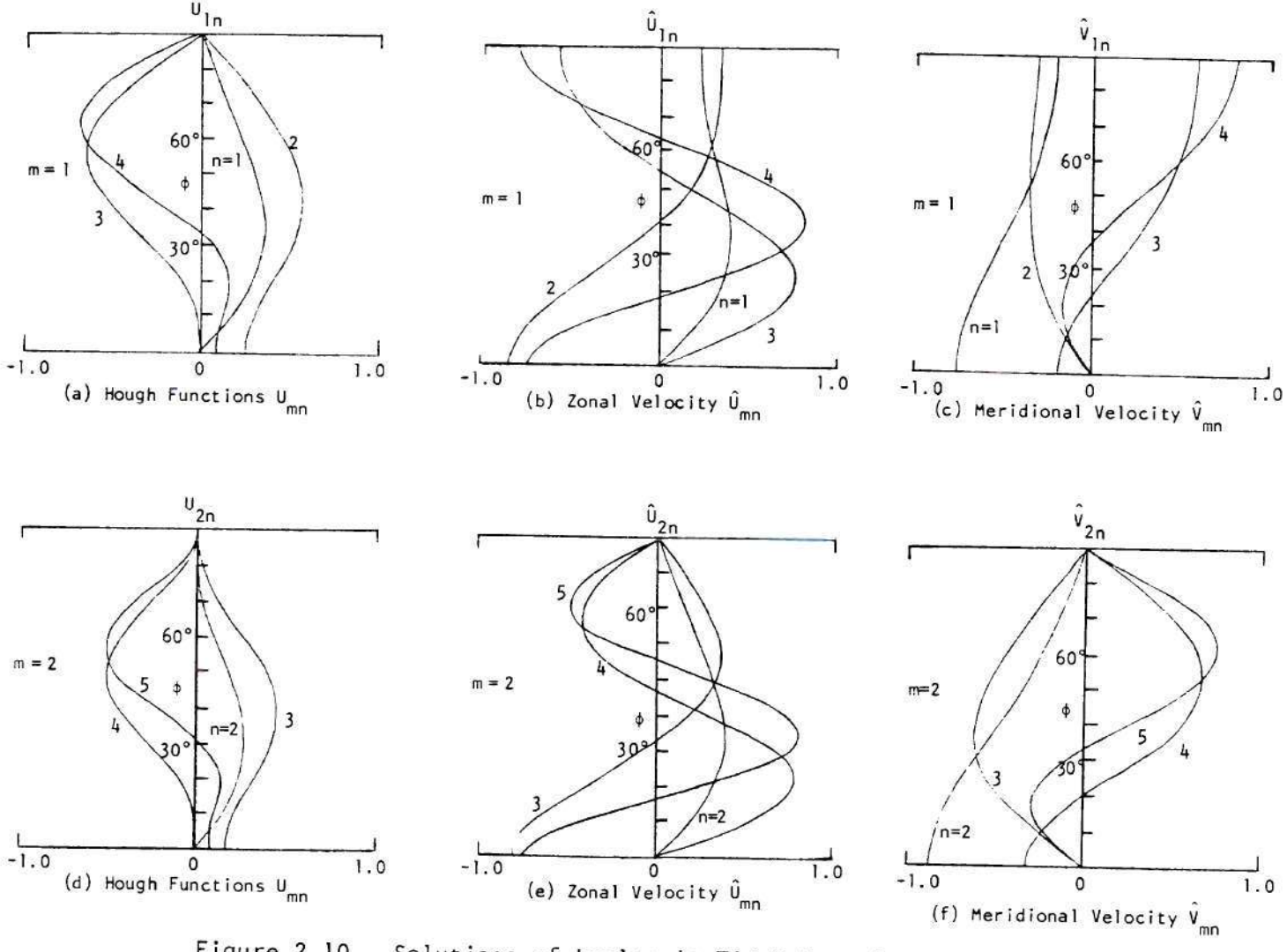

Figure 2.10. Solutions of Laplace's Tidal Equation as Functions of Latitude.

Table 2.2 Ratio of Potential to Total Energy for Solutions of Laplace's Tidal Equation

m \ (n-m)	0	1	ν_{mn}^{k} 2	3	4
			K=1		
1	.8650E+00	.6500E+00	.7300E+00	.8000E+00	.8500E+00
2	.8700E+00	.6500E+00	.7300E+00	.8100E+00	.8600E+00
			K=2		
1	.8450E+00	.5800E+00	.6500E+00	.7300E+00	.7800E+00
2	.8500E+00	.6000E+00	.6650E+00	.7500E+00	.8000E+00

It appears that the rate of change of these with m for the (n-m)th mode is very small and hence these may be taken as representative for the first few values of m.

2.7 Discussion of the Mathematical Model

Under the restrictions that have been imposed, two vertical modes with a large energy to leakage ratio have been found for a barotropic atmosphere. For each of these, there corresponds a discrete set of eigenfrequencies and horizontal modes. These motions are Rossby-gravity waves, whereas in a thin film of infinitesimal depth (LTE), the motions are pure Rossby waves. The vertical motion of these solutions is that of a gravity wave, while the horizontal motion is that of a Rossby wave. The equivalent depths that correspond to the vertical modes are

$$h_k = \bar{H}/\alpha_k;\ k = 1,2 \qquad (2.97.1)$$

Using $\bar{H}$ = 7.3km (corresponding to a mean temperature of 250°K), this yields

$$h_k = \begin{cases} 9.94 \text{ km} & k = 1 \\ 6.38 \text{ km} & k = 2 \end{cases} \qquad (2.97.2)$$

Jacchia and Kopal (1952) and Siebert (1961) have made similar studies for a restricted region of h (i.e., α) pertaining to resonance tidal theory. The former study examined several temperature profiles for the lowest 12 scale heights. By varying the profile parameters, they determined a profile and two equivalent depths, 10.4 and 7.9 km, having the greatest tidal amplification, the amplification factor of the first being infinite and that of the second finite. Siebert, using two simplified model profiles, determined a resonant equivalent depth of 10.0 km, also corresponding to an infinite amplification factor.

The first equivalent depth of Jacchia and Kopal and that of Siebert correspond closely to the first one found in this investigation, except that this corresponds to a large but finite energy to leakage ratio. The second equivalent depth of Jacchia and Kopal seems also to be related to the second one here, the difference probably due to the different profiles used. The values of α corresponding to these are shown on Figure 2.6. It is interesting to note that of all the profiles examined some 25 years ago when our knowledge of the upper atmosphere was crude at best, the one yielding the greatest response to tidal forcing has similar resonant characteristics to the atmosphere as we now know it.

Jacchia and Kopal found that for the second equivalent depth the amplification factor was very sensitive to the profile in the

vicinity of 50km. This is easily understood now by examining Figure 2.8 a for the refractive index of the second mode. This height corresponds to $\zeta = 7$ and roughly the second turning point or barrier away from the surface. The significance of the strato-mesospheric cavity for this mode was discussed in the previous section. This also explains the absence of this equivalent depth in Siebert's results. The simplified temperature profiles used in that study lacked the true nature of the atmosphere in this region and hence, the ability to form a resonant cavity for this value of α. Jacchia and Kopal also found that the amplification was insensitive to profile changes at the mesopause and above.

Finally, whereas the study of Jacchia and Kopal demonstrated the existence of two resonant equivalent depths in a rather restricted regime of h, this investigation seems to indicate that there are only two for the entire range.

The global energy and flux of these disturbances may now be evaluated. (2.76) gives the kinetic energy density. The potential energy density is essentially due to the buoyance motion, i.e., thermobaric, and is given by

$$P = \frac{1}{2} \left(\frac{N^2}{\omega^2}\right) \rho_o |w'|^2 \qquad (2.98.1)$$

(Gossard and Hooke, 1975, p. 106) where

$$N^2 = g\left\{\frac{g}{c^2}(\gamma - 1) + \frac{2}{c}\frac{\partial c}{\partial z}\right\} = \frac{g}{\tilde{H}\tilde{H}}(\tilde{H}' + \kappa) \qquad (2.98.2)$$

is the Brunt-Välsäilä frequency squared and c is the sound speed. With (2.93.3) this becomes

$$p = U^2(\mu)\,\frac{p_o(0)\,\delta^2\,\bar{u}^2}{2(2\hat{\Omega})^2\bar{H}^2\alpha^2}\cdot\frac{(\tilde{H}'+\kappa)}{\tilde{H}^2}\,\left|(\alpha\tilde{H}-1/2)v+\tilde{H}v'\right|^2 \qquad (2.98.3)$$

The ratio of the total potential energy to kinetic energy of the disturbance is then

$$\sum = \frac{PE}{KE} = \frac{\iiint_V P\,dV}{\iiint_V E\,dV}$$

which becomes

$$\sum = \frac{\delta^2 g}{(2\hat{\Omega})^2\,\bar{H}}\cdot\frac{\int_o^\infty \frac{(\tilde{H}'+\kappa)}{\tilde{H}^2}\left|(\alpha\tilde{H}-1/2)v+\tilde{H}v'\right|^2 d\zeta}{\int_o^\infty \frac{1}{\tilde{H}}\left|\frac{v}{2}-\tilde{H}v'\right|^2 d\zeta}\cdot\frac{\iint_S U^2 dS}{\iint_S(\hat{U}^2+\hat{V}^2)dS}$$

or with (2.96)

$$\sum{}^{k}_{mn} = \frac{\delta^2 g(1-\nu^k_{mn})}{(2\hat{\Omega})^2\,\bar{H}\,\nu^k_{mn}}\cdot\frac{\int_o^\infty \frac{(\tilde{H}'+\kappa)}{\tilde{H}^2}\left|(\alpha\tilde{H}-1/2)v_k+\tilde{H}v_k'\right|^2 d\zeta}{\int_o^\infty \frac{1}{\tilde{H}}\left|\frac{v_k}{2}-\tilde{H}v_k'\right|^2 d\zeta} \qquad (2.99)$$

We have computed the integrals

$$\psi_k = \int_o^\infty \frac{1}{\tilde{H}}\left|\frac{v_k}{2}-\tilde{H}\,v_k'\right|^2 d\zeta = \begin{cases} 1.65 \quad 10^4 & k=1 \\ 2.15 \quad 10^2 & k=2 \end{cases} \qquad (2.100.1)$$

$$\chi_k = \int_o^\infty \frac{(\tilde{H}' + \kappa)}{\tilde{H}^2} \left| (\alpha\tilde{H} - 1/2)v_k + \tilde{H} v_k' \right|^2 d\zeta = \begin{cases} 2.8\ 10^1 & k=1 \\ 8.8\ 10^1 & k=2 \end{cases}, \quad (2.100.2)$$

taking $|v_\infty| = 1$ and truncating after $\zeta = 60$. Then $\sum_{mn}^{k}$ becomes

$$\sum_{mn}^{k} = \eta \frac{\chi_k}{\psi_k} \frac{(1 - \nu_{mn}^k)}{\nu_{mn}^k} \quad (2.101)$$

Table 2.3 shows several values of $\sum_{mn}^{k}$ for m = 1,2, which should be representative of the (n-m)th mode for the first few values of m (cf., p. 90). By recalling that the potential energy is essentially thermobaric (gravitational), and the kinetic energy is essentially due to coriolis dominated horizontal motions (Rossby), one can see from Table 2.3 that the first Rossby-gravity mode, is, in an energy sense, strongly Rossby, while the second is more gravity.

Table 2.3 Ratio of Potential to Kinetic Energy of Both Vertical Modes for Several Horizontal Modes

m \ (n-m)	0	1	2	3	4
		$\sum_{mn}^{k}$			
		k = 1			
1	.2995E-02	.1033E-01	.7098E-02	.4798E-02	.3387E-02
2	.2868E-02	.1033E-01	.7098E-02	.4501E-02	.3124E-02
		k = 2			
1	.8490E+00	.3352E+01	.2492E+01	.1712E+01	.1306E+01
2	.8168E+00	.3086E+01	.2332E+01	.1543E+01	.1157E+01

A characteristic relaxation time for the disturbance may be defined as the ratio of the total energy to the leakage rate

$$\tau = \frac{\iiint_V (E+P)\,dV}{\iint_S \langle I_z \rangle_\infty \, dS} = \frac{\iiint_V E\,dV\{1 + \sum\}}{\iint_S \langle I_z \rangle_\infty \, dS} \tag{2.102.1}$$

which becomes

$$\tau^k_{mn} = \frac{1}{\omega^k_{mn}} \cdot \frac{(1 + \sum^k_{mn})\,\psi_k\,\nu^k_{mn}}{\eta k_\infty |v_\infty|^2 \alpha_k (1 - \nu^k_{mn})\tilde{H}_\infty} \tag{2.102.2}$$

Thus,

$$\tau^k_{mn} = \frac{s^k_{mn}}{\omega^k_{mn}} \tag{2.103.1}$$

where

$$s^k_{mn} = \frac{(1 + \sum^k_{mn})\,\psi_k \nu^k_{mn}}{\eta k_\infty |v_\infty|^2 \alpha_k (1 - \nu^k_{mn})\tilde{H}_\infty} \tag{2.103.2}$$

Table 2.4 lists values of τ^k_{mn} for m = 1,2. Again, these values should be representative for the (n-m)th mode for the first few values of m.

A more fundamental quantity is s^k_{mn}, with which a complex angular frequency may be defined as

$$\hat{\omega}^k_{mn} = \omega^k_{mn}\left(1 + \frac{i}{s^k_{mn}}\right) \tag{2.104}$$

Table 2.4 Relaxation Time (Days) for Several Modes

m \ (n-m)	0	1	2	3	4
		τ^k_{mn}			
		k = 1			
1	.2928E+04	.3644E+04	.8725E+04	.1932E+05	.3769E+05
2	.4189E+04	.2692E+04	.6159E+04	.1395E+05	.2755E+05
		k = 2			
1	.3182E+02	.8791E+02	.1496E+03	.2587E+03	.3771E+03
2	.4574E+02	.6683E+02	.1117E+03	.1830E+03	.2724E+02

The imaginary part is the decay rate and accounts for the relaxation of the disturbance due to leakage. Thus $s^k_{mn}/2\pi$ represents the number of cycles that elapse before the amplitude drops by a factor of e. Table 2.5 lists the corresponding values of $s^k_{mn}/2\pi$.

Table 2.5 Number of Cycles that Elapse During One Relaxation Period

m \ (n-m)	0	1	2	3	4
		$s^k_{mn}/2\pi$			
		k=1			
1	.2471E+04	.7215E+03	.1047E+04	.1545E+04	.2186E+04
2	.2581E+04	.7215E+03	.1047E+04	.1647E+04	.2369E+04
		k=2			
1	.2418E+02	.1442E+02	.1556E+02	.1759E+02	.1961E+02
2	.2470E+02	.1470E+02	.1587E+02	.1830E+02	.2070E+02

The decay rates of both modes are small fractions ($1/s^k_{mn}$), (shown in Table 2.6) of the oscillation rate, that of the first mode being some 2 orders of magnitude smaller than that of the second.

Table 2.6 Ratio of Imaginary Part to Real Part of the Complex Frequency

m \ (n-m)	0	1	2	3	4
		$1/s^k_{mn}$			
		k=1			
1	.6441E-04	.2206E-03	.1520E-03	.1030E-03	.7280E-04
2	.6167E-04	.2206E-03	.1520E-03	.9666E-04	.6717E-04
		k=2			
1	.6581E-02	.1104E-01	.1023E-01	.9048E-02	.8116E-02
2	.6444E-02	.1082E-01	.1003E-01	.8696E-02	.7688E-02

It appears that for all intents and purposes, the first mode may be considered as a contained evanescent wave. The second mode, although much "leakier," also has a large residence time. The smallest decay rates shown occur for the lowest modes n=m and decreases with increasing n-m. Apparently, those modes with $n - m > 5$ will have even smaller decay rates than those for $n = m$.

These solutions may be used to estimate the signal time between the surface and a particular height via the two vertical modes. The signal or group velocity is related to the energy density and flux by

$$\langle I_z \rangle = C_G (E + P) \qquad (2.104)$$

The time for the disturbance to travel from the surface to an elevation z can be estimated as

$$T(z,\mu) = \int_o^z \frac{dz'}{C_G} = \int_o^z \frac{(E+P)dz'}{\langle I_z \rangle} \tag{2.105.1}$$

The global mean is then

$$\overline{T}(z) = \frac{1}{4\pi a^2} \iiint_V \frac{(E+P)}{\langle I_z \rangle} dV \tag{2.105.2}$$

After some manipulation, this becomes

$$\overline{T}(\zeta) = \frac{r_{mn}^k(\zeta)}{\omega_{mn}^k} \tag{2.105.3}$$

$$r_{mn}^k = -\frac{\nu_{mn}^k}{4\pi\alpha_k(1-\nu_{mn}^k)\eta} \int_o^\zeta \frac{\left|\frac{v_k}{2} - \tilde{H}v_k'\right|^2}{\tilde{H}^2 \operatorname{Im}\{v_k' v_k^*\}} d\zeta' - \frac{1}{\alpha_k} \int_o^\zeta \frac{(\tilde{H}'+\kappa)\left|(\alpha\tilde{H}-1/2)v_k + \tilde{H}v_k'\right|^2 d\zeta'}{\tilde{H}^3 \operatorname{Im}\{v_k' v_k^*\}} \tag{2.105.4}$$

Now the quantity

$$-\tilde{H} \operatorname{Im}\{v_k' v_k^*\}$$

is proportional to $\langle I_z \rangle$ and is for all practical purposes independent of ζ (cf., 2.93.5). Therefore (2.105.4) becomes

$$r_{mn}^k = \frac{1}{-\tilde{H} \operatorname{Im}\{v_k' v_k^*\}\alpha_k} \left\{ \frac{\nu_{mn}^k}{4\pi\eta(1-\nu_{mn}^k)} \int_o^\zeta \frac{1}{\tilde{H}} \left|\frac{v_k}{2} - \tilde{H}v_k'\right|^2 d\zeta' + \int_o^\zeta \frac{(\tilde{H}'+\kappa)\left|(\alpha\tilde{H}-1/2)v_k + \tilde{H}v_k'\right|^2 d\zeta'}{\tilde{H}^2} \right\} \tag{2.105.5}$$

(cf., 2.100). Figure 2.11 shows $\overline{T}(\zeta)$ for both vertical modes for $m = n = 1$. A surface disturbance in the first mode is strongly confined to the lower atmosphere and has a time lag of some 200 days before reaching the mesosphere. However, the second vertical mode, being much leakier, allows a similar disturbance to reach the mesosphere in roughly 16 days for this horizontal mode. Paulin (1970) found a time lag between disturbances at the 25 mb and 500 mb levels of 5 to 7 days. These heights correspond to $\zeta = 3.37$ and .76 respectively. The time lag for the (1,1,2) mode indicated by Figure 2.11 is 4.8 days. Other horizontal structures of the second vertical mode have similar lags consistent with Paulin's results.

It should be pointed out that although τ_{mn}^{k} represents the mean decay time, the local time for decay from some initial configuration may be substantially shorter, particularly in the upper atmosphere where there is less reflection (cf., Figures 2.8, a; 2.9,a).

This may have important implications to spectral analysis of these disturbances at great heights, because the time series may be nonstationary, their spectral content changing over a sample period due to leakage and transient forcing.

Finally, Yanowitch (1967, a, b; 1971) has indicated that the radiation condition may be inappropriate as an upper boundary condition in stratified media for vertical wavelengths much larger than the scale of the stratification. He found that in the limit of small viscosity, there exists a thin viscous reflection layer at some finite elevation which reflects nearly all of the energy of those disturbances

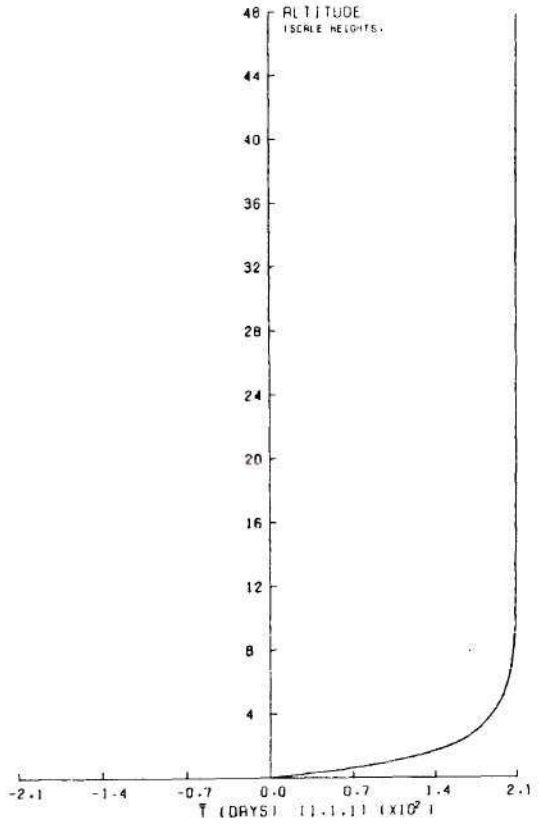

(a) (1,1,1) Mode

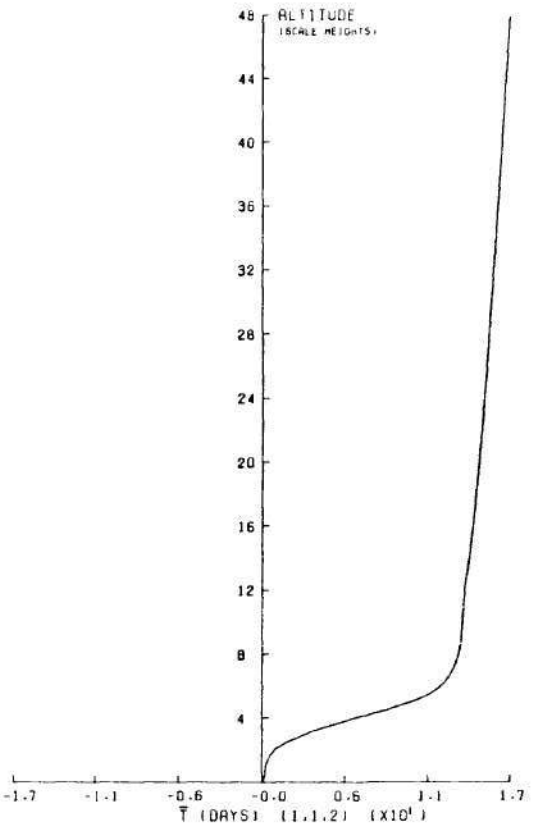

(b) (1,1,2) Mode

Figure 2.11. Mean Signal Time Between Surface and a Given Height.

where $k^2 \to 0$. Apparently, this study was motivated by Siebert's (1961) comment that the tidal resonance curves seemed discontinuous near $k^2 = 0$, the point of transition from oblique to horizontally propagating waves (cf., Figure 2.6). Since both of the vertically propagating modes found in this study lie in this regime of k^2, it appears that these results may be significant in changing both the values and perhaps the number of α's possible. An important consequence of this study is that apparently for many disturbances, the exponentially growing amplitudes of the inviscid, linear theory are restrained sufficiently by this limiting small viscosity so that they do not attain nonlinear values at large heights.

CHAPTER III

RADIO METEOR WIND DECOMPOSITION USING FINITE ELEMENT APPROXIMATION

The intention of this chapter is to develop a method for reducing meteor wind data to a form acceptable to spectral analytic techniques, when the fundamental period is not known a priori.

3.1 Introduction to the Meteor Technique

The radio-meteor technique for measuring upper atmospheric winds has been in use internationally for many years. Briefly, radio waves are transmitted from one site, reflected by an ionized meteor trail (which is assumed to drift with the ambient velocity) and finally received at another site. Because of the drift velocity of the trail, the frequency of the reflected waves is doppler shifted. The direction of arrival and the range of the reflected wave or "echo" gives the location of the reflecting point, and the doppler shift yields a velocity component at that point. Unfortunately, the velocity determined by this measured doppler shift is not the true velocity $\vec{V}$, but rather the line of sight velocity $\vec{V}_L$, i.e., the component of the actual wind velocity along the line of sight between the receiving station and the reflecting point on the trail (Figure 3.1).

In general the velocity field is expected to be a vector valued function of space and time:

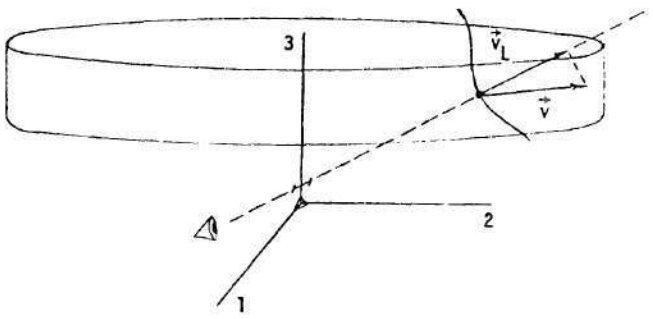

Figure 3.1. Meteor Wind Measurement Configuration. Only the Line of Sight Component of the True Velocity is Measured.

$$\vec{V} = \vec{V}(x_1, x_2, x_3, t) = V(\vec{x}, t)$$

or equivalently it may be represented by the three component functions:

$$v_1 = v_1(\vec{x}, t)$$

$$v_2 = v_2(\vec{x}, t)$$

$$v_3 = v_3(\vec{x}, t)$$

Here the standard coordinate convention is used: subscripts 1, 2 and 3 denote EW, NS and vertical directions respectively. A typical measurement volume might be a circular slab of atmosphere centered above the receiving site 400 km in diameter extending from 70 to 120 km in the vertical (Figure 3.1).

It is often assumed that the wind field is independent of the horizontal position in the measurement volume, which implies

$$\vec{V} = \vec{V}(z, t)$$

where we let $z = x_3$. The motivation for this is that horizontal scales of interest are expected to be considerably larger than the horizontal dimensions of the volume (A. Spizzichino, 1971). Thus, the problem is reduced to determining a vector valued function $\vec{V}$, or equivalently the three component functions v_k, over a two dimensional domain of height X time. (X is the Cartesian product e.g., if A and B are two intervals then the Cartesian product A X B is the rectangle given by $\{(t, z); t\varepsilon A, z\varepsilon B\}$). Typically, the problem might be to determine the vector values over a strip of length T, ranging from 70 to 120 km.

Any three-dimensional vector may be determined by resolving (measuring) three linearly independent components. Unfortunately, most meteor wind facilities have only one receiving site and hence measure velocity along only one line of sight. Thus, only one of the three required components is measured at any (t, z) in the domain. Moreover, since the incidence of meteors is random in space and time, the points where measurements are taken are randomly distributed across the domain, as are the direction cosines associated with the lines of sight.

The line of sight velocity at any point (t, z) is given by:

$$\vec{V}_L = (\vec{V} \cdot \vec{e}_L)\vec{e}_L \qquad (3.1)$$

where:

$\vec{V}$ is the true velocity

$\vec{V}_L$ is the line of sight component

$\vec{e}_L$ is a unit vector along the line of sight (Figure 3.2).

Now:

$$e_{L_j} = \cos \alpha_j = d_j \tag{3.2}$$

where d_j are the direction cosines associated with the line of sight (Figure 3.2). Thus the "signed magnitude" of the line of sight velocity is given by:

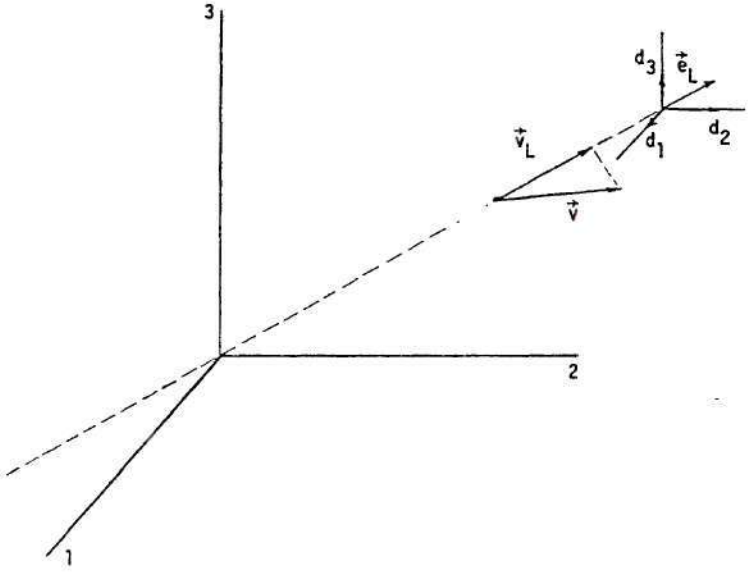

Figure 3.2. Line of Sight Observation of the True Velocity - The Line of Sight Unit Vector $\vec{e}_L$ has the Corresponding Direction Cosines d_1, d_2, d_3 as its Components.

$$V_L = \vec{V} \cdot \vec{e}_L = v_k d_k \tag{3.3.1}$$

or

$$V_L = d_1 v_1 + d_2 v_2 + d_3 v_3 \tag{3.3.2}$$

We see that the measured line of sight velocity $\vec{V}_L(t, z)$ is a linear combination of the three components of the true velocity $\vec{V}(t, z)$, where the coefficients are the "random" direction cosines. This gives but one equation in the three unknowns v_k at the point (t, z). Still needed are two other linearly independent equations in the velocity components. Thus, if there are N measurements at points $\{(t_\mu, z_\mu)\}_{\mu=1}^{N}$ there are 3N corresponding unknowns: $\{v_k(t_\mu, z_\mu)\}_{\mu=1}^{N}$, $k = 1,2,3$.

Obviously, some assumptions must be introduced to close the problem. One of the earlier techniques, which remains in use (Clark, 1975), partitions the time height domain into several subregions in which $\vec{V}(t, z)$ is assumed constant. This method has obvious drawbacks in consideration of velocity height variations, evolution of the wind field, and spectral resolution. Another alternative is to sample only echoes arriving along a given direction, thereby measuring a <u>given</u> component at different (t, z). This closes the problems mathematically yet fails to give a complete description of the velocity field.

In 1959 G. V. Groves (Groves, 1959) established a technique which solved the problem in a "least squares" sense. The unknown velocity components were assumed to be given functions of time and height containing arbitrary parameters. These parameters were then chosen so as to minimize the error in V_L, as formed by these functions, compared with the actual measurements of V_L. The general technique as used at the

University of Adelaide in South Australia and the Georgia Institute of Technology in Atlanta employs a cubic polynomial in height and the first four terms of a Fourier series in time where the fundamental period is chosen to be the length of the interval under study. This is usually taken as 24 hours. Motivation for this choice of the temporal behavior is to provide a harmonic decomposition of the wind field. Thus after performing the Groves analysis, at any fixed height z there will exist three time sequences for the three velocity components v_k, each of which will have exactly three spectral constituents. Similarly at any fixed time t, there will exist three velocity height profiles, each of which may vary as at most, a cubic polynomial. Also, in order to have a large ensemble of data points in the period of interest, data from several adjacent periods is superimposed - as if it occurred in the same period.

There are several points that must be questioned concerning the previous technique. Of primary importance is the connection of spectral analysis to the velocity components v_k. If one assumes a discrete set of harmonic components for the temporal behavior of $v_k(t, z)$, one expresses a priori knowledge of not only the number of such components, but more importantly the frequencies associated with them (see Clark, 1975). That is, the data is "pre-analyzed" to have a spectrum containing only these frequencies. In general such an omniscient assumption is unwarranted. If a fundamental (largest) period is known to exist in the data, then a harmonic analysis may be performed using a Fourier series with the first harmonic term having period equal to this fundamental. Unfortunately, this is very unlikely in almost all geophysical

data, in particular atmospheric data. Probably the best choice for a fundamental period would be one year, but even this would have its limitations due to solar cycle variations, etc. Classical spectral and harmonic analyses require stationarity - in essence the mean and spectral content are independent of time. Again, unlike laboratory situations, this is not so in most geophysical phenomena. If this is not the case nonstationarities must be accounted for so as not to distort the spectrum. Assuming $v_k(t, z)$ to behave as a truncated fourier series in t implies the existence and knowledge of a fundamental period. Obviously this is not the case, and the consequences will fall into the temporal behavior and spectral content of the velocity components.

Recall that the Groves technique as used in Adelaide and Atlanta employs superposition of data in several adjacent time intervals. This amounts to averaging adjacent time spans. The effect of this is to cancel the Fourier transform and hence the power spectrum for all frequencies other than those periodic in T (see Appendix D for details). Therefore after sufficient averaging, only those frequency components that are "window periodic" will survive.

If the velocity functions were stationary, and if this averaging were performed sufficiently, then only the window periodic frequency components would remain. Then a Fourier series might be fitted to the data with fundamental period equal to the length of the time interval. However, stationarity does not exist, and the question of an appropriate fundamental period or sample time remains unanswered. Additionally,

the destruction of the spectral content except at the window periodic frequencies is also a questionable point. Indeed, the dominant features of the spectrum may be lost in such a process. It is worth noting that the spectral resolution, i.e., the number of harmonic components, obtained with the Groves analysis is sharply limited by machine capacity. Although this may not be so serious for the investigation of forced phenomena of "known" frequency, e.g., tides, it is certainly a detrimental feature in the analyses of more general phenomena where the frequencies are not known a priori, e.g., gravity waves and planetary waves.

Finally, resolution of the wind field in the vertical is limited to that of a cubic polynomial, which may have at most two critical points.

The Groves technique was unquestionably a major step in the reduction and analysis of meteor wind data. Yet, the previous discussion seems to indicate that a somewhat different approach would be warranted.

3.2 Development of the Problem

Construction of the problem is merely outlined in this section. The reader is referred to Appendix E for the details. The problem is to determine representations of the unknown velocity component functions over a suitable domain of interest. We take this to be a strip in the t - z plane of length:

$$T = t_F - t_0$$

and width $z_F - z_0$ (Figure 3.3)

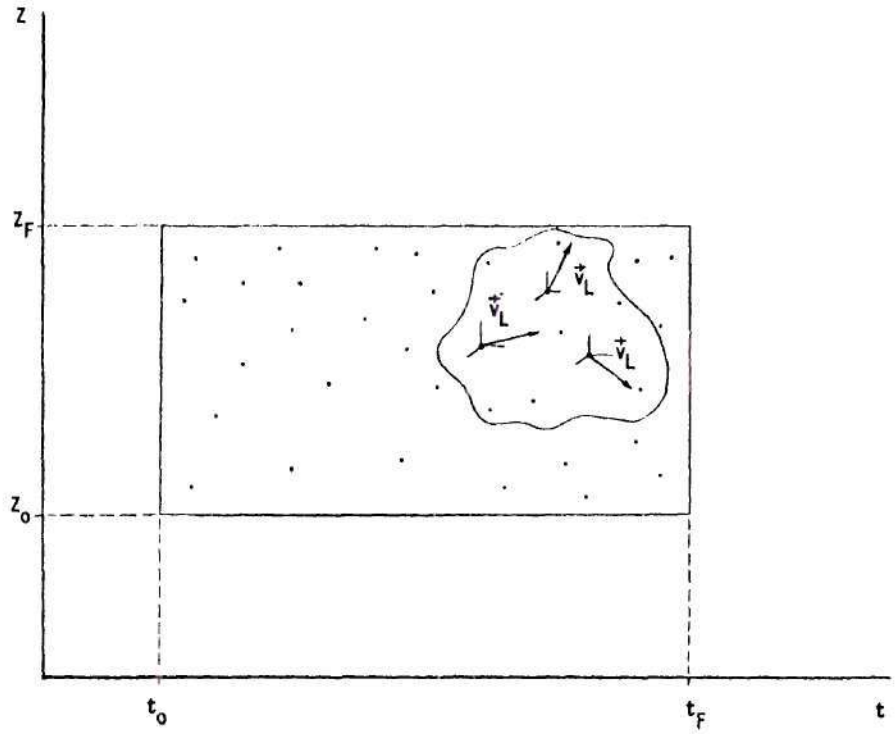

Figure 3.3. Nearby Observation Points in the Velocity Domain, The Rectangular Strip $[t_o,t_f) \times [z_o,z_f)$, are to be Related in Order to Close the Problem.

Since it takes three linearly independent measurements at a single point (t, z) to determine the three unknowns $v_k(t, z)$, we attempt to relax the problem and relate observations at nearby points (Figure 3.3). We do this by allowing the velocity functions to vary in some continuous manner between the different observation points.

We assume that there are N line of sight observations: $\{V_{L\mu}\}_{\mu=1}^{N}$ at N points: $\{(t_\mu,z_\mu)\}_{\mu=1}^{N}$ in the domain with N corresponding sets of direction cosines: $\{d_{1\mu}\}_{\mu=1}^{N}$, $\{d_{2\mu}\}_{\mu=1}^{N}$, $\{d_{3\mu}\}_{\mu=1}^{N}$. Thus we have N equations:

$$V_{L\mu} = d_{1\mu}\, v_1(t_\mu, z_\mu) + d_{2\mu}\, v_2(t_\mu, z_\mu) + d_{3\mu} v_3(t_\mu, z_\mu)$$

$$\mu = 1,2,\ldots,N \qquad (3.4)$$

As in the classical Least Squares (LS) Problem, we assume the unknown functions $v_k(t,z)$ to be composed of a linear combination of p_k approximating functions: $Z_j^k(t,z)$ $j = 1,2,\ldots,p_k$, plus an error term $\varepsilon_k(t,z)$, $k = 1,2,3$. That is

$$\begin{cases} v_1(t,z) = \alpha_1 Z_1^1(t,z) + \alpha_2 Z_2^1(t,z) + \ldots + \alpha_{p_1} Z_{p_1}^1(t,z) + \varepsilon_1(t,z) \\ v_2(t,z) = \beta_1 Z_1^2(t,z) + \beta_2 Z_2^2(t,z) + \ldots + \alpha_{p_2} Z_{p_2}^2(t,z) + \varepsilon_2(t,z) \\ v_3(t,z) = \gamma_1 Z_1^3(t,z) = \gamma_2 Z_2^3(t,z) + \ldots + \gamma_{p_3} Z_{p_3}^3(t,z) + \varepsilon_3(t,z) \end{cases} \qquad (3.5)$$

or

$$\begin{cases} v_1(t,z) = \sum_{j=1}^{p_1} \alpha_j Z_j^1(t,z) + \varepsilon_1(t,z) \\ v_2(t,z) = \sum_{j=1}^{p_2} \beta_j Z_j^2(t,z) + \varepsilon_2(t,z) \\ v_3(t,z) = \sum_{j=1}^{p_3} \gamma_j Z_j^3(t,z) + \varepsilon_3(t,z) \end{cases} \qquad (3.6)$$

The α_j, β_j, and γ_j are the as yet undetermined coefficients of the approximating functions $Z_j^1(t,z)$, $Z_j^2(t,z)$ and $Z_j^3(t,z)$, where there are p_1, p_2, and p_3 of each respectively.

To simplify matters we will approximate all three of the velocity functions by the same set of functions: $Z_j(t, z)$, i.e.,

$$Z_j^k(t,z) = Z_j(t,z) \qquad j = 1,2,3,\ldots,p \tag{3.7}$$

(3.6) then reduces to:

$$\begin{cases} v_1(t,z) = \sum_{j=1}^{p} \alpha_j Z_j(t,z) + \varepsilon_1(t,z) \\ v_2(t,z) = \sum_{j=1}^{p} \beta_j Z_j(t,z) + \varepsilon_2(t,z) \\ v_3(t,z) = \sum_{j=1}^{p} \gamma_j Z_j(t,z) + \varepsilon_3(t,z) \end{cases} \tag{3.8}$$

We must now choose the set of approximating functions: $\{Z_j(t,z)\}_{j=1}^{p}$. Criteria for these should be:

(i) They do not bias the spectral content of the velocities.

(ii) They do not require stationarity of the wind field.

(iii) The resulting approximation functions for $v_k(t,z)$ should be sufficiently flexible to conform to the data, i.e., the resolution of the velocity functions be limited by only the data.

We will choose as our set of approximating functions a "basis set" of spline functions.

The strip in question is divided into nm subrectangles by partitioning the interval $[t_o, t_f)$ into n subintervals and the interval $[z_o, z_F)$ into m subintervals. This forms the mesh or "partition" Π

(Figure 3.4). The approximating functions $Z_j(t,z)$ are then chosen such that any linear combination of them results in a piecewise cubic polynomial in t and z over any subrectangle and is coupled to different polynomials over adjacent subrectangles through smoothness considerations. Thus any linear combination is a bicubic spline on the partition Π.

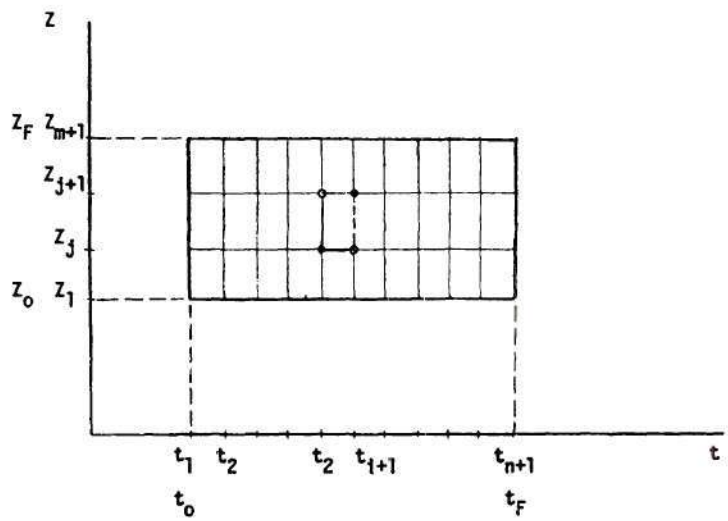

Figure 3.4. A Partition: $\Pi = \{(t_i,z_j)\}_{i=1\ j=1}^{n+1\ m+1}$, of the Rectangular Strip $[t_o,t_f) \times [Z_o,z_f)$ is Obtained by Dividing $[t_o,t_f)$ into n Subintervals and $[z_o,z_f)$ into m Subintervals. This Results in nm Subrectangles.

The problem then reduces to determining the 3p coefficients α_j, β_j, γ_j. This is accomplished by minimizing the mean square error between the observed line of sight velocities $\{V_L(t_\mu, z_\mu)\}_{\mu=1}^{N}$ and the

approximations to these. Once the expansion coefficients are determined, the velocity components may be obtained from (3.8).

3.3 Test Results

Initially the method was tested with the following known input functions:

$$\begin{cases} v_1(t,z) = \sin(4\pi t) \\ v_2(t,z) = \sin(\pi z) \\ v_3(t,z) = (t+z)^3 \end{cases} \tag{3.9}$$

with (t,z) in the unit square. Observation points were selected randomly (uniform in t and z) as were the corresponding direction cosines. The solution remained stable for different ensembles of observation points. It also remained stable for different ratios of the number of observations to the number of unknowns being determined: N/3p. For fixed ensemble of observations, different partitions, i.e., different temporal and vertical mesh sizes n and m, were used. For almost all partitions the resulting approximation functions for $v_k(t,z)$ represented the true (known) functions quite well.

Figure 3.5 shows a plot of the variance (mean square error) of known values of $v_1(t,z)$ about the approximate values. These are shown as a function of temporal mesh size n (for m = 1) and the ratio N/3p. Also shown are the variances of V_L about the approximate values. It can be seen that for increasing partition number the resulting variances of the velocity functions v_k and V_L decrease to quite acceptable values

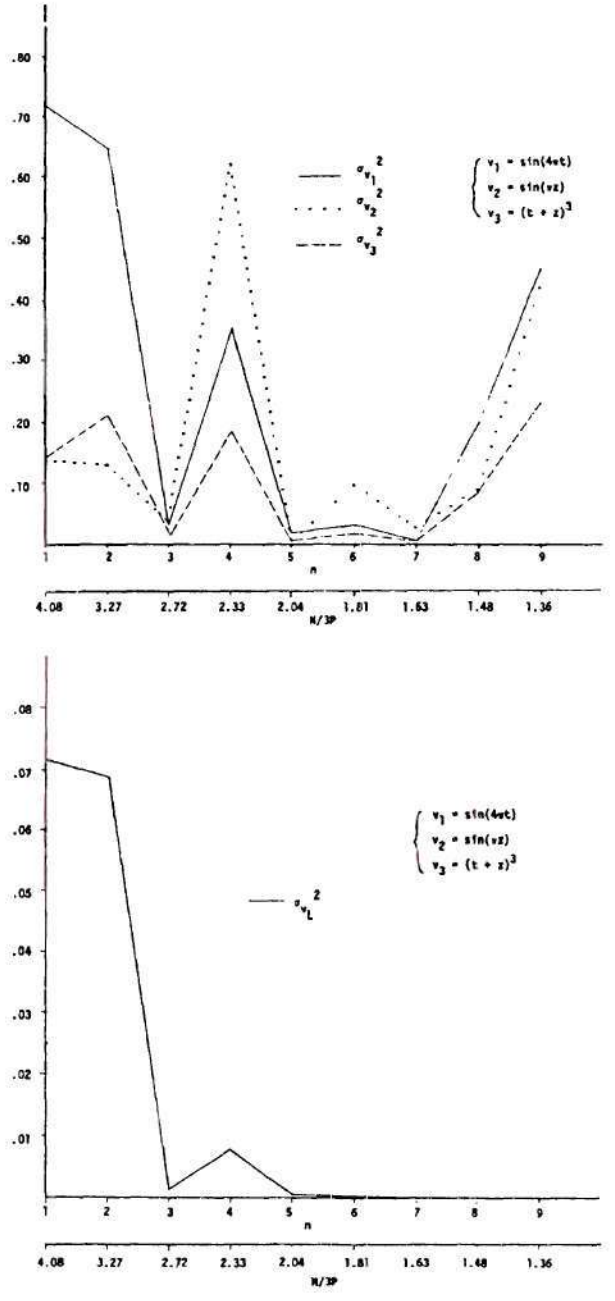

Figure 3.5. Variances of the True Velocities about their Approximations vs. Temporal Partition Number n and Overspecification Ratio N/3P (m = 1). As the Problem Approaches Determinancy, $N/3P \to 1$, the Variance of the Line of Sight Velocity (bottom): $\sigma_V^2 \to 0$, but the Variance of the Individual Components (top) Grows Unacceptably Large; $\sigma_{v_k}^2 \to \infty$. $v_1 = \sin(4\pi t)$ $v_2 = \sin(\pi z)$ $v_3 = (t + z)^3$.

except possibly at even values of n. This may be related to the fact that the spline functions used were cubic. Also as n increases past the value where $N/3p < 1.63$ the variances of the velocity functions v_k starts increasing while the variance of V_L decreases monotonically to zero. The ratio N/3p may be considered as a measure of the overspecification of the problem. Thus as N/3p tends to unity the linear problem becomes determinate. However, Figure 3.5 indicates that although $\sigma_{V_L}^2$ tends to zero as N/3p tends to one, $\sigma_{v_k}^2$ grows unacceptably large. This is consistent with the development since it is $\sigma_{V_L}^2$ which is being minimized, and only through the excess of constraints do we achieve small values for $\sigma_{v_k}^2$. That is as N/3p tends to unity the "data points" V_{L_μ} are interpolated exactly, but the "decomposition" of v_k is lost. This minimum usable ratio of N/3p = 1.63, although expected to vary with the data, compares favorably with a corresponding ratio of 3 or 4 that has been found to yield reasonable results in the Groves Analysis.

Similar results are shown in Figure 3.6 for different choices of $v_k(t,z)$. In virtually all cases examined the majority of the variance could be traced to regions of the domain where there was an absence or sparse scatter of data points, (t_μ, z_μ). In such regions, the resulting approximation functions are relatively unconstrained and may behave in essentially whatever manner needed in order to better fit the data where it occurs in greater abundance.

In particular if an <u>interior</u> region of the domain has a low data density, i.e., few sample points (t_μ, z_μ), the resulting approximation is quite well behaved and seems to vary "naturally" with the function

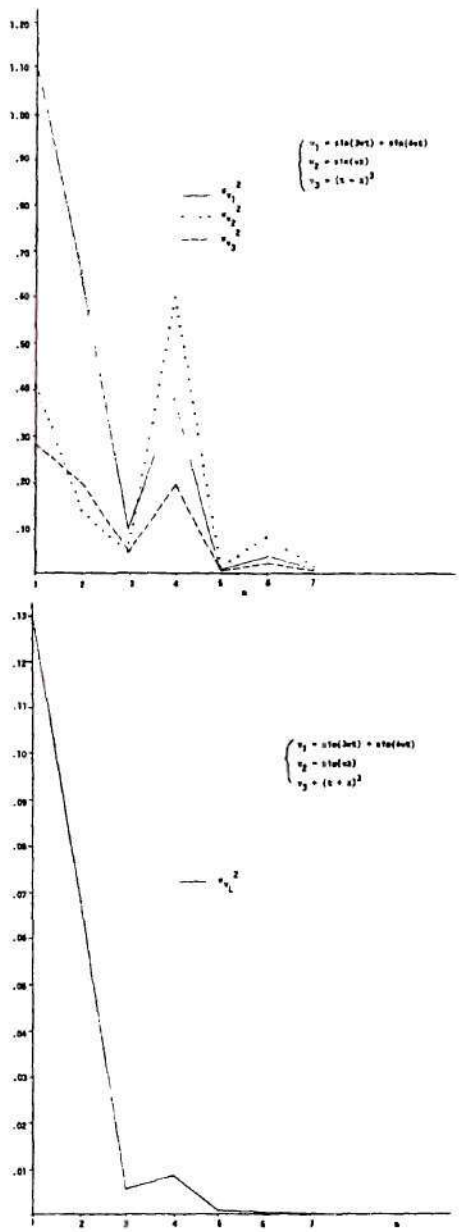

Figure 3.6. As for Figure 3.5 with $v_1 = \sin(3\pi t) + \sin(4\pi t)$, $v_2 = \sin(\pi z)$, $v_3 = (t + z)^3$.

in the rest of the domain. The region is surrounded by constraints (observation points $V_L(t_\mu, z_\mu)$). These constraints "project" the behavior of the velocity functions into this region. On the other hand, if a region adjacent to the boundary of the domain is poorly constrained, the approximation functions in this region may grow unreasonably large. Recall for the one-dimensional domain, a spline is a series of coupled polynomials over adjacent intervals. In general polynomials grow unbounded as x tends to $\pm\infty$. Thus each of the polynomials used in the spline does grow large, but not in the interval of use. Consider the outermost intervals. If the spline elements over these intervals are not constrained sufficiently, they need only meet additional constraints from one side - towards the interior of the partition. Thus we might expect the polynomials to grow quite large near the end points in order that the interior spline better fit the data where it occurs in greater abundance. A similar argument holds for the two-dimensional domain.

Finally, Figure 3.6 indicates a relatively large value of $\sigma_{v_1}^2$ for n = 1. Since over any subrectangle the approximate functions may vary at most as a cubic polynomial along either axis, and since a cubic has at most two critical points, we should not expect good representation of periodic functions having more than one cycle over any one rectangle. This has particular significance to the spectral resolution of this decomposition. In general, there will not be spectral content of frequencies of more than one cycle per partition interval. This has been verified by all of the cases examined. Thus Figure 3.6 indicates

the approximation functions for n = 1 are incapable of conforming to two cycles contained in the v_1 velocity function. It is important to note that $\sigma_{v_2}^2$ and $\sigma_{v_3}^2$ remain relatively low at the same time, indicating that they are essentially unaffected by the inability to conform to v_1. As the partition number n is increased, the approximation function gains additional degrees of freedom and is better able to conform to the data. For n = 2, $\sigma_{v_1}^2$ has decreased greatly, and by n = 3 it is quite small.

We have solved the problem with reasonably good success over a given domain in the t-z plane - a strip of length T. The resolution in t and z of the decomposed functions $v_k(t,z)$ (i.e., the size of the partition Π) is limited by:

(i) the number of observations N.

(ii) the uniformity of the observation points (t_μ, z_μ) in the domain - if there are gaps or holes in the domain where there are few observations, in particular near the boundaries, a cruder partition must be used.

(iii) computational capabilities - the number of unknowns being solved for simultaneously (size of the linear system) is of course limited by the machine used.

The last of these implies that a compromise must be reached between the degree of resolution (partition size) and the size of the domain being examined. Since ultimately, long time series are to be examined, this technique would be of little value if the resolution was lost. We now explore a method of attaining high resolution in the

approximations of $v_k(t,z)$ over adjacent strips of suitable length - say T, and coupling the functions over these domains.

Consider a strip in the t-z plane of length 3T, width $z_f - z_o$ (Figure 3.7). First we divide this region into three substrips each of length T. If the data were decomposed over disjoint strips, the resulting velocity approximates would be uncoupled. For many purposes, if there is sufficient data, this would probably be adequate. In order to couple these strips, we increment each by an amount ΔT on both sides, i.e.,

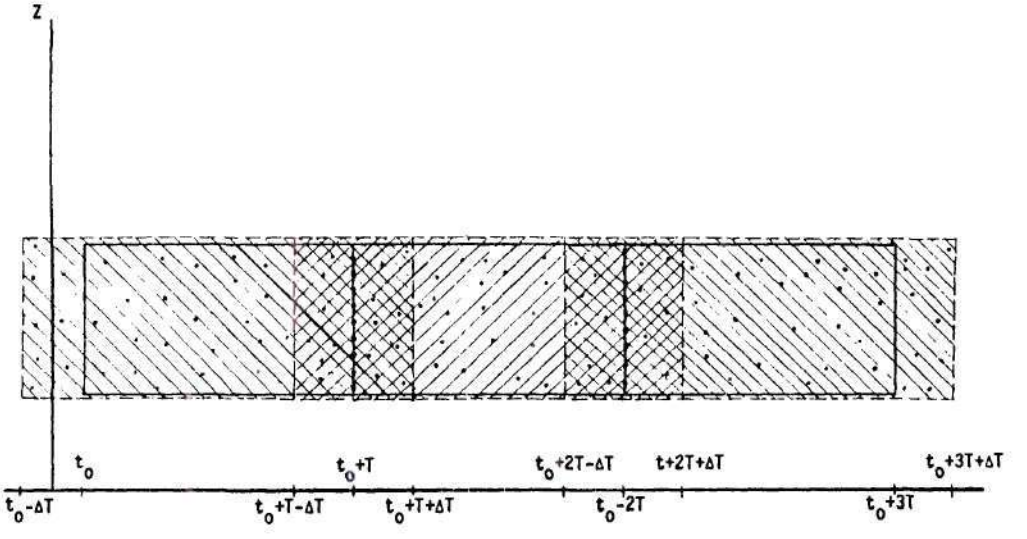

Figure 3.7. Adjacent Time Periods of Length T may be Coupled by Extending each Temporally on Both Sides by ΔT so That They all Overlap. Data over these Extended Domains is then Decomposed but the Resulting Velocity Functions are Retained only over the Original Periods of Length T. Continuity between these Periods (in a Least Squares Sense), may be Achieved by Producing Data Points, along the Border between the Strips of Length T.

$$[t_o, t_o + T) \rightarrow [t_o - \Delta T,\ t_o + T + \Delta T)$$

$$[t_o + T,\ t_o + 2T) \rightarrow [t_o + T - \Delta T,\ t_o + 2T + \Delta T)$$

$$[t_o + 2T,\ t_o + 3T) \rightarrow [t_o + 2T - \Delta T,\ t_o + 3T + \Delta T)$$

The data is then decomposed on the first "augmented" strip, but the resulting velocity functions are retained only over the smaller strip of length T. If this is done with all the strips the regions used to produce the approximations will overlap, and thus information is fed both forwards and backwards. Moreover, continuity (in a least squares sense) may be obtained by actually producing data points at the interfaces of the regions from the approximation functions of the previously analyzed region (Figure 3.7). The procedure just outlined not only couples adjacent domains, but also minimizes undesirable behavior near the boundaries of these domains due to insufficient data. The resulting approximates for $v_k(t,z)$ represent the "instantaneous" wind field. Of course adjacent sampling periods may be superimposed, as in other techniques, to yield a higher data density thereby increasing the resolution, but at the expense of the spectral content at non window periodic frequencies. The resulting approximations would then represent some "average sense" wind field.

The following set of test functions was then used on the strip given by $\{(t,z);\ t \in [0,3),\ z \in [0,1)\}$

$$\begin{cases} v_1(t,z) = \sin(3\pi t) + \sin(4\pi t) \\ v_2(t,z) = \sin(\pi z) \\ v_3(t,z) = (t+z)^3 \end{cases}$$

The domain was divided into three substrips each of length T = 1; 300 data points were randomly scattered on each. The decomposition was performed as previously discussed - but without projecting data points into adjacent regions to achieve continuity. Figure 3.8 shows approximate values of $v_1(t, 2/3)$ for m = 1, n = 1,3,5. The actual input function is essentially identical with the approximate for n = 5. As previously discussed, the approximation functions for n = 1 cannot conform to the variation of $v_1(t, z)$ over any interval. This is primarily responsible for the discontinuities between the strips at t = 2. It is interesting to note that despite this handicap, the approximation for n = 1 does indicate the general trend.

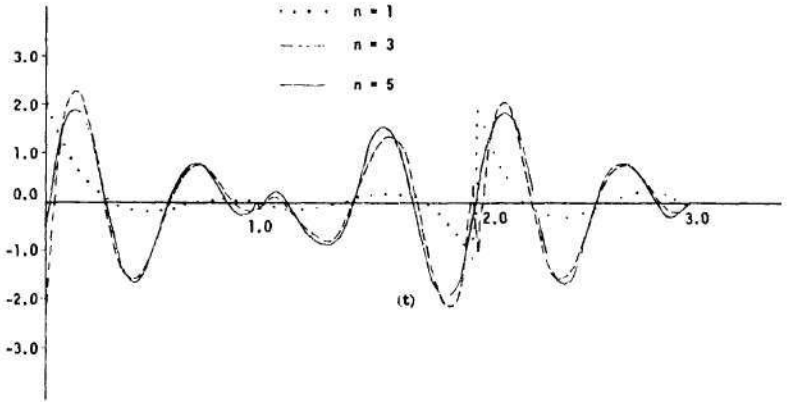

Figure 3.8. Approximation for $v_1(t, 2/3)$ for n = 1,3,5; m = 1. The Spline for n = 1 Lacks Sufficient Flexibility to Conform to the Input Function and a Discontinuity Results at t = 2. Approximations for n = 3 and n = 5 are Nearly Identical and the Discontinuity at t = 2 Disappears. The Actual Input Function is Indiscernible from the Approximation for n = 5.

Figure 3.9 shows the corresponding power spectra of these time series. The spectrum for n = 1 has peaks at the correct frequencies, but the discontinuities have introduced noise throughout the spectrum. This is evidenced greatest by the higher frequency content, which this spline approximation is incapable of producing. Spectra for n = 3 and n = 5 are essentially identical with the true spectrum.

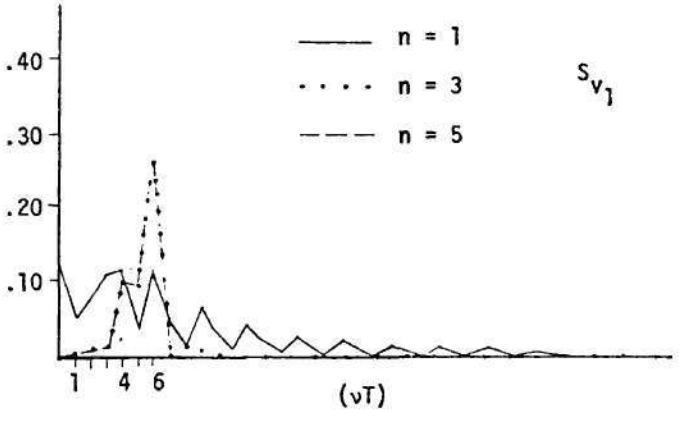

Figure 3.9. Power Spectra of Approximations for $v_1(t, 2/3)$ for Temporal Partition Numbers n = 1,3, and 5. Broad Band Noise for n = 1 Primarily Due to Substantial Discontinuity (see Figure 3.8). Power Spectra for n = 3 and 5 are Essentially Identical and Identical with the Power Spectrum of the Actual Input Function.

We now perform a similar decomposition: $v_2(t,z)$ and $v_3(t,z)$ are as before, but now allow $v_1(t,z)$ to have two widely separated spectral components (as may be expected in a true wind field):

$$v_1(t,z) = \sin(2\pi t) + \sin(12\pi t)$$

The approximation for n = 3 and the true behavior of $v_1(t,1/2)$ are shown in Figure 3.10. Again the approximation is incapable of conforming to

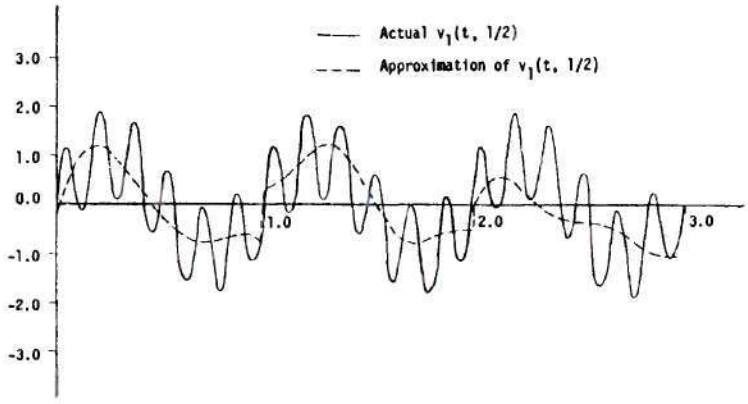

Figure 3.10. Actual and Approximate Values for $v_1(t, 1/2)$. Actual Input Function $v_1 = \sin(2\pi t) + \sin(12\pi t)$; Temporal Partition Number $n = 3$.

6 cycles over any strip of length T = 1. Yet aside from the discontinuities at the boundary points: t = 1 and t = 2 (data points were not projected into adjacent regions), the approximation is the one most desirable - it indicates the general trend of $v_1(t, 1/2)$. The associated spectra reinforce this (Figure 3.11). Except for the peak missing at the higher unattainable frequency, the predicted spectrum is very close to the true spectrum. Even without projecting data points into adjacent regions, the discontinuities are not excessive and produce only a very small amount of noise in the spectrum. This is very important; not only is the decomposition spectrally unbiased, but also this indicates that inability of the approximation functions to represent higher frequency content of the velocity field (as will surely be the case in actual wind data) does not distort the spectrum at frequencies that can be represented.

It should be noted that when used on actual data, the only means of evaluating the error in the approximation is relative to the

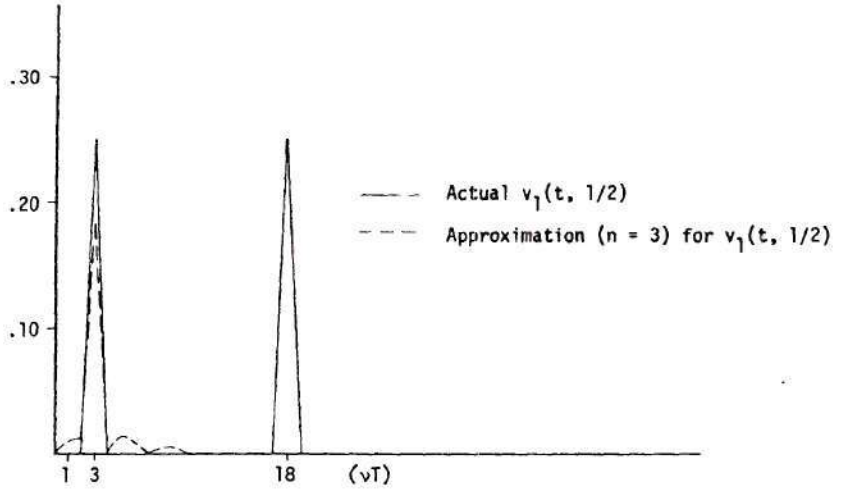

Figure 3.11. Power Spectra of Actual and Approximate (n = 3) Velocity Function $v_1(t, 1/2)$. The Spectrum of the Approximate Function is very Close to that of the True Function except for the Higher Frequency Spike which the Approximation is Incapable of Reproducing.

observations in V_L, i.e., linear combinations of the $v_k(t,z)$. Even this may be quite large. In the previous example, where a large portion of the spectral content was unrepresentable, $\sigma_{v_1}^2$ was roughly 50% of the maximum value achieved by $v_1(t,z)$. Despite this, the approximation yields the appropriate trend. In general, we expect the true wind field to have contributions (possibly quite substantial) from frequencies that neither the observations nor the approximations are able to resolve. Therefore the variance of the data about the approximation, $\sigma_{v_L}^2$, is a questionable criteria for the reliability of the approximation.

3.4 Final Results

The finite element method was used to decompose meteor wind data taken at Georgia Tech over the 8-day period from July 19, 1975 to July 26, 1975. The height range considered was from 70 km to 120 km.

The period was divided into 8 one-day strips, each of which was augmented by 8 hours on either side and then partitioned into 7 intervals along the time axis and 1 along the vertical (i.e., $T = 24$ hr, $\Delta T = 8$ hr, $n = 7$, $m = 1$). Thus we expect no spectral resolution of periods shorter than roughly 40/7 or 5.7 hr. A typical time trace of the resulting approximation $v_1(t, 100\ \text{km})$, is shown in Figure 3.12. Figures 3.13 - 3.14 show power spectra for the horizontal velocity components at the heights 80, 90, and 100 km. There is marked spectral content at 24, 12, and 8 hrs., but there are also striking features in the vicinities of 96, 48, 32, 19.2 and 13.7 hrs. The total velocity power spectrum was obtained by adding the power spectra for the three components. These are shown in Figure 3.15 for the three heights considered. Among other features, the spectral content in the vicinity

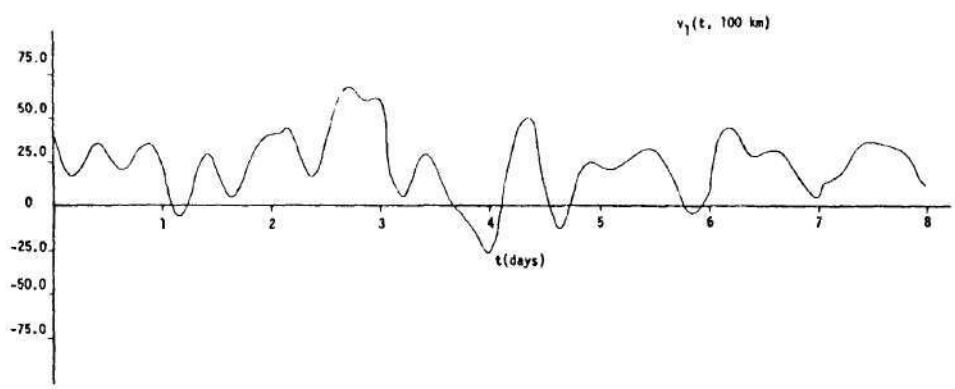

Figure 3.12. Approximation for Zonal Velocity v_1 at $z = 100$ km over 8-Day Sample Period: July 19 - July 26, 1975.

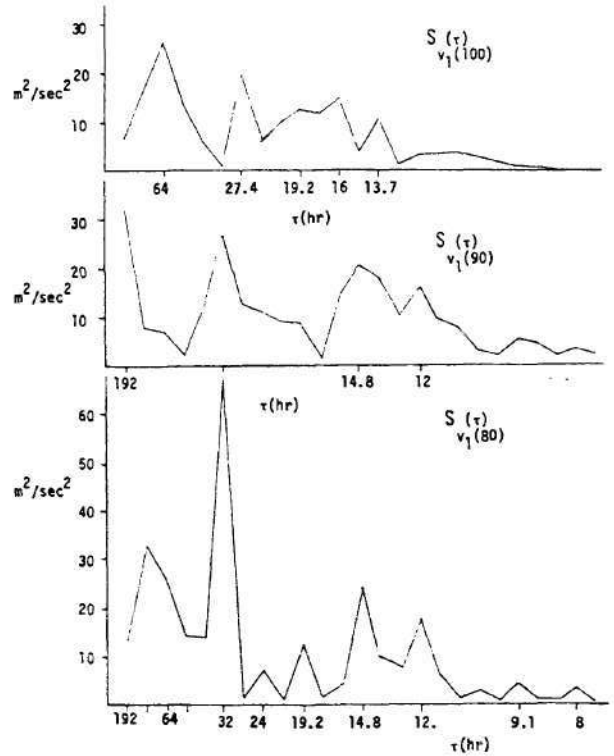

Figure 3.13. Power Spectra of Zonal Velocity Approximation $v_1(t,z)$ at the Heights 80, 90, and 100 km for the Period July 19 - July 26, 1975.

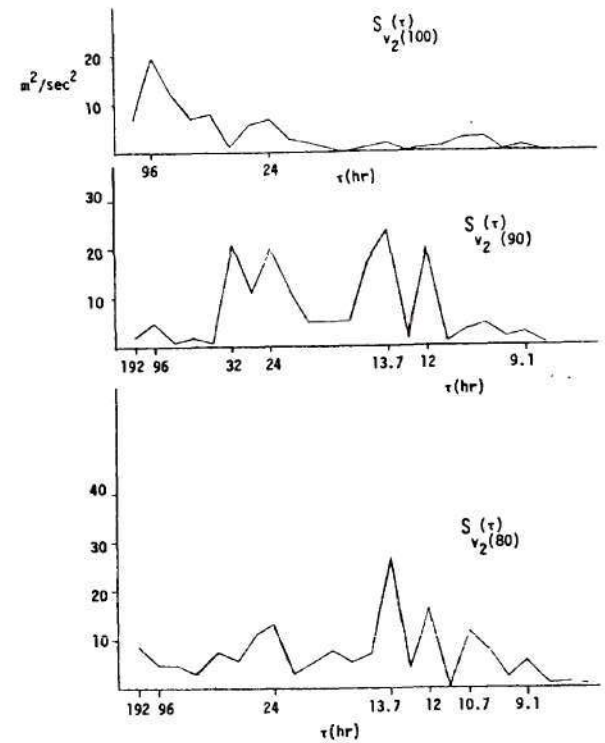

Figure 3.14. Power Spectra of Meridional Velocity Approximations $v_2(t,z)$ at the Heights 80, 90, and 100 km for the Period July 19 - July 26, 1975.

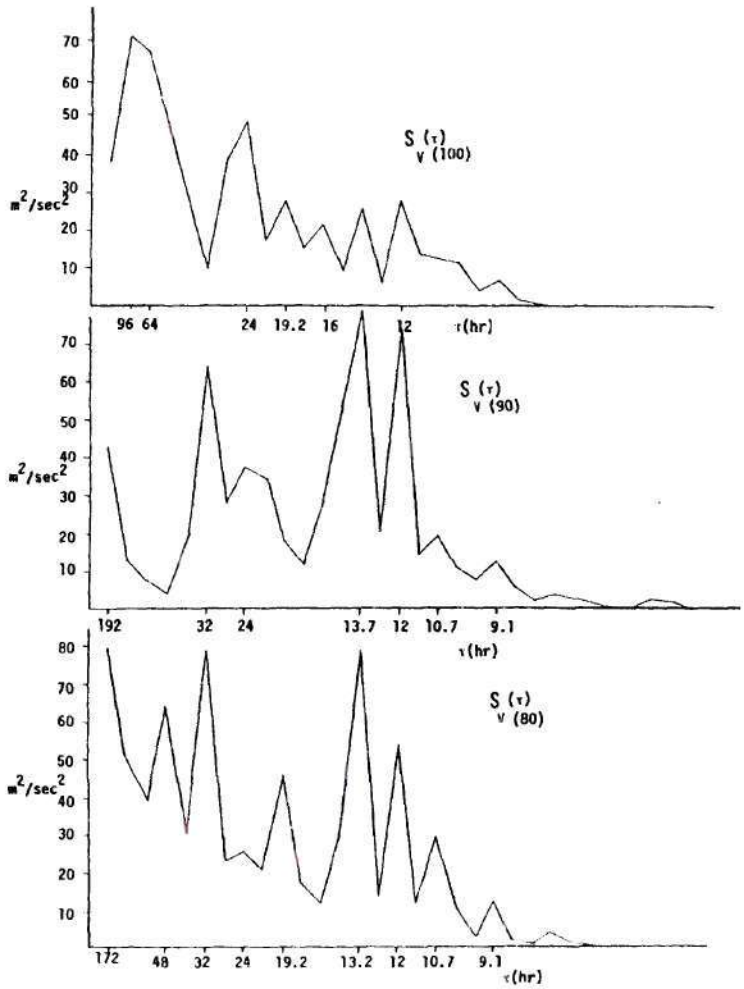

Figure 3.15. Total Velocity Power Spectra at the Heights 80, 90, and 100 km for the Period July 19 - July 26, 1975.

of 24 hours seems to increase monotonically with height (see Roper, 1972). The 12 and 32 hr. contributions are also striking.

CHAPTER IV

ANALYSIS OF OBSERVATIONS AND COMPARISON WITH THEORY

4.1 Limitations of the Data

The method developed in the previous chapter is suitable for meteor wind data with regions of sparse observations and/or gaps in the data. The technique extrapolates the information into these regions from those where it occurs in greater abundance. There is, of course, a limit to the sparsity of observations and size of the gaps beyond which neither this nor any technique of comparable utility will suffice. Now in standard constant mesh spectral analyses, a compromise must be reached between spectral resolution, $\nu = \nu_{min} = \frac{1}{T}$, dictated by the sample period T, and the high frequency limit, $\nu_{max} = \frac{1}{2\Delta t}$, determined by the time increment, Δt. For all but possibly the first modes, $n = m$, of interest to this investigation, sample periods of at least 20 days will be required, and 40 days would be more reasonable. However, the two effects just mentioned compete with each other in the Georgia Tech data primarily due to irregularly spaced gaps of random length. The investigation is restricted to data samples of suitable length that have no gaps larger than Δt. Because of this, it proves useful to divide the spectral studies into two categories according to the frequency range

(i) $[\frac{1}{3}, 1]$ cycles/day

(ii) $[0, \frac{1}{3}]$ cycles/day

Shorter samples and finer partitions can be used for the former, and larger gaps may be allowed in the latter. In each, the high frequency limit in the spectrum is dictated by the size of the partition used in decomposition, i.e., the maximum gap size. The partition acts as a low pass filter, and the spectra will have a high frequency roll off.

4.2 Detrending

Standard spectral techniques will be employed for analysis of the data. Unfortunately, it is usually quite evident (see Figure 4.1) that the time series contain substantial trends which must be removed in order that these be used. These trends are either seasonal in nature or due to longer period waves which cannot be resolved in the given sample period.

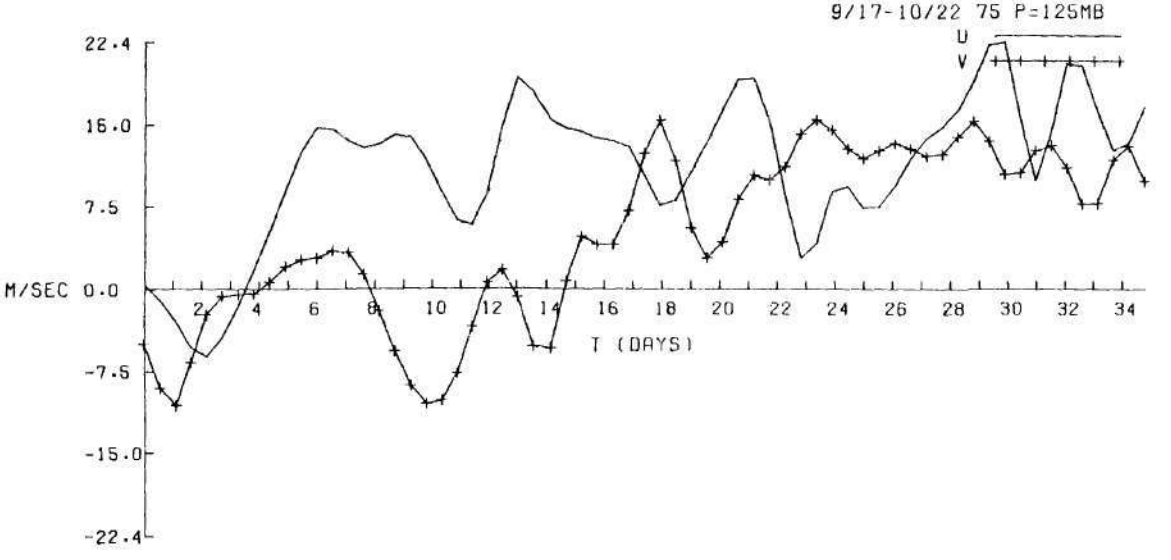

Figure 4.1. Typical Trends Appearing in Velocity Time Series.

The trends will be assumed to be piecewise quadratic and hence, may be removed by differentiation. Practically, however, there is a limit to how many times this may be done without altering the spectral content, because of discretization. The velocity functions may be written as

$$u(t) = at^2 + bt + c + \sum_{k=1}^{n/2} f_k e^{i\frac{2\pi k}{T}t} \tag{4.1}$$

where $S_{|u|^2} = \frac{|f_k|^2}{2}$ is the power spectrum of u at the kth frequency. The mth derivative is approximately

$$u^{(m)}_{(t)} = \frac{\hat{u}^{(m)}(t)}{h^m} \tag{4.2.1}$$

where $\hat{u}^{(m)}$ is the mth difference and h is the difference interval. Hence the mth difference of u is

$$\hat{u}^{(m)} = h^m (at^2 + bt + c)^{(m)} + h^m \left(\frac{i2\pi}{T}\right)^m \sum_{k=1}^{n/2} f_k k^m e^{i\frac{2\pi k}{T}t} \tag{4.2.2}$$

Assuming the trend to be eliminated, the power spectrum of this new function, $\hat{u}^{(m)}$, is recognized as

$$S_{|\hat{u}^{(m)}|^2} = \frac{1}{2} \left| \left(\frac{i2\pi}{T}\right)^m h^m k^m f_k \right|^2 \tag{4.3.1}$$

or

$$S_{|\hat{u}^{(m)}|^2} = \left(\frac{2\pi}{T}\right)^{2m} h^{2m} k^{2m} \frac{|f_k|^2}{2} = \left(\frac{2\pi kh}{T}\right)^{2m} S_{|u|^2} \tag{4.3.2}$$

By taking

$$h = \Delta t = T/n \tag{4.4}$$

the original spectrum (recolored) in terms of that of the differenced function is

$$S_{|u|^2} = \left(\frac{n}{2\pi k}\right)^{2m} S_{|\hat{u}(m)|^2} \tag{4.5}$$

In a similar fashion, the magnitude and argument of the cross spectrum between two time series, u and v, are related to those of the differenced series by

$$\begin{cases} |S_{uv}| = \left(\frac{n}{2\pi k}\right)^{\ell+m} |S_{\hat{u}(\ell)\hat{v}(m)}| & (4.6.1) \\ \arg\{S_{uv}\} = \arg\{S_{\hat{u}(\ell)\hat{v}(m)}\} + (m-\ell)\frac{\pi}{2} & (4.6.2) \end{cases}$$

4.3 Wind Spectra and Analysis

Before proceding with any comparisons between observations and the results of Chapter II, the angular velocity, A, of the atmosphere must be specified. Now as already mentioned, the variation of mean zonal wind is a small perturbation on the rotational velocity of the earth i.e., to zero order the atmosphere rotates with the earth as a unit. Figure 4.2 shows the zonal velocity as a function of height and latitude and seems to indicate that even the vertical and global mean of the perturbation is near zero. Therefore A will be ignored and $\hat{\Omega} \cong \Omega$.

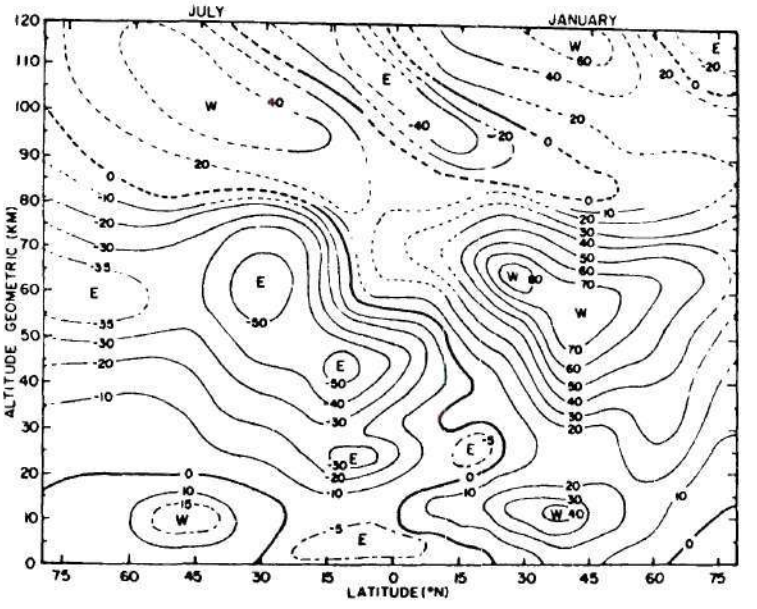

Figure 4.2. Mean Zonal Velocity as a Function of Latitude and Height (after Groves, 1971, p. 72).

Data samples suitable for either category (i) or (ii) were decomposed into the velocity functions. Now this decomposition distributes the error uniformly among the three components, and since the vertical velocity is expected to be appreciably smaller than the horizontal components, it will likely be buried in the error. Therefore, w' will be neglected in future discussion.

Time series of u' and v' were obtained at different heights using the results of the decomposition. After detrending by differencing an appropriate number of times, a standard Fast Fourier transform technique (IMSL, 1977, FTFFT1) was used to provide spectral estimates of the horizontal velocities. Of particular interest to this investigation is discrete spectral content associated with the two vertically propagating modes discussed in Chapter II. Of course, a

true indication of this would require simultaneous observations at different locations in order to identify the horizontal structure. Unfortunately, the Georgia Tech facility may be the only meteor radar making somewhat continuous observations of the meteor region. Thus the latter are not at our disposal at this time, and we must rely on the temporal variations alone. Discrete modes may appear as coincident spikes in the spectra of u' and v'. However, this certainly is not necessary. Examination of Figure 2.10 reveals that the latitudinal dependence of u' and v' may differ widely from one mode to another. In particular, the amplitude of v' may be quite small relative to that of u' if the point of observation is near a node of $\hat{V}$. Thus the spectra of u', $S_{|u|^2}$, may exhibit a substantial spike while the corresponding peak in $S_{|v|^2}$ is buried in the noise. This effect is enhanced when the spectral resolution is not comparable to the spectral distance between different modes. The reader may recall that for large values of $(n - m)$ the eigenfrequencies lie on the asymptotic branch of LTE corresponding to equation 1.3. In contrast to typical problems of this sort where the frequencies are increasing in the mode index, these eigenfrequencies behave as $1/n$ for large n and become closer and closer with increasing n. Thus, although the sample length may be sufficiently long to estimate the spectral content from several modes, it may be too short to resolve the content between them. The result of several modes of nearly identical frequency would be blending of the corresponding peaks, and the spectrum might display a gradual maximum rather than a spike because of leakage to adjacent frequencies. Figure 4.3 displays several of these features.

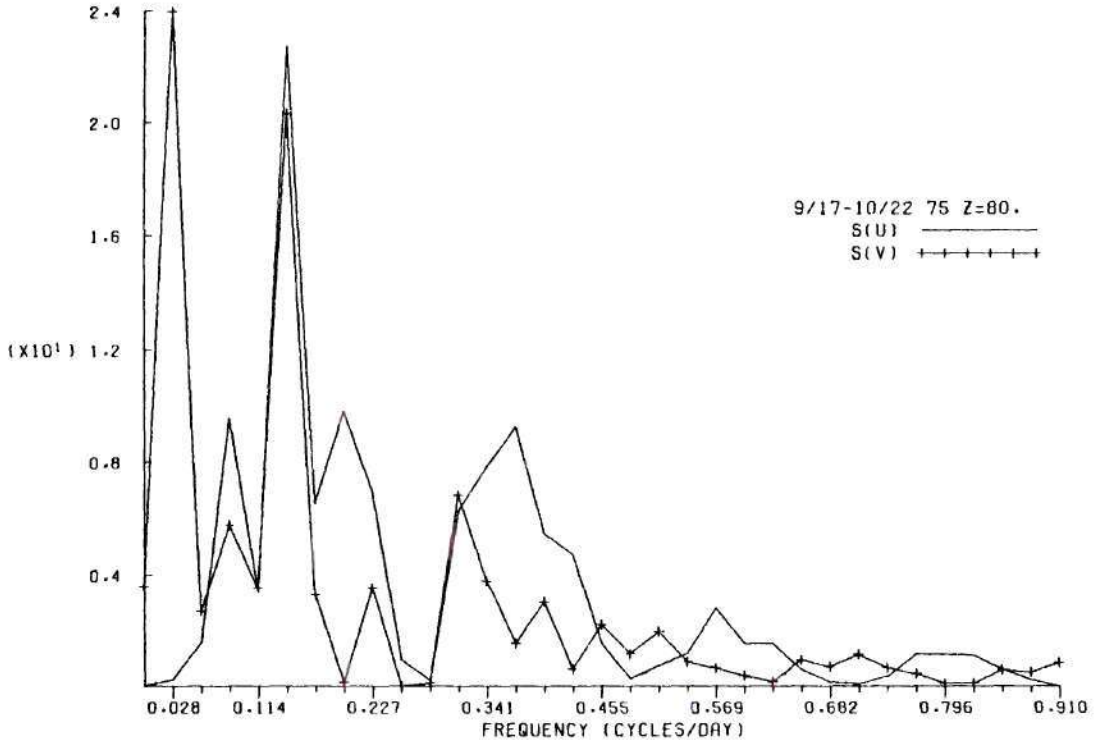

Figure 4.3. Power Spectra of u, S(u), and S, S(v).

In an attempt to alleviate these difficulties, the cross spectrum between u' and v' will be examined. Since it is the complex product of the transforms of u' and v', it should have greater reliability in exhibiting discrete spectral content than either of the individual power spectra. The argument also gives the phase between u' and v'. Unfortunately, it does little to obviate the problem of distinguishing between adjacent modes. Beneath the spectra presented, are two bars corresponding to the vertically propagating modes, $k = 1,2$. The spectral lines underneath the bars represent the eigenfrequencies for the modes (m,n), $m = 1,2,3,4,5$, $n - m = 0,1,2,3,4,5$, and those above represent the doppler shifted values due to local zonal mean over the

sample. Now in the presence of moving media, the frequency relative to the source remains invariant, the intrinsic frequency being doppler shifted (see Bretherton and Garret, 1969, p. 212). Thus the lower lines should be compared with the spectrum; the doppler shifted frequencies have been presented for comparison with critical levels. (The lower spectral lines are easily identified by recalling that for fixed m and k, ω_{mn}^{k} is monotone decreasing in n.) However, if the source of the disturbance is in motion, e.g., baroclinic instability travelling with the mean, the appropriate frequencies will be doppler shifted. This is one source of uncertainty. A more important cause of discrepancy is the neglect of the vertical wind variation, which is known to alter the vertical index of refraction. The pair of values of ID shown on the spectra, represent the differencing order of u' and v', i.e., ℓ and m respectively from Section 4.2. If only one value is indicated, the two were equal.

The results from data samples of category (i) will be presented first. Figures 4.4 - 4.9 show the magnitude squared of cross spectra of u' and v' at heights 80, 90, and 100 km. For the most part these data samples are long enough to allow identification of only the first modes, $n = m$.

It should be kept in mine that the high frequency rolloff is dictated by the partition size used in decomposition and not by aliasing, and this may vary from sample to sample.

Figure 4.4 indicates possible contribution at 80 km from all of the lowest modes (m,m,k), $m = 1,2,3,4,5$ $k = 1,2$. The highest frequency content is probably of tidal original. The

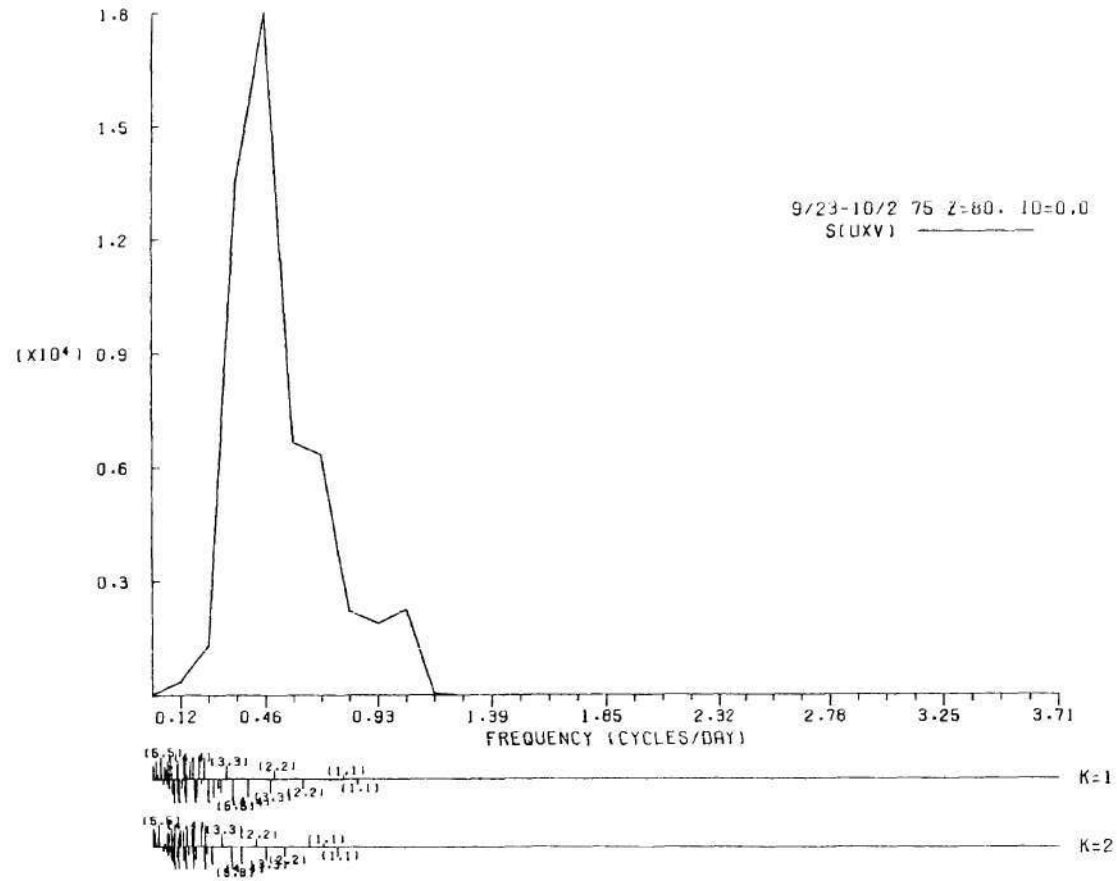

(a) 80 km

Figure 4.4. Magnitude Squared of the Cross Spectrum Between u and v for Autumn.

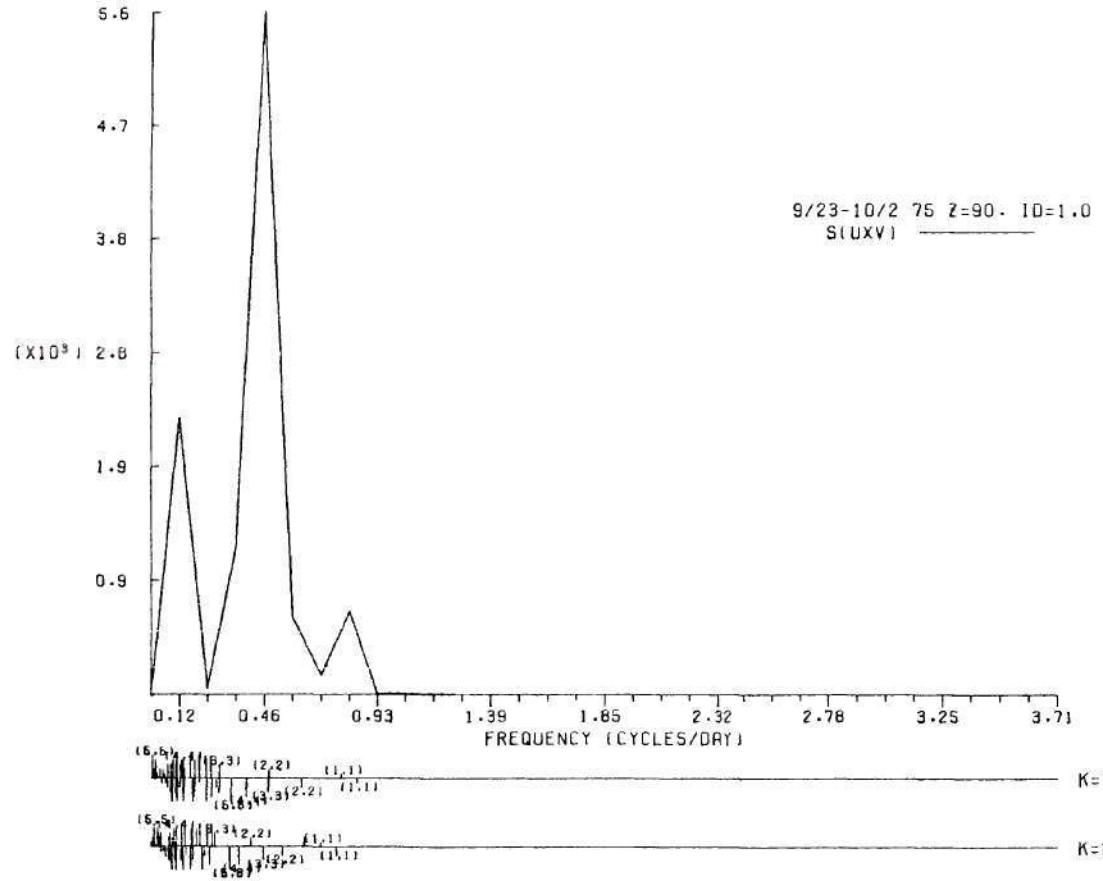

(b) 90 km

Figure 4.4. (Continued)

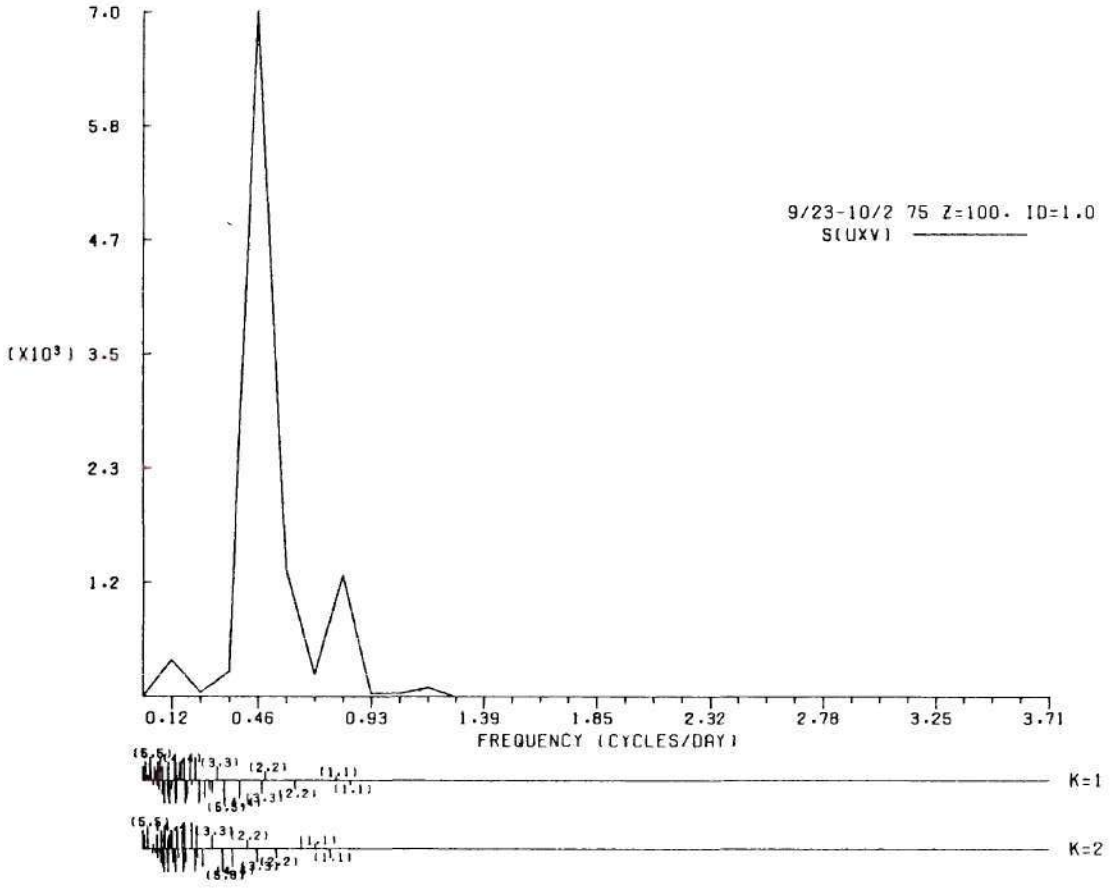

(c) 100 km

Figure 4.4. (Continued)

spectral content appears to become more discrete with increasing height, but is not monotone in height. The spectra at 90 and 100 km seem to implicate either of the (3,3) modes of roughly a 2-day period. This leads one to believe that they are responsible for the peak at 80 km as well. Possible contribution from the (1,1) horizontal modes appears more distinct at these heights also, the (1,1,1) mode being nearest to the peak. The phases of the cross spectra at the peak frequency (.46 cycles/day) for the heights 80, 90, 100 km are 204, 280, and 205 degrees respectively.

Figures 4.5 a and b show time traces at 80 and 90 km for a similar time of year. The 80 km series indicates a regular oscillation of roughly a 2-day period superimposed upon a much longer period trend.

The latter part of the trace exhibits an apparent change in the spectral content (cf., discussion p. 99). Unlike the trend, this type of nonstationarity is difficult if not impossible to compensate for. If the time scale of the frequency modulation is large compared with the length of the sample, the spectra will be unaffected. This is not the case here, and unfortunately, this phenomenon is not restricted to this sample alone. The 90 km trace indicates substantially lower frequency content. Cross spectra of these are shown in Figure 4.6. Again, the (3,3) modes appear to be associated with the 2-day periodicity at 80 km;the corresponding phase is 279 degrees. The absence of higher frequency content is due to a larger partition size than that of the previous sample. At 90 km this peak has vanished as

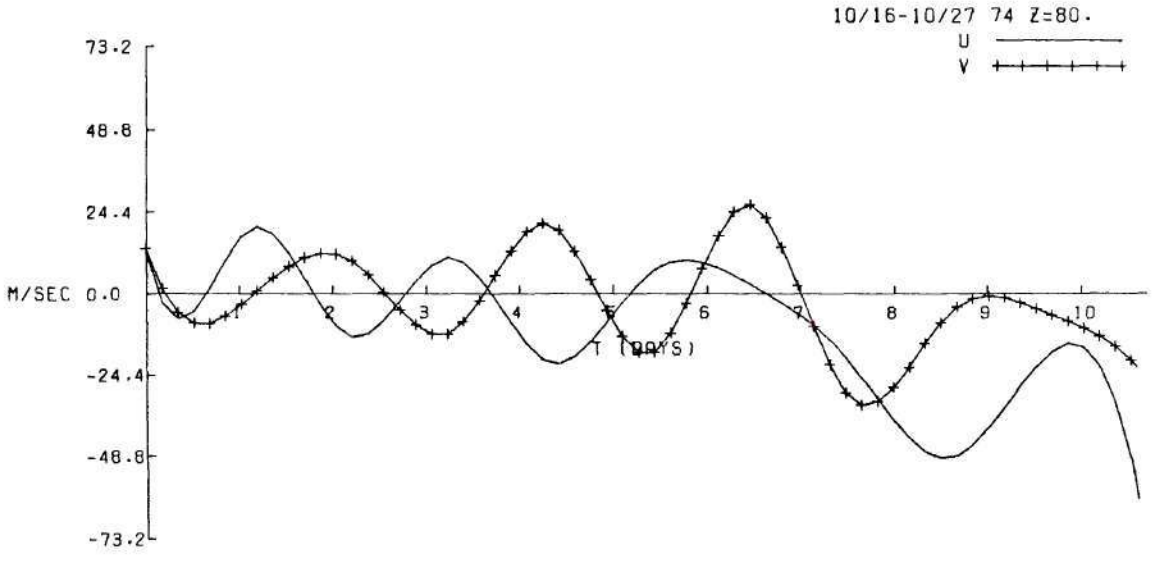

(a) 80 km

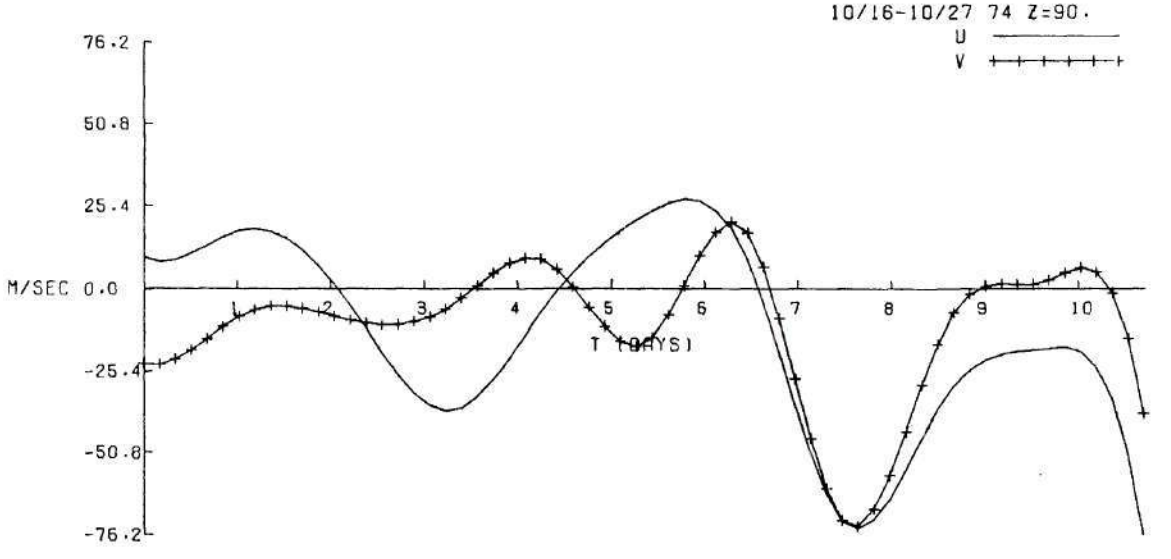

(b) 90 km

Figure 4.5. Time Traces at 80 amd 90 km.

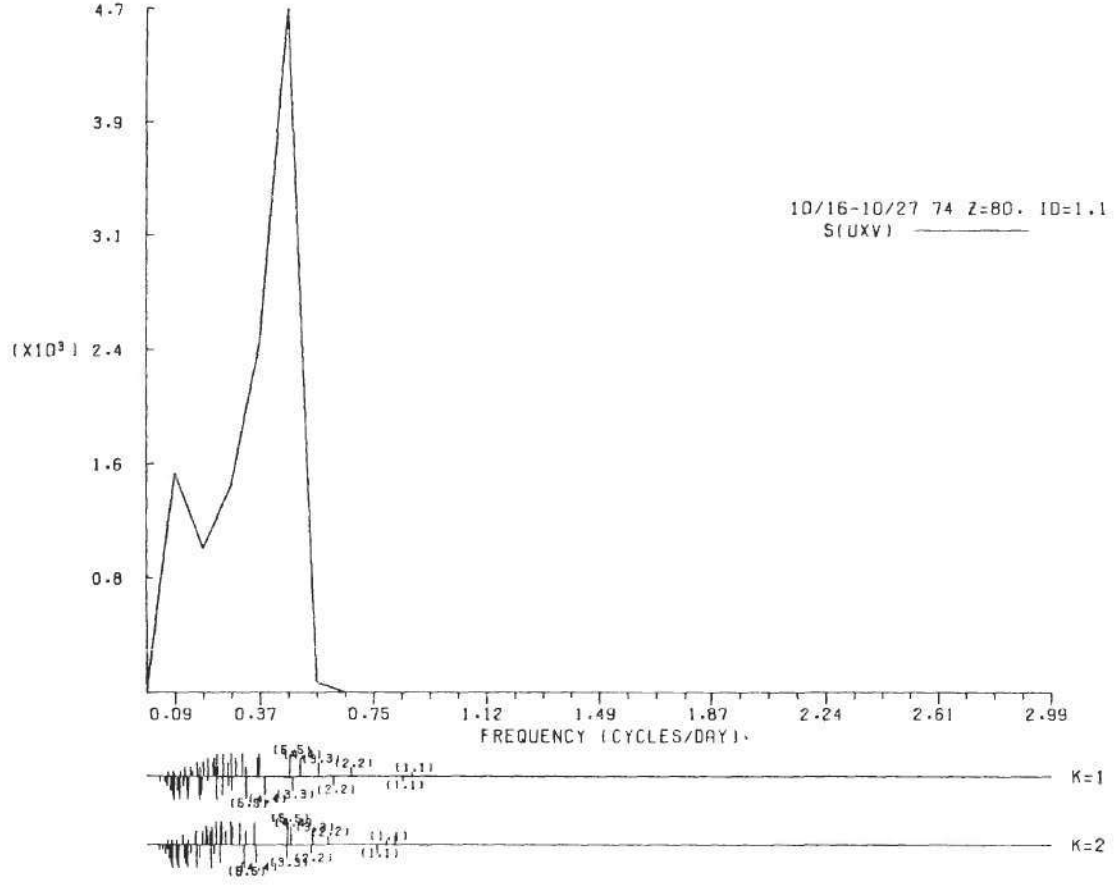

(a) 80 km

Figure 4.6. Magnitude Squared of the Cross Spectrum Between u and v for Autumn.

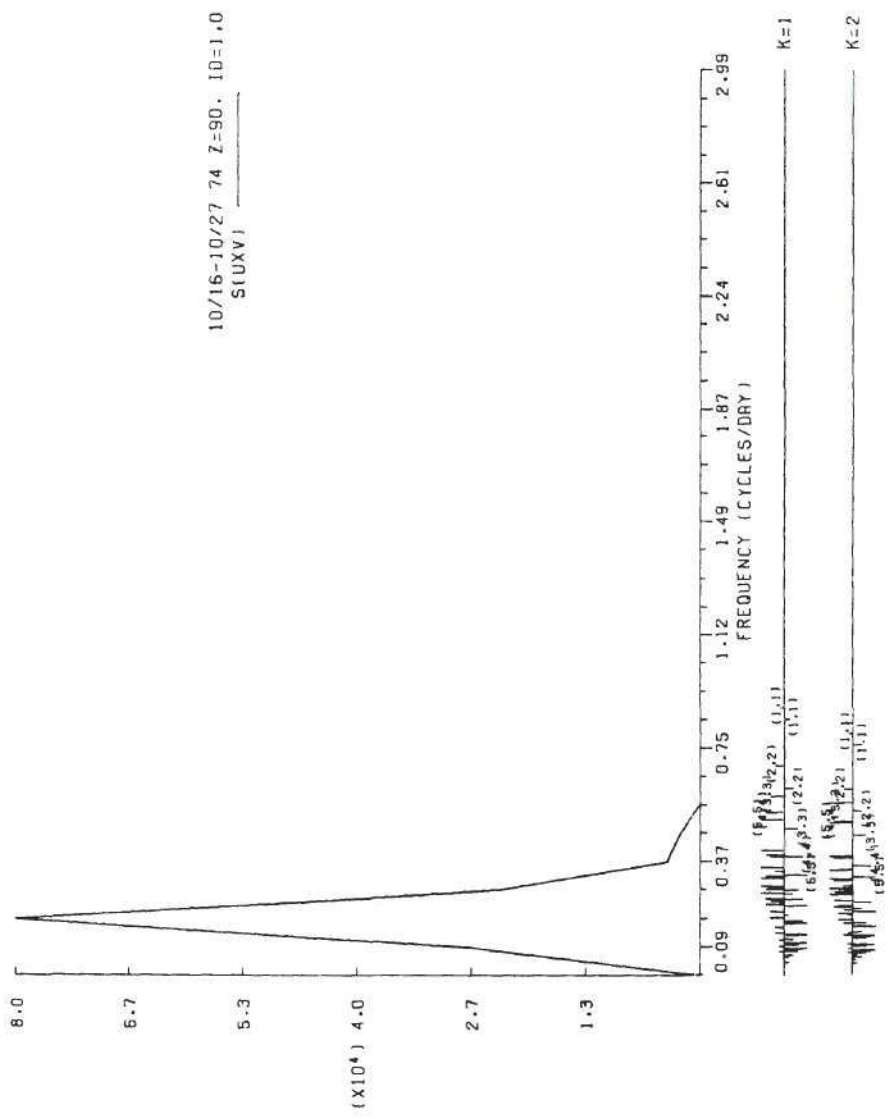

(b) 90 km

Figure 4.6. (Continued)

indicated by the time trace, and the lower frequency content has increased significantly. This effect is probably due to zonal wind variation.

A late fall sample, Figure 4.7, also indicates evidence for the (3,3) modes. The second peak may be attributed to any of the (2,3) or (4,5) modes. As in earlier samples, a large portion of the spectral content appears at the lowest frequency. There also appears to be some evidence of the (2,2,1) mode.

Figure 4.8 shows the results of an early winter sample when one expects strong transient forcing from the lower atmosphere. The amplitudes of these spectra are not significantly greater than those of earlier samples which may indicate insensitivity or at least a lag in the response of the upper atmosphere to action in the lower atmosphere. The 80 km spectrum appears more discrete than the previous periods and indicates evidence of the (1,1,1), (3,3) and (2,2) modes. These peaks are dwarfed by the lower frequency content near the mesopause (of phase 248 degrees) which is subsequently diminished at 100 km. This may be related to the behavior of the second mode near $\zeta = 13$ (cf., Figure 2.8 a, c). The (1,1,1) and (2,2) modes appear to emerge strong at this level along with the diurnal tide. The spectra associated with the (2,2) modes have phases of 292, 341, and 282 degrees at the heights 80, 90, and 100 km respectively.

Finally, Figure 4.9 contains results of a sample in early summer, when the lower atmosphere exhibits relative calm. These spectra are of smaller amplitude than those of previous samples, and seem to contain

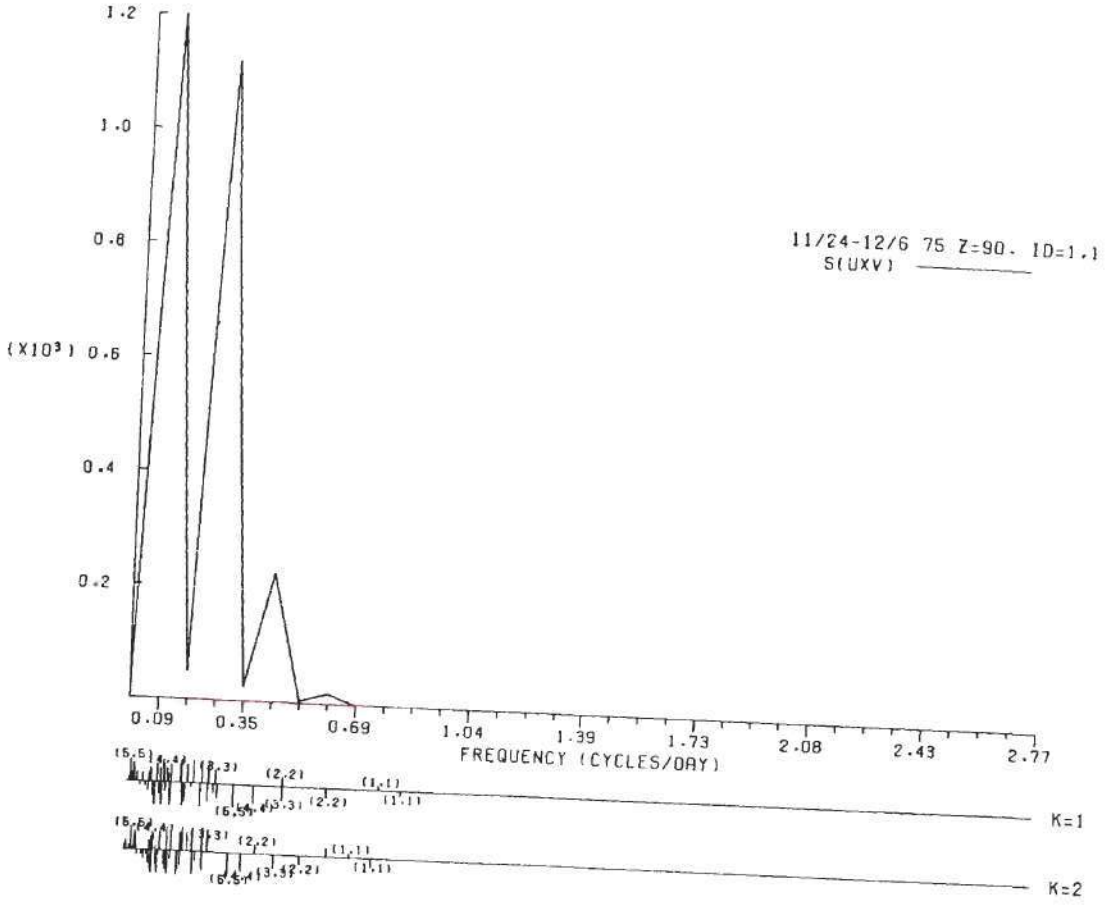

Figure 4.7. Magnitude Squared of the Cross Spectrum Between u and v for Late Autumn (90 km).

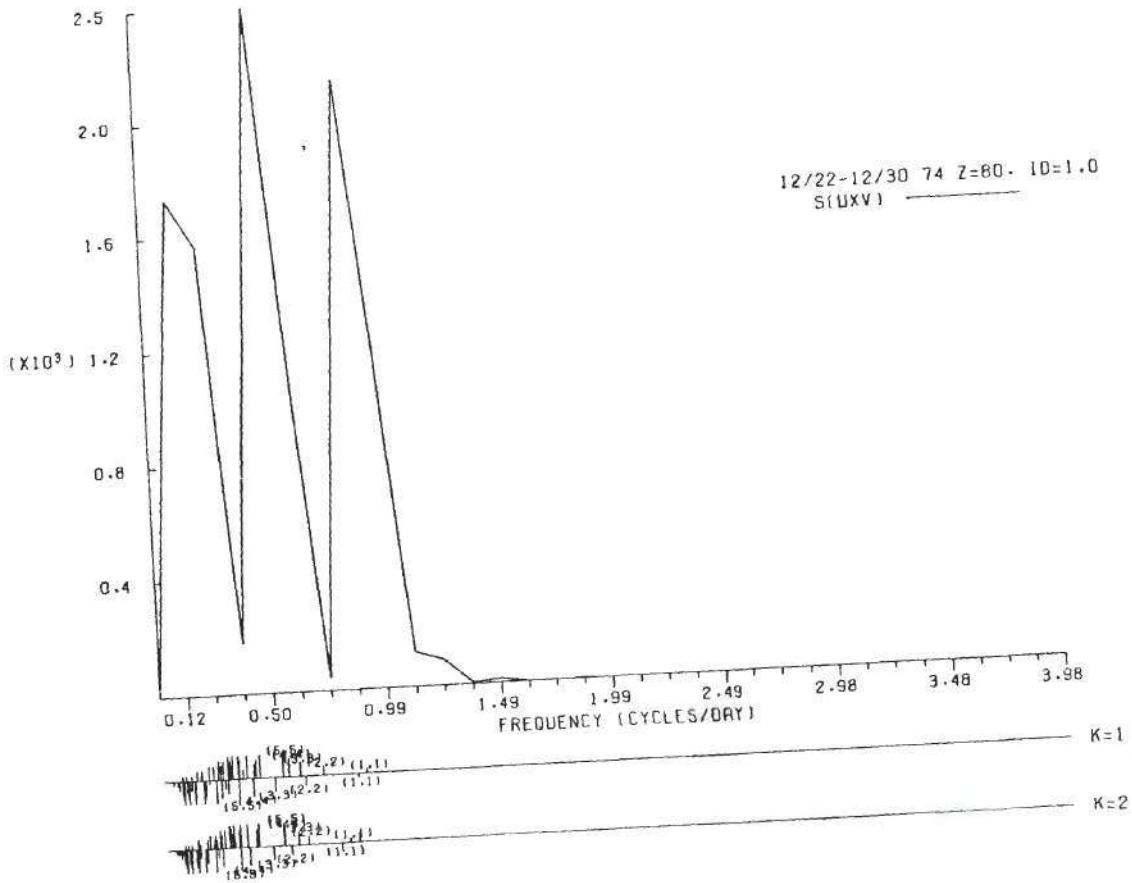

(a) 80 km

Figure 4.8. Magnitude Squared of the Cross Spectrum Between u and v for Winter

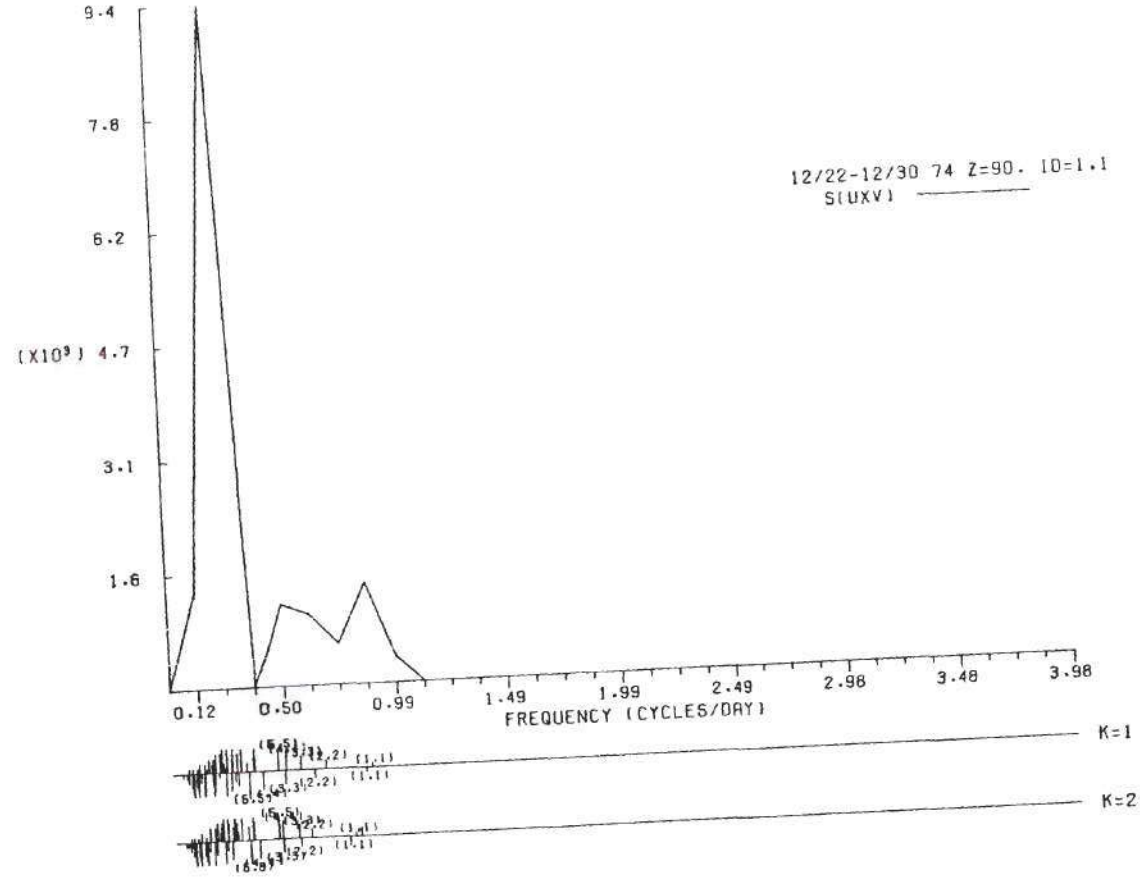

(b) 90 km

Figure 4.8. (Continued)

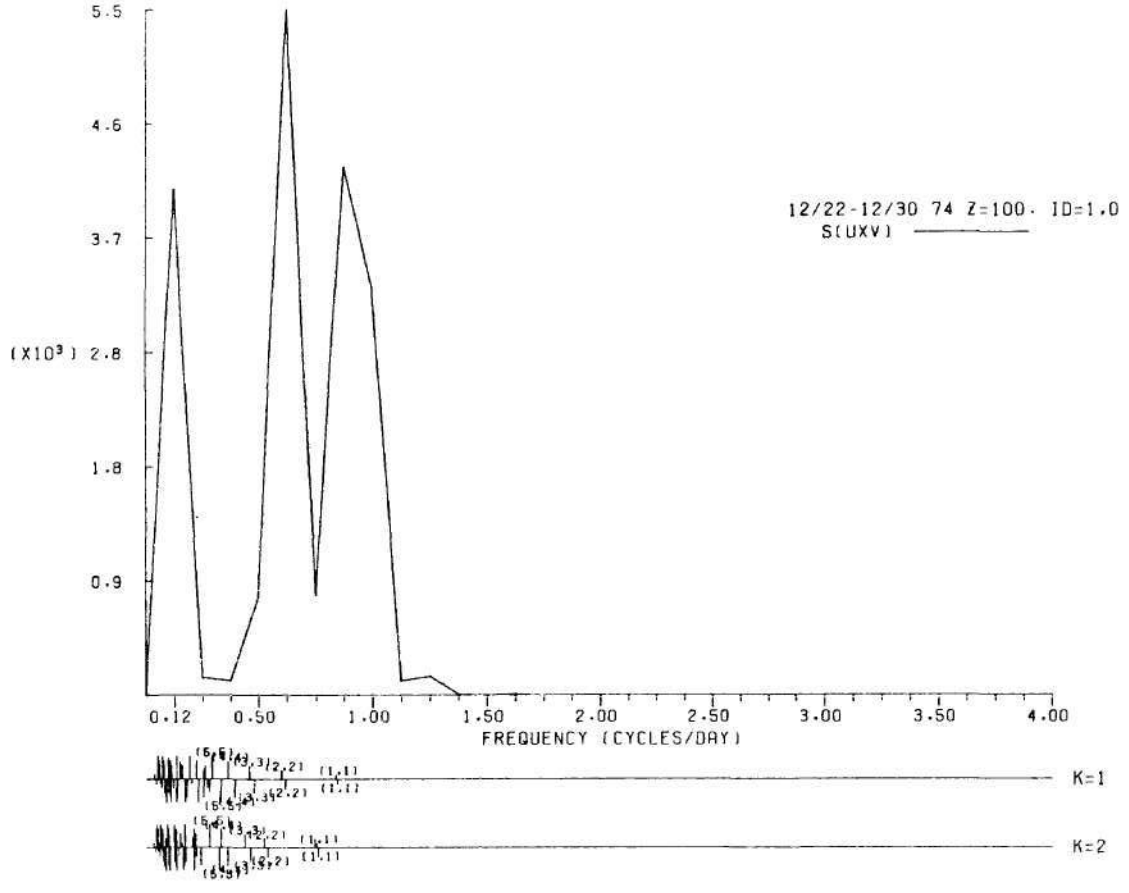

(c) 100 km

Figure 4.8. (Continued)

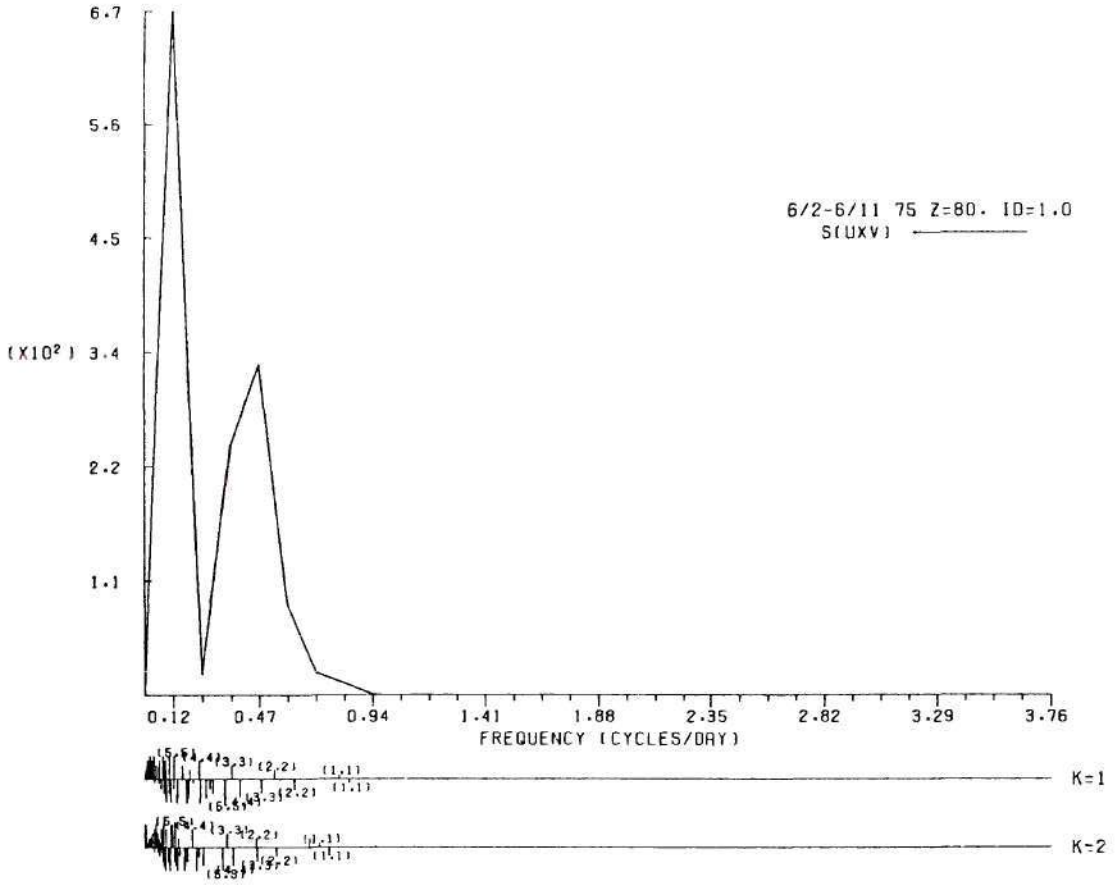

(a) 80 km

Figure 4.9. Magnitude Squared of the Cross Spectrum Between u and v for Summer.

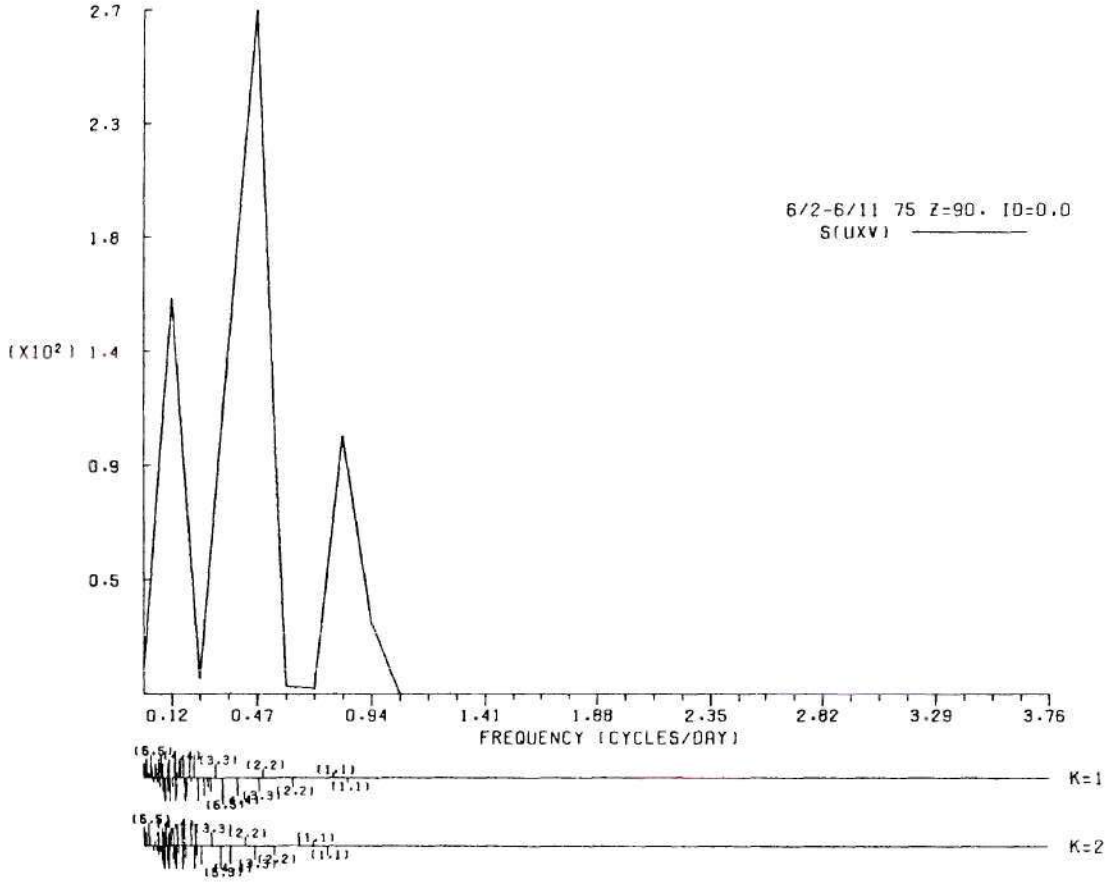

(b) 90 km

Figure 4.9. (Continued)

evidence of the (2,2), (3,3), (4,4) and (5,5) modes at 80 km. However, the 90 km spectrum appears to narrow the field down to the (3,3) modes with additional content from either (4,4) or (5,5). The (1,1) modes also appear prevalent at this altitude. The phases of the spectra associated with (4,4) and (5,5) at 80 and 90 km are 227 and 317 degrees respectively.

Results for category (ii) data samples will now be presented. In addition to observations from the meteor region, wind spectra are also computed from rawinsonde data at pressure heights in the lower stratosphere.

Figure 4.10 shows cross spectra for a period during autumn. Most of the spectrum at 125 mb is dwarfed by the values at the lowest frequency which may be associated with the (1,6) and (1,7) modes as well as those of higher index than is shown. The adjacent peaks may be related to the (3,8), (4,9), (5,10) and the (3,5), (4,6), (5,7) and (1,2,2) modes respectively. At 80 km the spectrum is quite different, displaying a sharp spike at .14 cycles/day an order of magnitude larger than the largest peak at 125 mb. This peak of phase 285 degrees, may be related to the (2,4,2) mode. Other spectral peaks may be associated to the (3,8), (4,9), (5,10) modes at .08 cycles/day with corresponding phase of 313 degrees, the (5,6,1) and (2,3,2) at .23 cycles/day and the (5,5) and (4,4) modes at .30 and .40 cycles/day. The phases of the latter two are 265 and 240 degrees respectively. Once again the spectrum near the mesopause is diminished in magnitude from that at 80 km. Spectral content at other frequencies has become more pronounced.

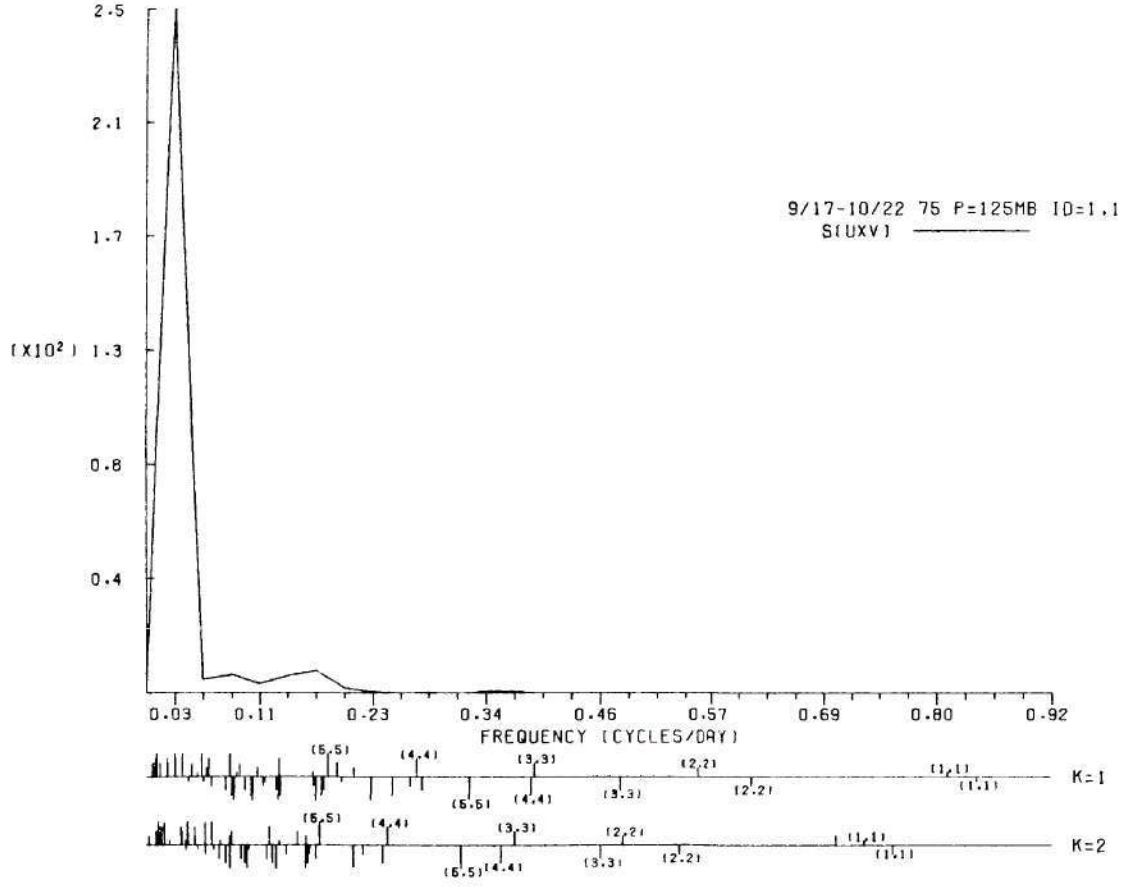

(a) 125 mb

Figure 4.10. Magnitude Squared of Cross Power Spectrum Between u and v for Autumn.

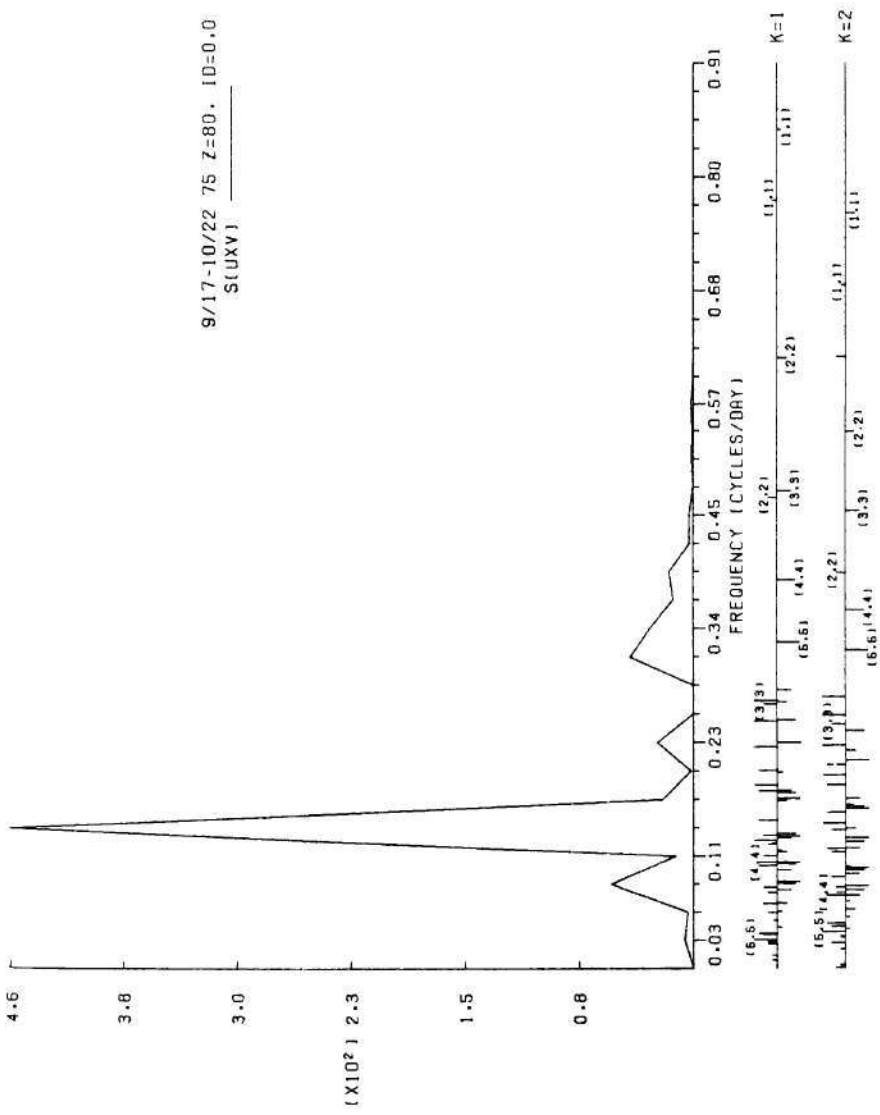

(b) 80 km

Figure 4.10. (Continued)

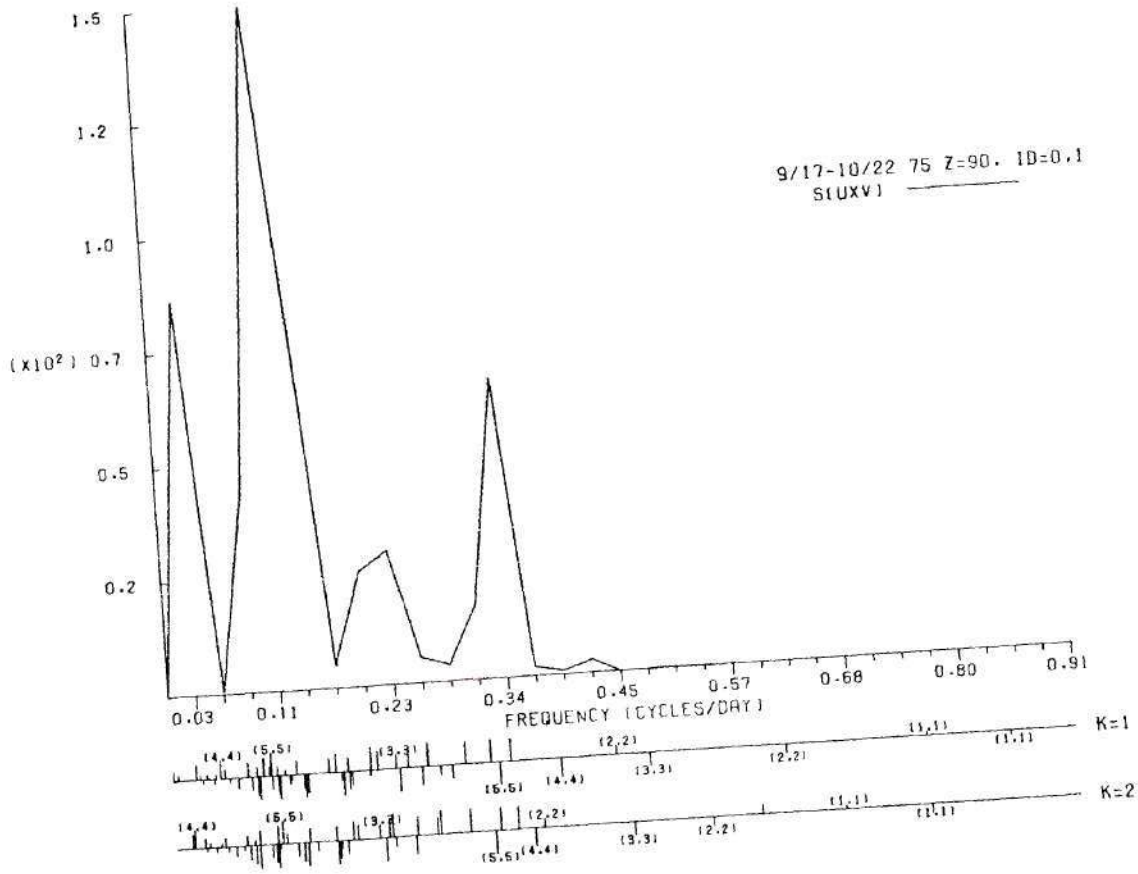

(c) 90 km

Figure 4.10. (Continued)

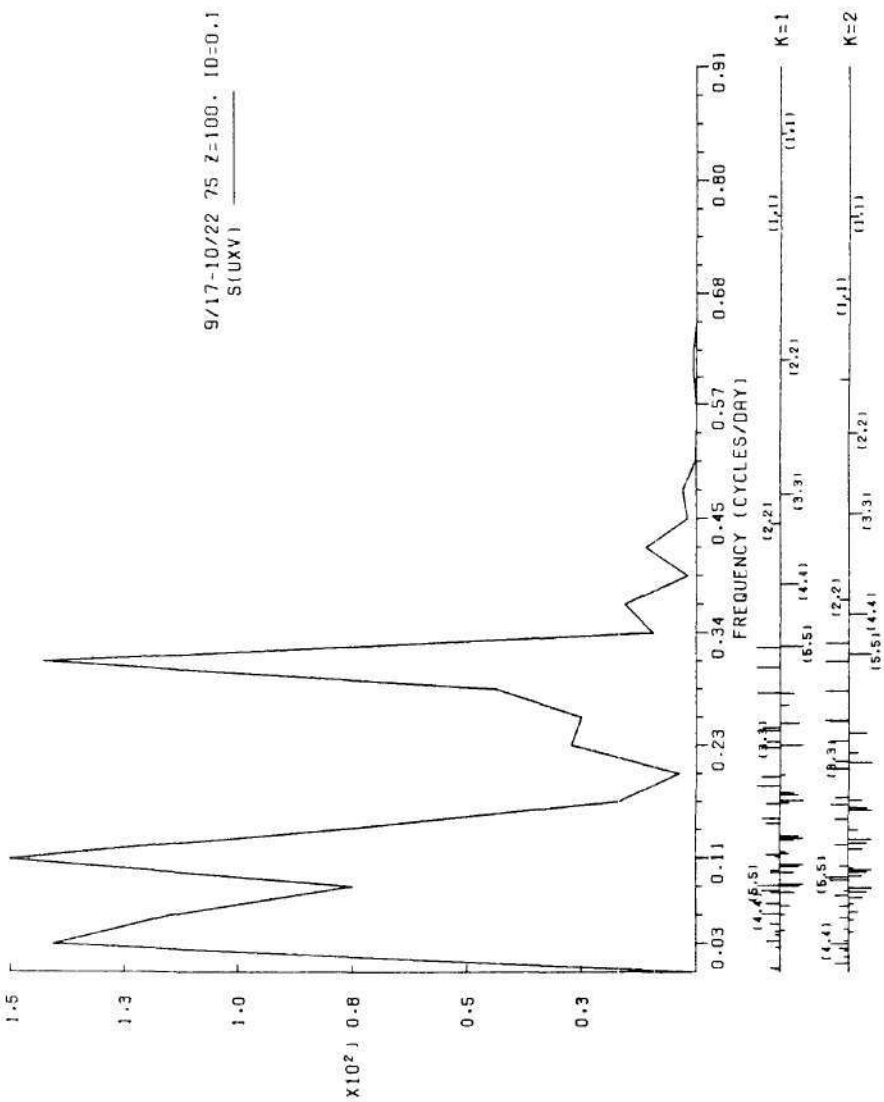

(d) 100 km

Figure 4.10. (Continued)

Aside from the peaks associated with the 80 km spectrum, the content at .03 and .19 cycles/day may be evidence for the (1,6), (1,7) and (1,2,1) modes. The latter has a period of 5.3 days which is precisely the period Geisler and Dickinson (1976) found to grow resonantly with steady surface forcing in the presence of realistic zonal winds. They concluded that this mode was insensitive to the vertical wind structure. Rodgers (1976) has observed this wave in satellite radiance data. Figure 1.10 shows a spectral peak corresponding to a wavenumber 1 disturbance of period 6.2 days. In general the period of this wave was found to vary from 4.5 to 6.3 days. The periods of the (1,2,1) and (1,2,2) modes are 5.3 and 6.1 days respectively. It appears that the (5,5) modes are closest to the peak at .34 cycles/day. The 100 km spectrum displays an enhancement of these features with contribution apparently from (5,5,2) being prominent. The phases at this level corresponding to the frequencies .03, .14, .23 and .31 cycles/day are 277, 302, 259, and 272 degrees respectively.

Results of an early winter sample are given in Figure 4.11. As for the previous examples, the bulk of the lower atmosphere's energy lies in the lowest end of the spectrum. However, it appears that some of the higher frequency modes are also excited in this more active time of year. In particular, the (1,2) modes may be associated with the 5-day peak and the (5,5) modes with the 3-day peak. Also, similar to other samples, the spectra are more discrete in the upper atmosphere, but the magnitudes in this case are up some 3 orders from those of the stratosphere (the spectra shown are the magnitude squared of the cross

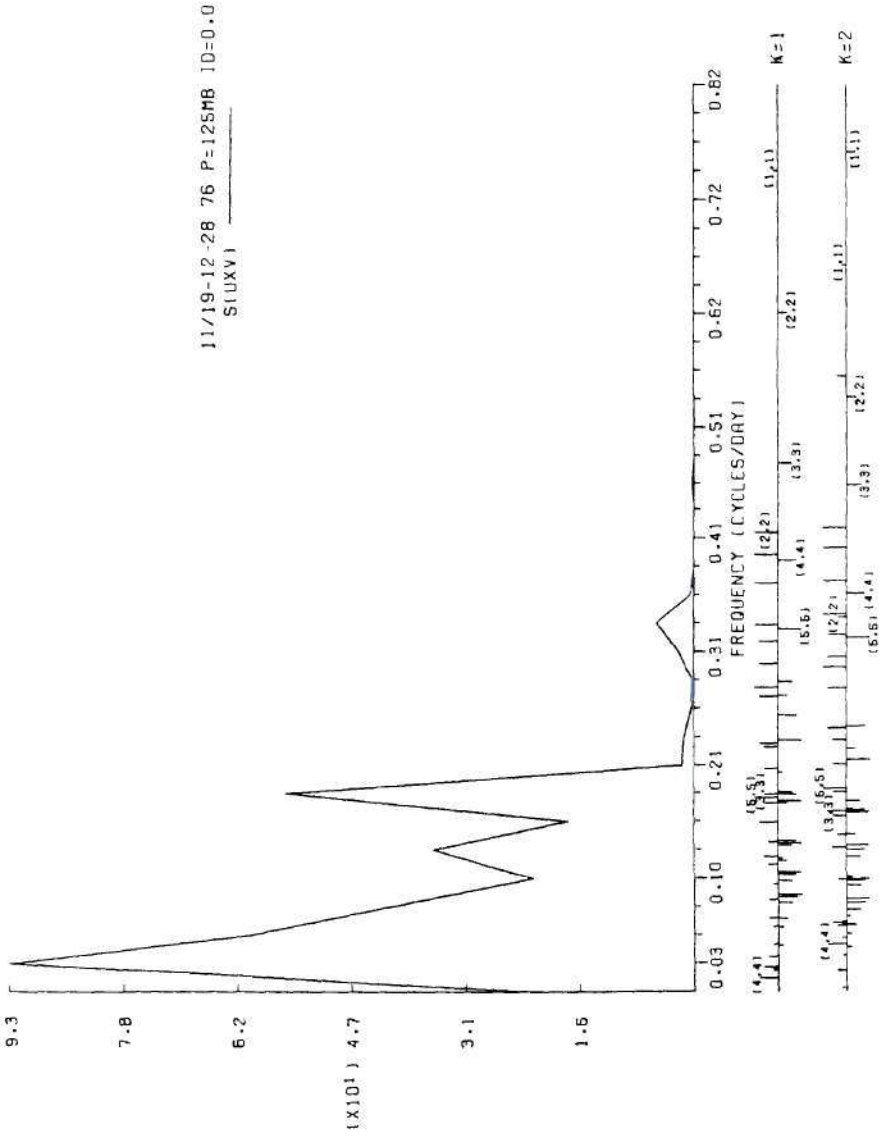

(a) 125 mb

Figure 4.11. Magnitude Squared of Cross Power Spectrum Between u and v for Autumn.

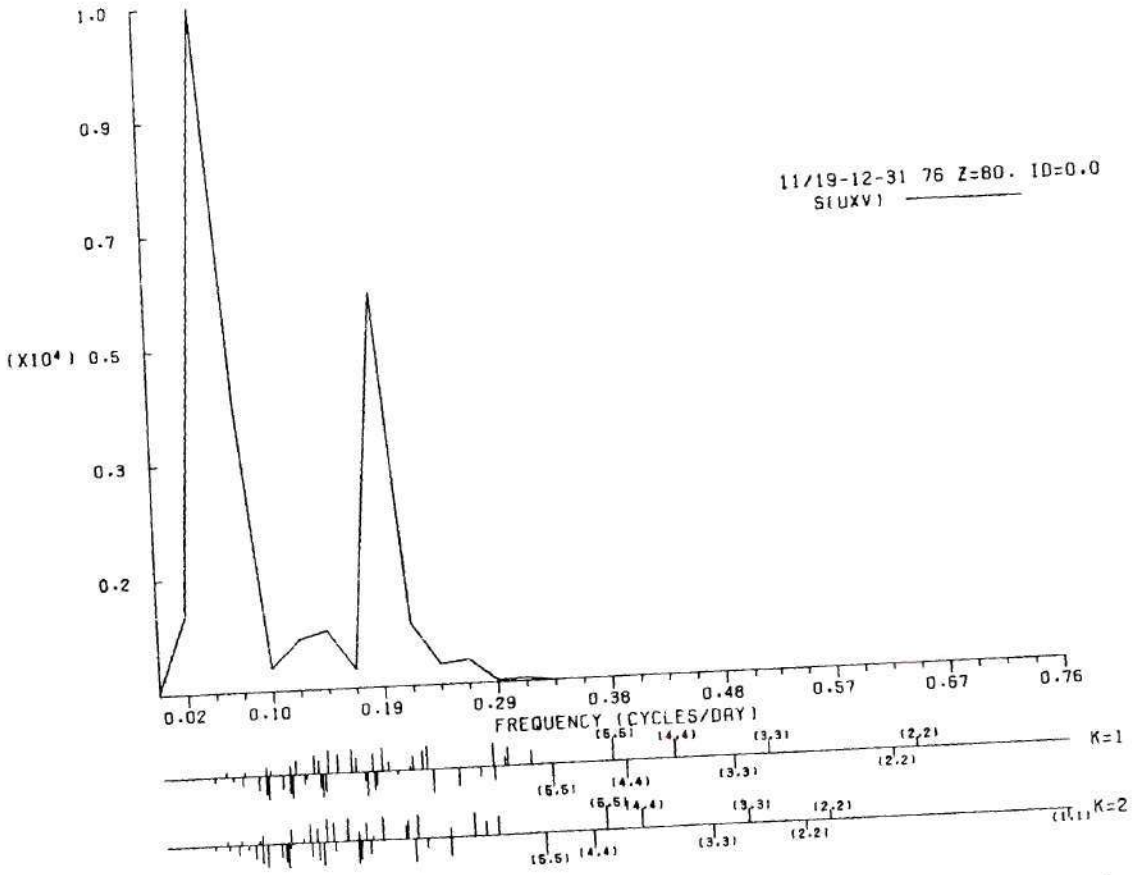

(b) 80 km

Figure 4.11. (Continued)

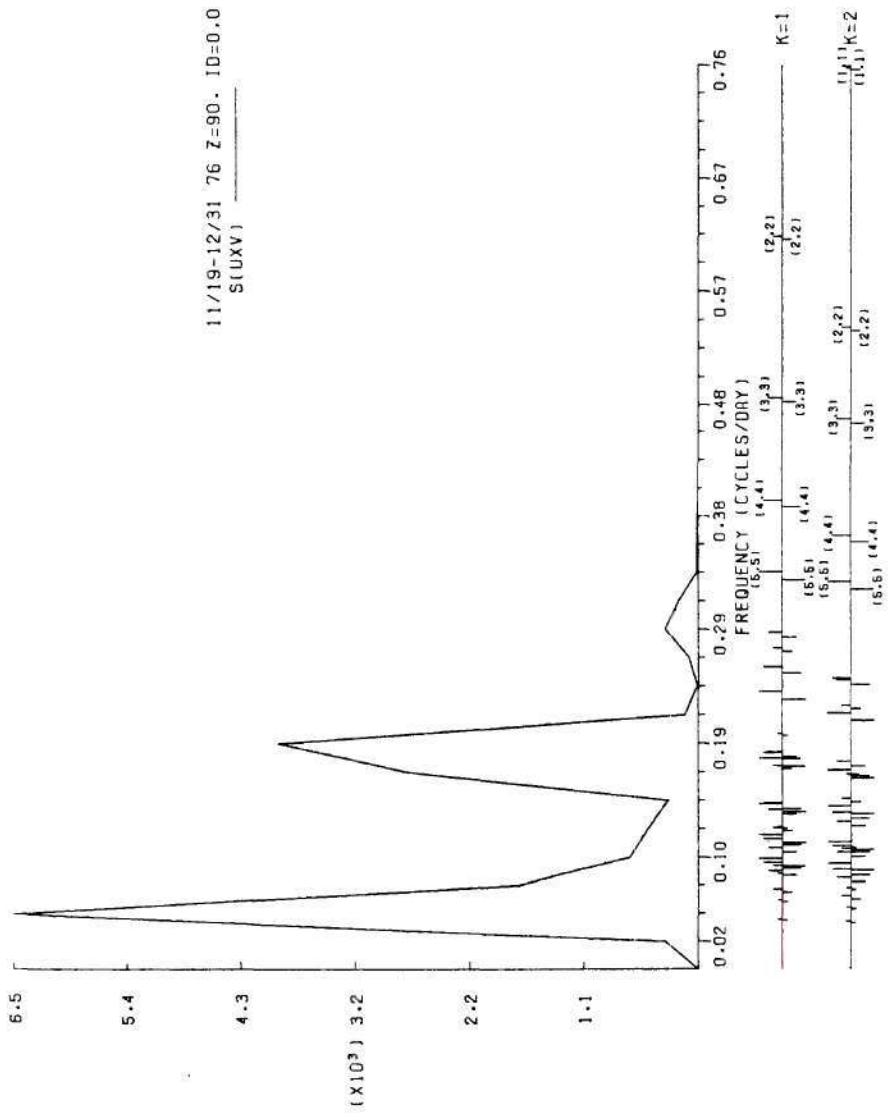

(c) 90 km

Figure 4.11. (Continued)

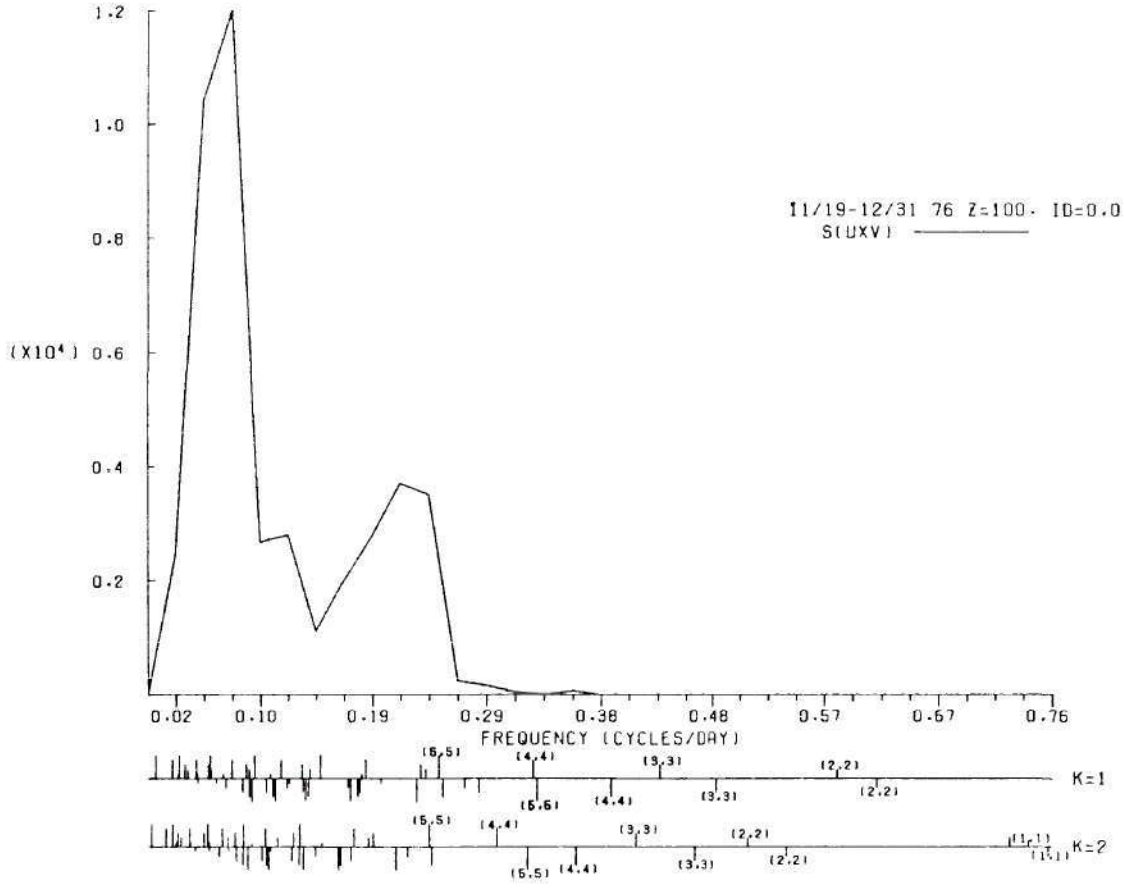

(d) 100 km

Figure 4.11. (Continued)

spectra; hence, amplitudes of discrete constituents are proportional to the 4th root of these). The largest peaks at 80 and 90 km may be associated with the (1,6) and (1,7) modes and the 5-day wave bears clear association to the (1,2,1) mode, with possibly an increase in contribution from (1,2,2) at the latter height. At 100 km the 5-day wave appears to be submerged in the contribution of other sources; however, it seems that its magnitude is roughly constant across the meteor region.

Figure 4.12 shows a spectrum for the stratosphere similar to that of Figure 4.10 for autumn, except for the stronger peaks at .13 - .16 cycles/day. The upper atmospheric spectra are again of greater magnitude. Apparently, the (1,2,1) mode has been replaced by another, possibly (1,2,2) evident from the peak at .16 cycles/day at several levels. The phases for this peak at the last three levels are 204, 256, and 286 degrees respectively.

The final upper atmospheric set corresponds to mid-summer, and is shown in Figure 4.13. Once again, evidence for the (1,2,1) mode appears in the stratospheric spectrum and the upper-air spectra. However, the 90 km spectrum indicates negligible contribution from this mode. Although not obvious at 70 mb, the (1,2,2) mode seems to appear at all of the upper levels, and seems to vary little in amplitude across the region. The character of these (1,2) modes is in line with the results of Geisler and Dickinson (1976); however, the large amplitudes that their model predicted in the summer mesosphere is not confirmed by these observations. Evidence for modes of frequency near .10

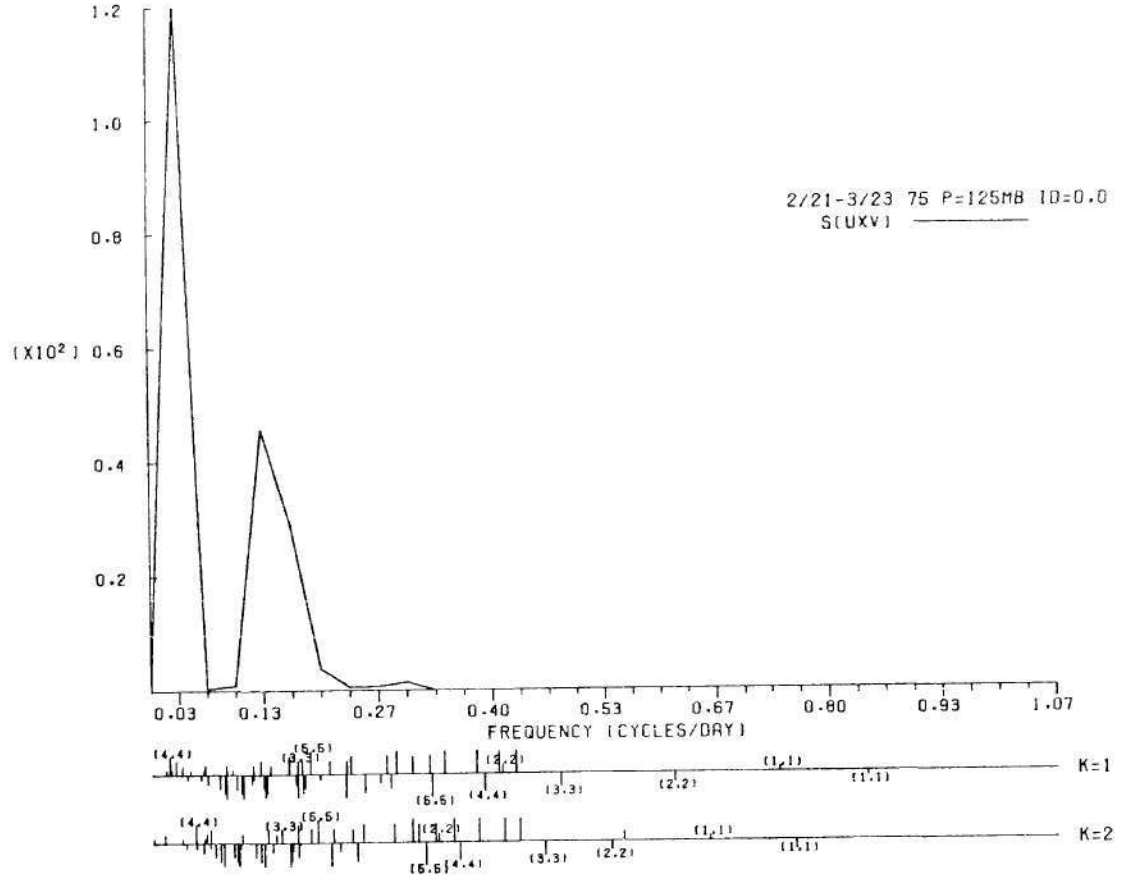

(a) 125 mb

Figure 4.12. Magnitude Squared of Cross Power Spectrum Between u and v for Spring.

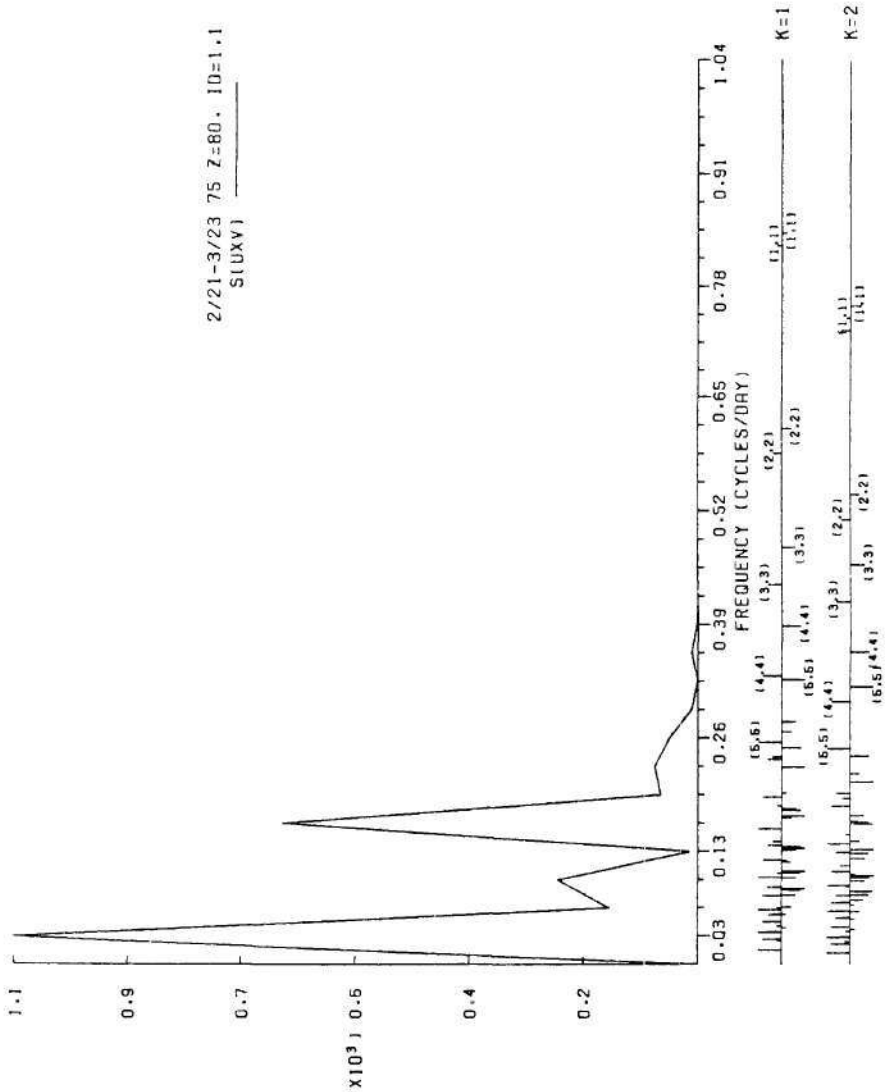

(b) 80 km

Figure 4.12. (Continued)

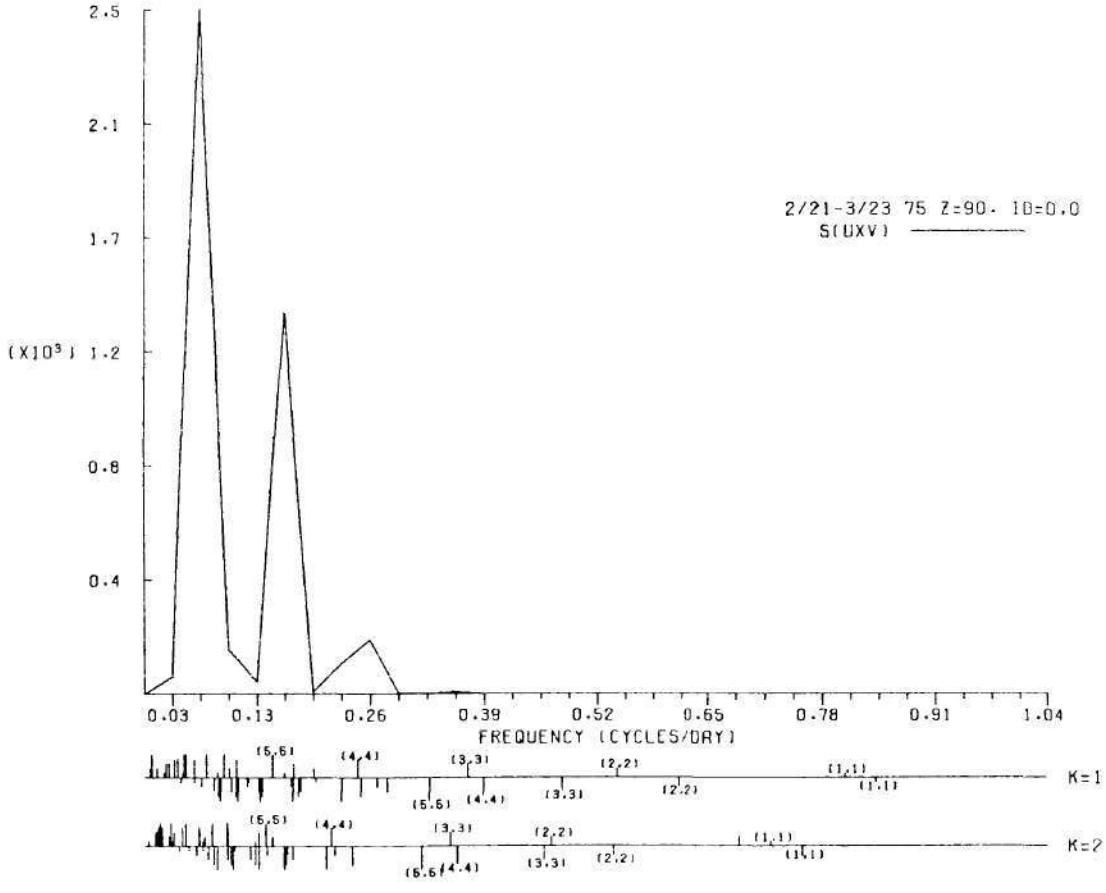

(b) 90 km

Figure 4.12. (Continued)

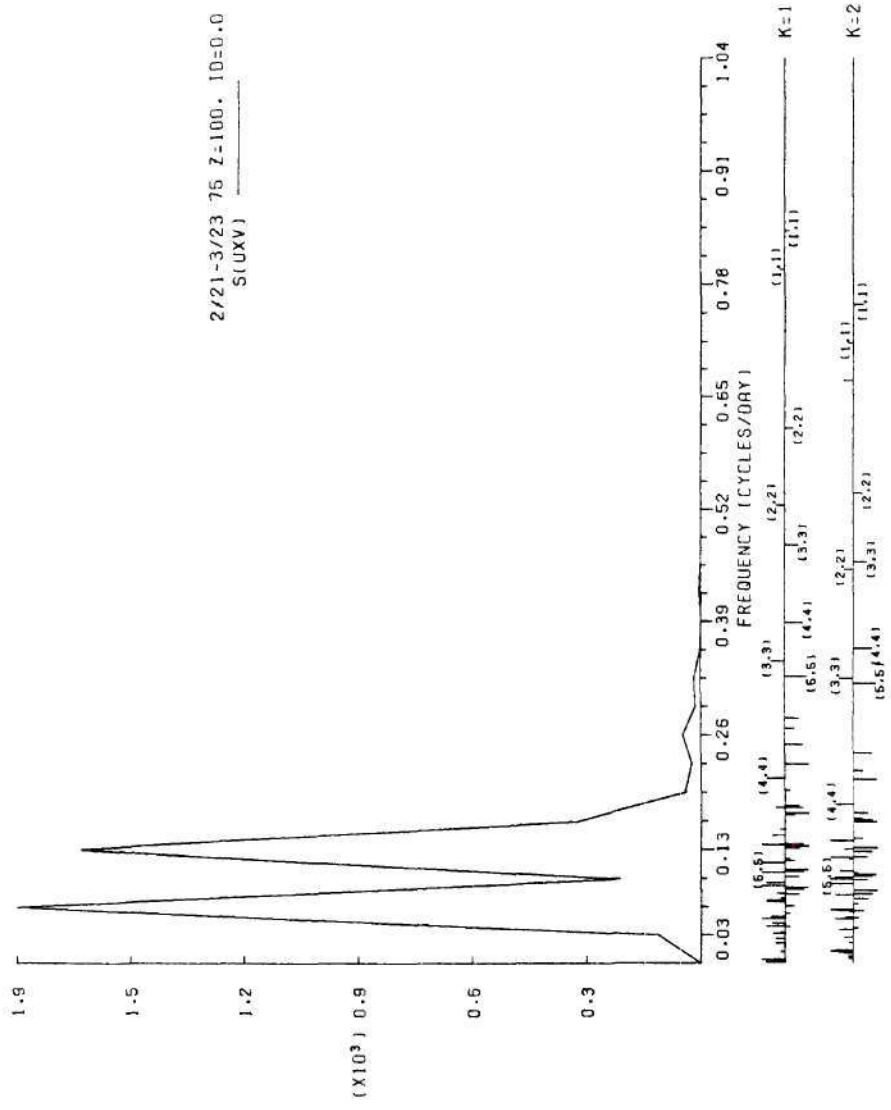

(d) 100 km

Figure 4.12. (Continued)

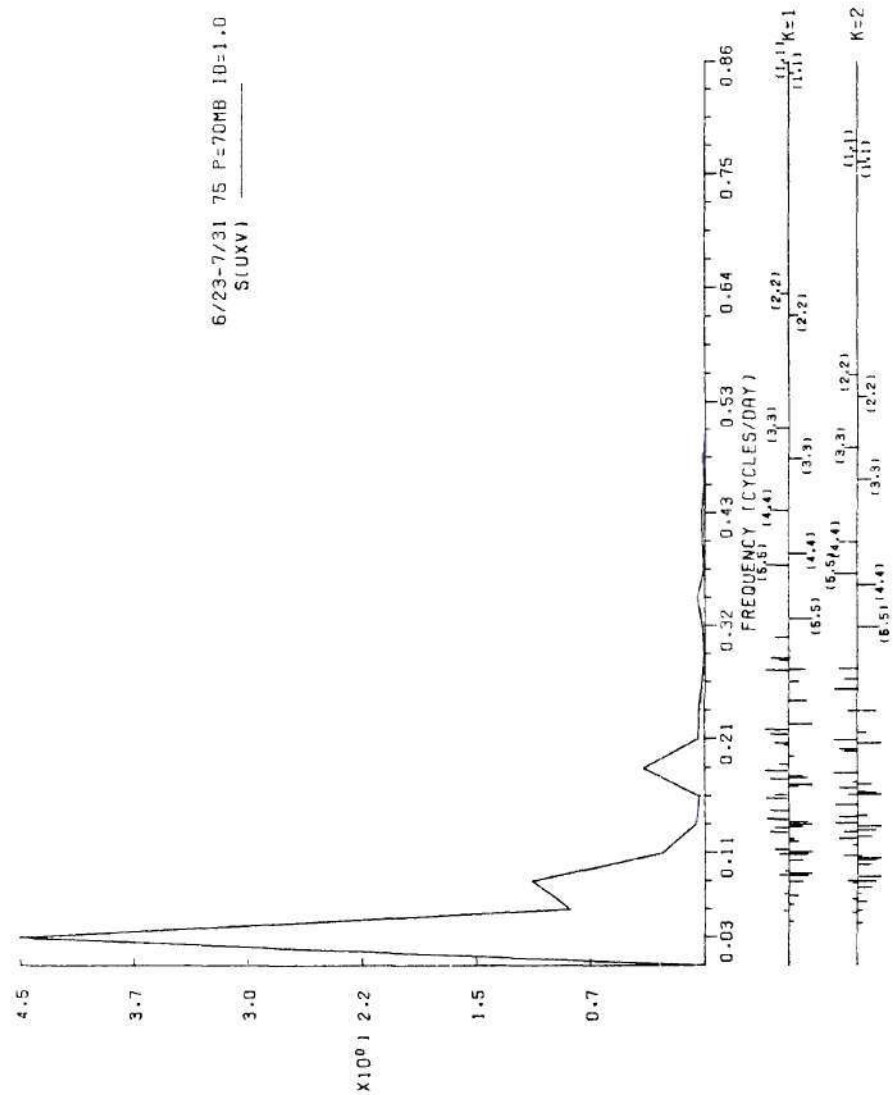

(a) 70 mb

Figure 4.13. Magnitude Squared of Cross Power Spectrum Between u and v for Summer.

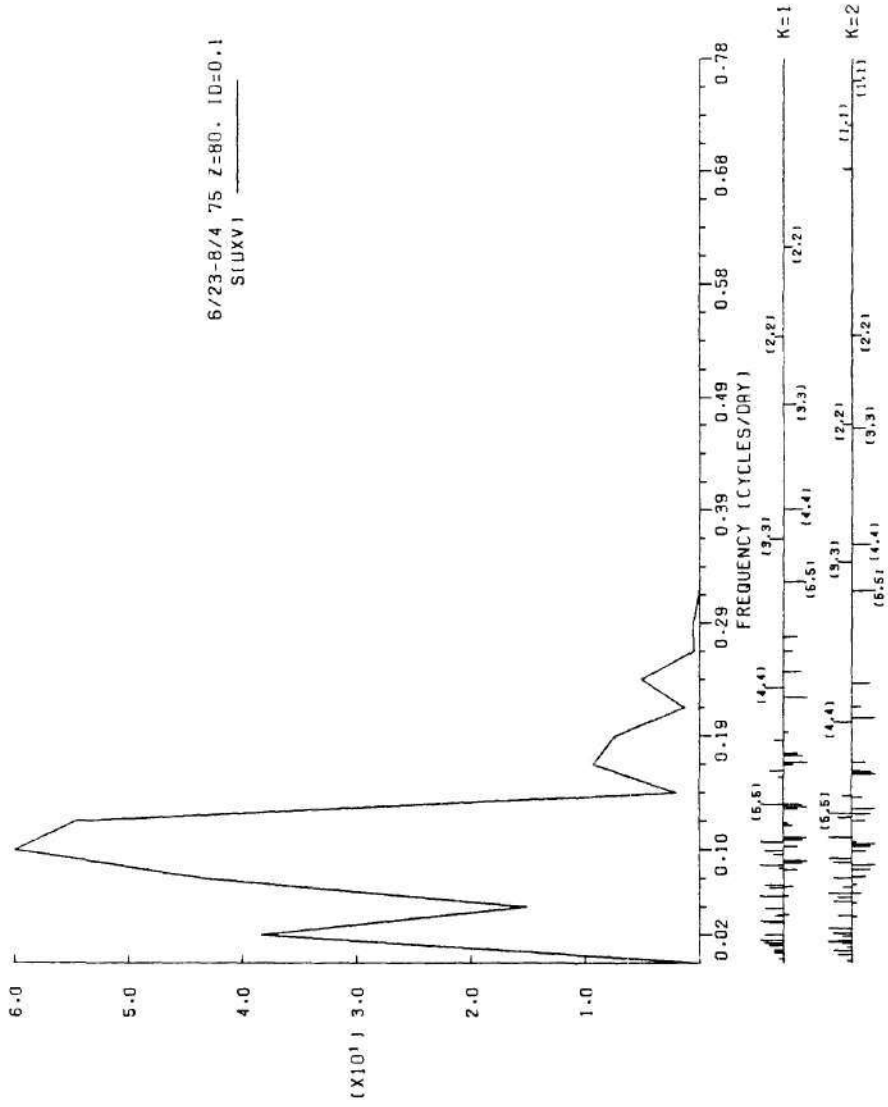

(b) 80 km

Figure 4.13. (Continued)

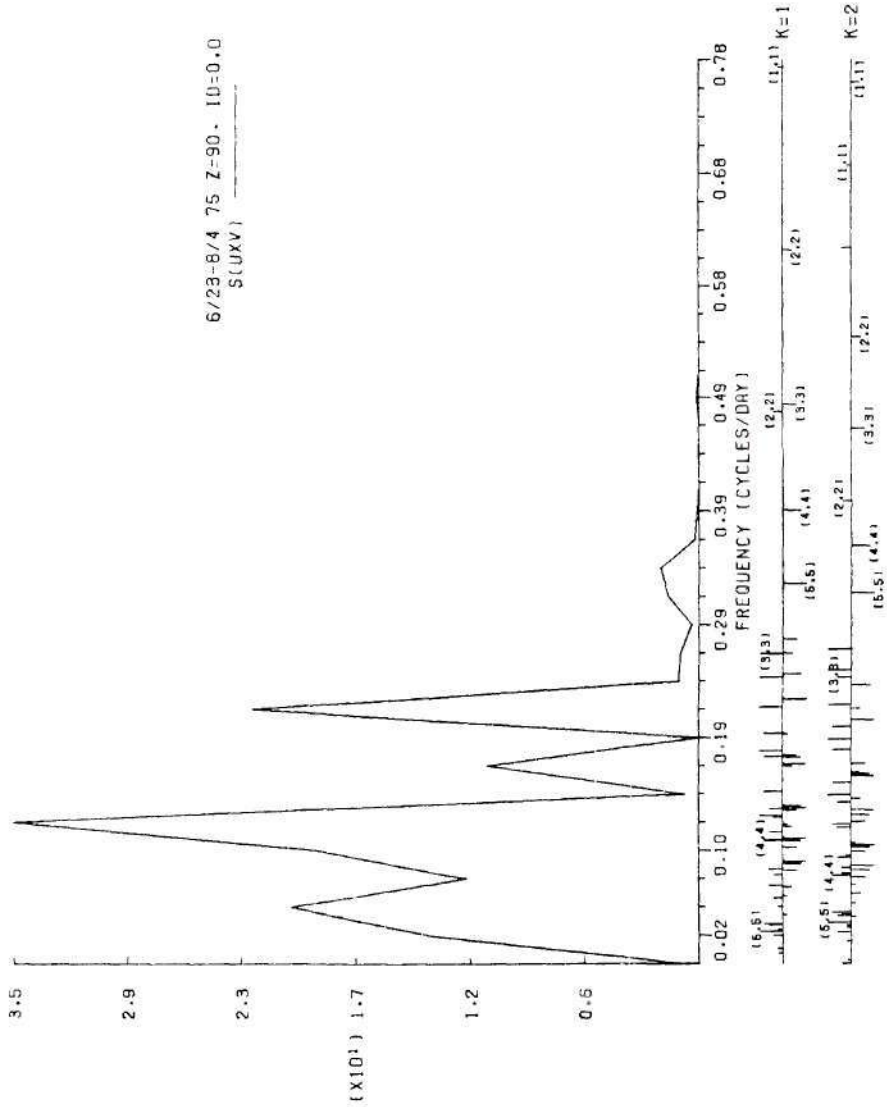

(c) 90 km

Figure 4.13. (Continued)

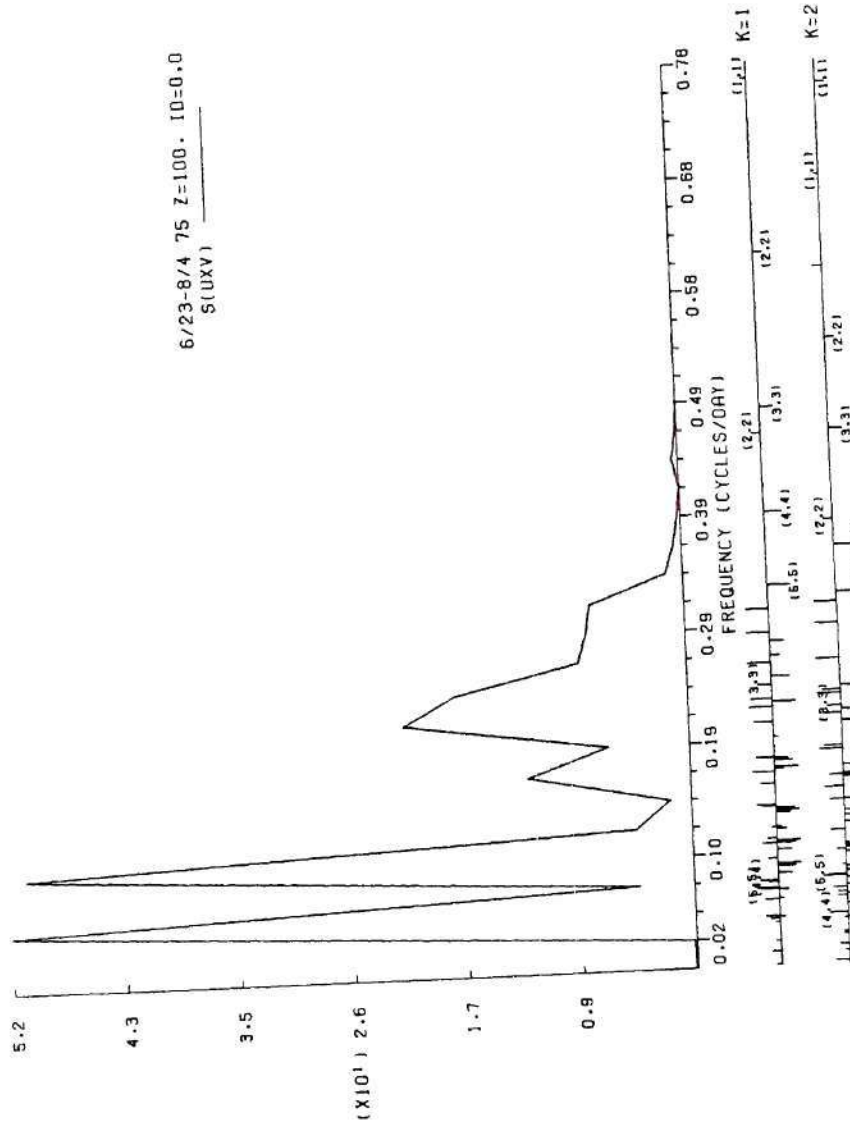

(d) 100 km

Figure 4.13. (Continued)

cycles/day also seems to exist at all of the upper levels.

One final spectrum is presented for the stratosphere in order to illuminate the lower frequency content in this region of the atmosphere. Figure 4.14 shows the spectrum for a 4-month sample period. Whereas the upper-level spectra readily indicated discrete content, those of the stratosphere lacked the resolution to rule out continuous spectral content, particularly in the lowest frequencies. This spectrum indicates that even these are composed essentially of discrete contribution. Moreover, the phases associated with the peaks at .03, .08, .11, .13, .15, .18 and .20 cycles/day are 253, 262, 267, 297, 330, 278 and 334 degrees respectively.

4.4 Discussion of the Observations

A general feature of the stratospheric time series examined indicates that the largest amplitudes are associated with the ultra-long period motions, appearing as trends over the sample period. These, apparently due to all of the higher meridional indices seem to be contained to the lower atmosphere where they constitute the bulk of the energy, because such gradual trends rarely appeared in the meteor time series. There may be two explanations for the large amplitudes of these modes. The baroclinic interaction terms of equations 2.47 depend upon the meridional derivative $\frac{\partial}{\partial \phi}$. For large meridional index, n, these terms may dominate. Hence, these large n disturbances may absorb energy (vorticity) out of the mean state efficiently. The other possible explanation follows from the results of Chapter II where it was indicated that the decay rates decrease with (n-m). Figures 4.4 - 4.13

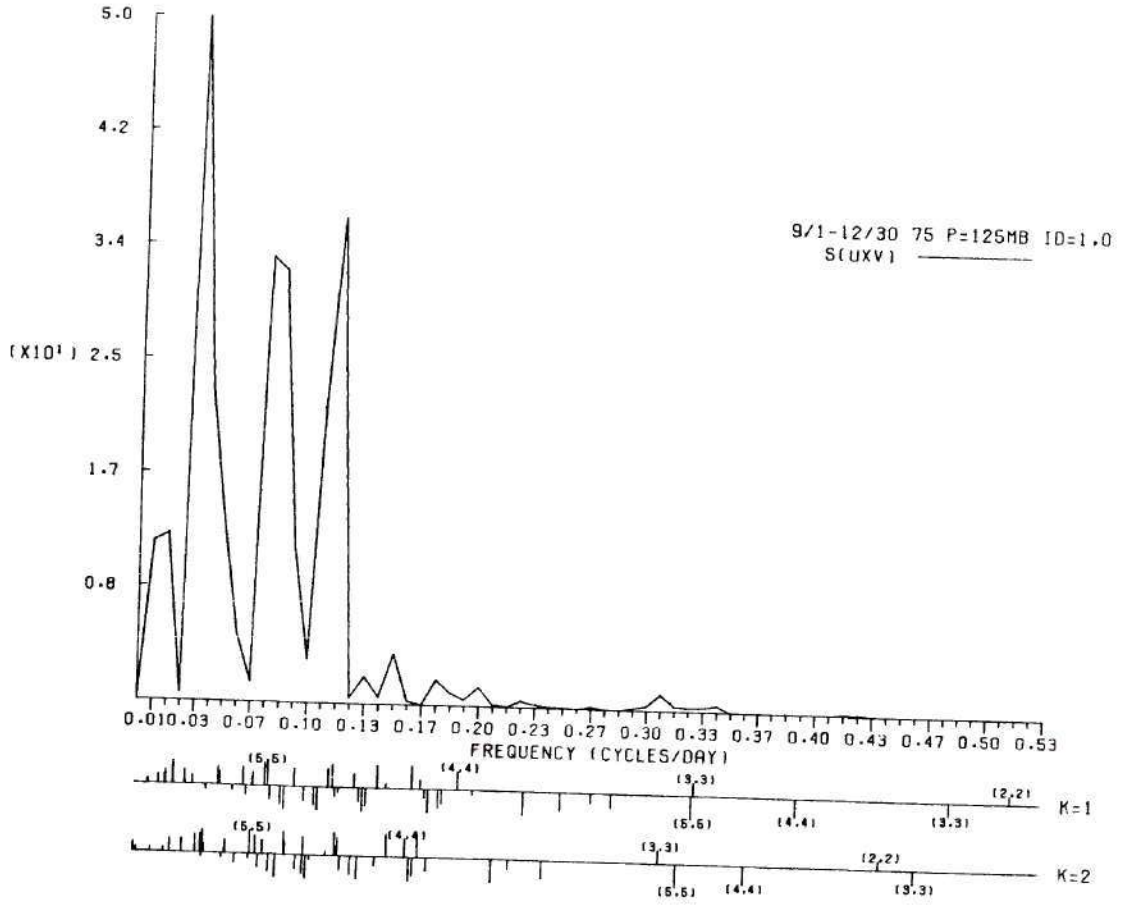

Figure 4.14. Magnitude Squared of Cross Power Spectrum of u and v at 125 mb for 4-Month Period.

indicate that the upper atmospheric spectra of the smaller wavenumbers (category (i)) appear to be consistently larger than those of the higher wavenumbers (category (ii)). Apparently the energy of the lower wavenumbers penetrates the stratospheric vortex better than that of the higher wavenumbers. Winter seems to be an exceptional season, when the amplitudes of the latter meet or exceed those of the former. Although this preferential transmission of lower wavenumbers agrees with the result of Charney and Drazin, the data does not collaborate their conclusion that significant planetary wave energy will penetrate only at the equinox. The major transmission seems to occur in winter and significant penetration must occur at all seasons since the meteor wind spectra are dominated by discrete content for the entire range of wavenumber considered. These results agree with the findings of Deland and Friedman (1972), Boville (1966), Theon et al. (1967), Deland and Johnson (1968), Muench (1968), and McNulty (1976). The discussion of signal time in Section 2.7 would indicate that the seasonal variation of spectral content in the upper atmosphere is related to the second vertical mode. This is confirmed by Paulin's (1970) study. The fact that several modes appeared at meteor heights but not in the stratosphere may be due to baroclinic instability at the stratopause (Simmons, 1974), or perhaps these modes are buried in the noise at lower levels, yet have sufficient vertical flux to appear in the mesosphere. The increased transmission during winter may be due to either an incorrect estimate of the dependence of the refractive index on season or increased forcing at the surface.

The spectra appear more and more discrete with increasing height and even the stratospheric spectra appear to be composed of essentially discrete content if a sufficiently long sample period is used. This seems to rule out the existence of the continuous band of modes mentioned in Section 2.5. No general variation with height was observed for the spectra, possibly indicating an important role played by the vertical wind shear. However, several of the spectra exhibited a minimum near 90 km. Aside from wind shear, there may be a connection with the last turning point of the second vertical mode near the mesopause. The associated magnitude of u' normalized by $e^{\xi/2}$ changes from decreasing to constant in this region (cf., Figure 2.8, c) and hence one might expect this sort of behavior. Although peaks in cross spectra were not always associated with a 270 degree phase, the two did occur simultaneously throughout the samples, and virtually all of the spikes in the spectrum computed for the 4-month sample indicated this.

The three most commonly observed periods were the 20 - 25 day waves corresponding to (1,5), (1,6) and (1,7) modes, the 5-day wave corresponding to the (1,2) modes, and the 2-day wave possibly due to the (2,2) or (3,3) modes. The first and third may be related to the smaller decay rates discussed in Section 2.7. Finally, the location of the spectral lines is uncertain according to the motion of the source of the disturbance. This may explain the few spectral peaks that did not appear to be associated with any of the modes.

CHAPTER V

CONCLUSIONS AND RECOMMENDATIONS

Two discrete vertical modes were found which satisfied the homogeneous problem in a relaxed sense, where the radiation condition was imposed as the upper boundary condition. This problem should be reevaluated using the results of Yanowitch and a viscous reflecting layer as the upper boundary condition to see how these modes are affected and if new ones are introduced.

Realistic zonal wind structure should then be incorporated, possibly as a perturbation on the angular velocity of the earth. Lastly, baroclinic interaction with the mean state might be investigated. This too might be treated as a perturbation on a basic barotropic state. It is likely that in this case the eigenvalues will be complex due to disturbance vorticity production. The mathematics will be considerably more involved, but if these complex eigenvalues are found, the growth rates for the unstable modes could be determined. A straightforward perturbation analysis for these two problems, however, may not be the most effective route to proceed along, because of the appearance of the eigenvalues in the boundary conditions and their appearance nonlinearly in the equations.

A spectrally unbiased finite element technique for decomposing meteor wind data was developed. The data examined with this technique indicates that winds in the meteor region are dominated by planetary

wave content and not by the diurnal tide. Application of the Groves analysis without sufficient averaging may produce spurious results. Future work might modify this decomposition for a variable mesh partition to allow better fit to the data density. Nonuniform distribution of error among the velocity components might also be studied.

Investigation of meteor wind data suffers from two major problems. Sufficiently long periods without temporal gaps are few, and even longer periods are needed to distinguish between adjacent modes and offer adequate spectral resolution. A variable mesh fourier transform would allow examination of longer data samples and increase the resolution of the spectra. It would eliminate the high frequency rolloff due to the larger partitions required to interpolate across gaps in the data. Autocorrelation studies might overcome the resolution difficulty since the periods for large $(n - m)$ should behave like $(n - m)$. Finally, the frequency modulation evident in several of the upper atmospheric samples might be more amenable to the Anharmonic Frequency Analysis (AFA) developed by A.K. Paul at ERL NOAA, Boulder, Co.

APPENDIX A

DERIVATION OF THE SURFACE BOUNDARY CONDITION

The surface boundary condition (2.60.2) follows immediately from the relation

$$\underline{P} = \frac{1}{\alpha}\left(\frac{1}{\tilde{H}} Z - Z'\right) \qquad \alpha \neq 0 \tag{A.1}$$

which will now be shown ($\underline{P}$ is given by 2.68.1).

Suppose Z is such that the equation

$$J \circ L[Z] + \alpha Z = 0 \tag{A.2.1}$$

is satisfied and

$$Z = J[\underline{P}] = \frac{1}{(\tilde{H}' + \kappa)} \frac{\partial}{\partial \zeta} (\tilde{H}\,\underline{P}) \,. \tag{A.2.2}$$

The original 2nd order PDE to be satisfied by $\tilde{p}$ given by (2.57) is

$$L \circ J[\tilde{p}] = \hat{M}[\tilde{p}] \tag{A.3}$$

and therefore separation results in

$$L \circ J[\underline{P}] + \alpha \underline{P} = 0 \tag{A.4}$$

Equation (A.2.1) may be written

$$J \circ L[Z] + \alpha J[\underline{P}] = 0 \tag{A.5}$$

By operating with

$$J^{-1}[\circ] = \frac{1}{\tilde{H}} \int (\tilde{H}' + \kappa) \circ d\zeta + \frac{c(\mu)}{\tilde{H}}, \qquad (A.6)$$

where $c(\mu)$ is arbitrary, (A.5) becomes

$$L[Z] + \alpha \underline{P} = \frac{\hat{c}(\mu)}{\tilde{H}} \qquad (A.7.1)$$

or

$$L \circ J[\underline{P}] + \alpha \underline{P} = \frac{\hat{c}(\mu)}{\tilde{H}} \qquad (A.7.2)$$

But, by (A.4)

$$\hat{c}(\mu) = 0 \qquad (A.8)$$

necessarily. Equation (A.1) then follows from (A.7.1) and (2.58.2) for $\alpha \neq 0$.

APPENDIX B

THE CASE $\alpha = 0$

For this case the surface boundary condition remains

$$Z - \underline{P} = 0 \tag{B.1}$$

It may be verified that for $\alpha = 0$, the general solution of (A.4) is

$$\underline{P} = \frac{A}{\tilde{H}} \int (\tilde{H}' + \kappa) e^{\tilde{\xi}(\zeta')} d\zeta' + \frac{c(\mu)}{\tilde{H}} \tag{B.2}$$

This solution is divergenceless, i.e.,

$$Z = J[\underline{P}] = 0 \tag{B.3}$$

The finite energy condition demands that

$$A = 0 \tag{B.4}$$

and (B.1) and (B.3) require

$$c = 0 \tag{B.5}$$

APPENDIX C

THE SURFACE BOUNDARY CONDITION FOR THE WKB APPROXIMATION

Case (i) $\hat{k}^2 >> 0 \quad (\alpha > 0)$

Substitution of (2.85.4) into the surface boundary condition (2.67.2) results in the following equation

$$2i\hat{k}_o^2 = (2\alpha\hat{H}_o - 1)\hat{k}_o - \hat{k}_o' \qquad (C.1)$$

where primes indicate differentiation with respect to $\tilde{\xi}$ and zero subscripts denote surface evaluation. Now $\hat{k}$ is assumed to be a real valued function of $\tilde{\xi}$ and therefore $\hat{k}_o$ and $\hat{k}_o'$ are real. Thus the right hand side is real the left hand side is imaginary and there are no real values of $\hat{k}_o$ and hence α which satisfy the equation.

Case (ii) $\hat{k}^2 = -\tilde{k}^2 << 0 \quad (\alpha < 0)$

Substitution of (2.86.4) into (2.67.2) yields

$$4\tilde{k}_o^3 = -\{2(1 - 2\alpha\hat{H}_o)\tilde{k}_o^2 + (\tilde{k}^2)_o'\} \qquad (C.2)$$

We will now assume the mean height profile to vary linearly near the surface (certainly not a departure from reality)

$$\tilde{H} \sim H_o(1 - \gamma\zeta) \qquad \zeta \to 0 \qquad (C.3.1)$$

Then it follows that

$$\hat{H}(\tilde{\xi}) = H_o e^{-\gamma H_o \tilde{\xi}} \tag{C.3.2}$$

The last term on the right of (C.2) becomes

$$(\tilde{k}^2)'_o = -\alpha\gamma H_o^2 (\gamma H_o - \kappa) \tag{C.4}$$

Now the Brunt-Väisälä frequency may be written as

$$N^2 = \frac{g}{\theta}\frac{d\theta}{dz} = \frac{g}{\bar{H}\hat{H}^2}(\hat{H}' + \kappa\hat{H}) \tag{C.5}$$

(cf., 2.98.2). Thus if the constant lapse γ is the adiabatic lapse, Γ, $\frac{d\theta}{dz} = 0$ and

$$\hat{H}' + \kappa\hat{H} = 0$$

or

$$\hat{H} = H_o e^{-\kappa\tilde{\xi}} \tag{C.6}$$

Therefore, from (C.3.2), at the adiabatic lapse, $\gamma = \Gamma$ and

$$\gamma H_o = \kappa \tag{C.7}$$

Now α is negative for this range of validity of the WKB approximation hence

$$(\tilde{k}^2)'_o \begin{cases} > 0 & \gamma > \Gamma \\ = 0 & \gamma = \Gamma \\ < 0 & \gamma < \Gamma \end{cases}$$

In any case, the global and temporal mean of γ cannot deviate substantially from Γ and hence the last term on the right of (C.2),

$(k^2)'_o$ is small, certainly with respect to the first term for this case. Also the first term is positive. ($\alpha < 0$); hence the entire right hand side is negative. However, in invoking the finite energy condition it was assumed that $\tilde{k} > 0$, and therefore, the left hand side is positive. Thus there are no real values of $\tilde{k}_o$ and hence α which satisfy the equation under these conditions.

APPENDIX D

THE EFFECT OF AVERAGING

Consider a time sequence of some function f(t) over an interval [0, NT). If the function values over adjacent intervals of length T are averaged, then the corresponding Fourier transforms will also be averaged due to linearity of the Fourier transform. Defining the kth function as:

$$f_k(t) = f(t + kT) \quad t \in [0, T) \quad k = 0,1,2,\ldots, N-1 \tag{D.1}$$

and assuming stationarity over intervals of length T, it is easily shown that f_k has the Fourier transform:

$$F_k(\nu) = F(\nu)e^{i2\pi\nu kT} \tag{D.2}$$

where $F(\nu)$ is the Fourier transform of $f(t)$ $t \in [0, T)$ (Bath, 1974, p. 44).

Averaging these functions we have:

$$\frac{1}{N} \sum_{k=0}^{N-1} f_k(t)$$

with corresponding Fourier transform:

$$\frac{1}{N} \sum_{k=0}^{N-1} F_k(\nu) = F(\nu) \frac{1}{N} \sum_{k=0}^{N-1} e^{i2\pi\nu kT} \tag{D.3}$$

In general the summation involved in the transform will lead to cancellation. That is for N sufficiently large, the value of the Fourier transform of the average will tend to zero for general ν. If however ν is such that

$$2\pi\nu kT = 2\pi n$$

for all k for some integer n

i.e., $$\nu = n/T \qquad (D.4)$$

then the Fourier transform of the average at these ν will in fact equal that of $f(t)$ $t \in [0, T)$.

APPENDIX E

B-SPLINES AND CONSTRUCTION OF THE LEAST SQUARES PROBLEM

At the N points of observation $\{(t_\mu, z_\mu)\}_{\mu=1}^{N}$, Equations (3.8) become:

$$\begin{cases} v_1(t_\mu, z_\mu) = \sum_{j=1}^{p} \alpha_j Z_j(t_\mu, z_\mu) + \varepsilon_1(t_\mu, z_\mu) & \mu = 1,2,\ldots,N \\ v_2(t_\mu, z_\mu) = \sum_{j=1}^{p} \beta_j Z_j(t_\mu, z_\mu) + \varepsilon_2(t_\mu, z_\mu) & \mu = 1,2,\ldots,N \\ v_3(t_\mu, z_\mu) = \sum_{j=1}^{p} \gamma_j Z_j(t_\mu, z_\mu) + \varepsilon_3(t_\mu, z_\mu) & \mu = 1,2,\ldots,N \end{cases} \tag{E.1}$$

or

$$\begin{cases} \vec{v}_1 = Z\vec{\alpha} + \vec{\varepsilon}_1 \\ \vec{v}_2 = Z\vec{\beta} + \vec{\varepsilon}_2 \\ \vec{v}_3 = Z\vec{\gamma} + \vec{\varepsilon}_3 \end{cases} \tag{E.2.1}$$

where $\vec{v}_k$ and $\vec{\varepsilon}_k$ are N dimensional vectors consisting of the velocities and errors at the points (t_μ, z_μ):

$$\vec{v}_k = \begin{vmatrix} v_k(t_1,z_1) \\ \vdots \\ v_k(t_\mu,z_\mu) \\ \vdots \\ v_k(t_N,z_N) \end{vmatrix} \qquad \vec{\varepsilon}_k = \begin{vmatrix} \varepsilon_k(t_1,z_1) \\ \vdots \\ \varepsilon_k(t_\mu,z_\mu) \\ \vdots \\ \varepsilon_k(t_N,z_N) \end{vmatrix} \quad k=1,2,3 \tag{E.2.2}$$

Z is an N x p matrix with the μjth entry $Z_j(t_\mu, z_\mu)$. That is the jth column vector of Z consists of the jth approximation function $Z_j(t,z)$ evaluated at the N observation points (t_μ, z_μ).

$$Z = \begin{vmatrix} Z_1(t_1,z_1) & \cdots & Z_j(t_1,z_1) & \cdots & Z_p(t_1,z_1) \\ Z_1(t_2,z_2) & & \vdots & & \vdots \\ \vdots & & \vdots & & \vdots \\ Z_1(t_\mu,z_\mu) & \cdots & Z_j(t_\mu,z_\mu) & & \vdots \\ \vdots & & & & \vdots \\ Z_1(t_N,z_N) & \cdots & \cdots & & Z_p(t_N,z_N) \end{vmatrix}_{N \times p} \qquad \text{(E.2.3)}$$

$\vec{\alpha}$, $\vec{\beta}$, and $\vec{\gamma}$ are p dimensional vectors composed of the unknown coefficients. (E.2.1) constitutes essentially three L S problems: determining the coefficient vectors $\vec{\alpha}$, $\vec{\beta}$, and $\vec{\gamma}$ such that the sums of the squares of the errors is minimized, i.e., such that $\langle \vec{\varepsilon}_k, \vec{\varepsilon}_k \rangle$ is a minimum (where $\langle \vec{a}, \vec{b} \rangle = \Sigma a_i b_i$). Also the errors are normally distributed with mean 0 and variance σ_k^2 ($\vec{\varepsilon}_k$ is $N(0, \sigma_k^2 I)$ where I is the identity matrix).

Unfortunately, we do not have the observations of the individual velocity components v_k, but only random linear combinations of them. Substitution of (E.1) into (3.4) yields:

$$V_{L\mu} = d_{1\mu} \sum_{j=1}^{p} \alpha_j Z_j(t_\mu,z_\mu) + d_{2\mu} \sum_{j=1}^{p} \beta_j Z_j(t_\mu,z_\mu) + d_{3\mu} \sum_{j=1}^{p} \gamma_j Z_j(t_\mu,z_\mu)$$

$$+ (d_{1\mu}\, \varepsilon_1(t_\mu,z_\mu) + d_{2\mu}\, \varepsilon_2(t_\mu,z_\mu) + d_{3\mu}\, \varepsilon_3(t_\mu,z_\mu)) \quad \mu = 1,2,\ldots,N \qquad \text{(E.3.1)}$$

If we assume

$$\sigma_1^2 = \sigma_2^2 = \sigma_3^2 = \sigma^2$$

we have:

$$V_{L\mu} = d_{1\mu} \sum_{j=1}^{p} \alpha_j Z_j(t_\mu, z_\mu) + d_{2\mu} \sum_{j=1}^{p} \beta_j Z_j(t_\mu, z_\mu)$$

$$+ d_{3\mu} \sum_{j=1}^{p} \gamma_j Z_j(t_\mu, z_\mu) + \varepsilon_\mu \quad \mu = 1,2,\ldots,N \qquad \text{(E.3.2)}$$

where ε_μ is $N(0, \sigma^2)$ since:

$$d_{1\mu}^2 \sigma_1^2 + d_{2\mu}^2 \sigma_2^2 + d_{3\mu}^2 \sigma_3^2 = (d_{1\mu}^2 + d_{2\mu}^2 + d_{3\mu}^2)\sigma^2 = \sigma^2$$

More compactly,

$$\vec{V}_L = D_1 Z \vec{\alpha} + D_2 Z \vec{\beta} + D_3 Z \vec{\gamma} + \vec{\varepsilon} \qquad \text{(E.4.1)}$$

where

$$\vec{V}_L = \begin{vmatrix} V_{L1} \\ V_{L2} \\ \vdots \\ V_{L\mu} \\ \vdots \\ V_{LN} \end{vmatrix} \qquad D_k = \begin{vmatrix} d_{k1} & & & & \\ & d_{k2} & & & \\ & & \ddots & & \\ & & & d_{k\mu} & \\ & & & & d_{kN} \end{vmatrix}_{N \times N} \qquad k = 1,2,3 \qquad \text{(E.4.2)}$$

and $\vec{\varepsilon}$ is $N(0, \sigma^2 I)$. Or finally,

$$\vec{V}_L = \hat{Z} \vec{\delta} + \vec{\varepsilon} \qquad \text{(E.5.1)}$$

where:

$$\hat{Z} = \left| D_1 Z \,\middle|\, D_2 Z \,\middle|\, D_3 Z \right|_{N \times 3p} \qquad \vec{\delta} = \left| \begin{array}{c} \vec{\alpha} \\ \hline \vec{\beta} \\ \hline \vec{\gamma} \end{array} \right|_{3p \times 1} \tag{E.5.2}$$

(E.5.1) is now in the form of the classical Least Squares Problem. The solution $\vec{\delta} = \vec{b}$ is the 3p dimensional vector of coefficients that makes $\vec{\epsilon}\, N(0, \sigma^2 I)$ with σ^2 minimized. The Gauss Markov Theorem states that $\vec{b}$ is a solution of this problem if it is a solution of the Normal Equations:

$$\hat{Z}^t \hat{Z}\, \vec{\delta} = \hat{Z}^t\, \vec{V}_L \tag{E.6}$$

In this case $\hat{Z}\vec{b}$ is a "best linear unbiased estimate" of $\vec{V}_L$.

The solution of (E.6), $\vec{b}$, yields the coefficient vectors $\vec{\alpha}$, $\vec{\beta}$, and $\vec{\gamma}$ and hence approximations of the velocity functions which are least squares in the sense of the observations of V_L - the line of sight velocities. The error that has been minimized is that between the linear combinations of the velocity approximations and the line of sight observations.

The approximating functions $Z_j(t, z)$ are chosen as follows. Consider a finite interval $[t_o, t_f)$ on the real line. The set of n + 1 uniformly spaced points: $\pi = \{t_i\}_{i=1}^{n+1}$ such that:

$$t_o = t_1 < t_2 < t_3 < \ldots\ldots < t_{n+1} = t_f$$

forms a uniform partition of the interval into n half open subintervals: $\{[t_i t_{i+1})\}_{i=1}^{n}$. Over this partitioned interval exists a collection or

"space" of functions: $S(\pi)$, consisting of all piecewise cubic splines with nodes at the points of the partition π. Contained in this space is a "basis set" of $n+3$ linearly independent functions $\{\ell_j(t)\}_{j=1}^{n+3}$, from which any other function in the space may be constructed by linear superposition. Thus if $s(t) \in S(\pi)$, then

$$s(t) = \sum_{j=1}^{n+3} \alpha_j \ell_j(t) \tag{E.7}$$

for suitable choice of the coefficients α_j. The choice of the basis set for $S(\pi)$ is not unique. Our choice will be the so called "B-splines" or "hump functions" (see DeBoor, 1972). Briefly, the B-splines have been chosen because they are local (no more than four of the basis functions are nonzero at any point), yielding fewer necessary computations and also they may be computed directly from a partition without solving additional linear systems.

First we augment the initial partition π by three points on each side of the interval and thus form the augmented partition $\hat{\pi} = \{t_i\}_{i=1}^{n+7}$ consisting of $n+6$ sub-intervals (Figure E.1). The ith "normalized cubic B-spline" $N_i(t)$ is non-zero on the interval (t_i, t_{i+4}) (Figure E.2) and is given by:

$$N_i(t) = (t_{i+4} - t_i) \sum_{\nu=i}^{i+4} \frac{(t\nu - t)_+^3}{\prod_{\substack{j=i \\ j\neq\nu}}^{i+4} (t\nu - t_j)} \tag{E.8.1}$$

Figure E.1. Augmented Partition $\hat{\pi} = \{t_i\}_{i=1}^{n+7}$ is Obtained by Extending the Uniform Partition π on Each Side by Three Equally Spaced Points. The Partition Points are Reindexed in Increasing Order as Shown.

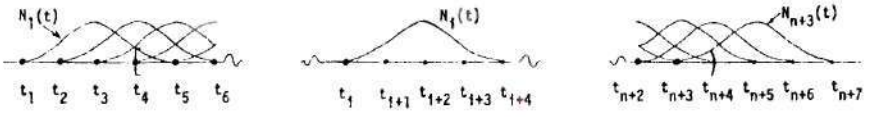

Figure E.2. $n+3$ B-Spline, Functions $N_i(t)$ $i = 1,2,\ldots,n+3$, on the Augmented Partition $\hat{\pi}$ Form a Basis for the Collection of All Spline Functions: $S(\pi)$ on the Uniform Partition π of the Interval $[t_o,t_f)$. No more than 4 Basis Functions are Nonzero at any Point in the Interval $[t_o,t_f)$. The ith Basis Function $N_i(t)$ being Zero Outside the Interval $[t_i,t_{i+4})$.

where

$$x_+^3 = \begin{cases} x^3 & x \geq 0 \\ 0 & x < 0 \end{cases} \qquad (E.8.2)$$

Then the set $\{N_i(t)\}_{i=1}^{n+3}$ comprises a basis set for $S(\pi)$ and thus any linear combination of these functions results in a piecewise cubic spline function.

Let us now return to the two-dimensional strip in the t-z plane: $[t_o,t_f) \times [z_o,z_f)$. Partitioning $[t_o,t_f)$ into n equilength half open subintervals and $[z_o,z_f)$ into m equilength half open subintervals

creates the partition $\Pi = \{(t_i,z_j)\}_{i=1}^{n}{}_{j=1}^{m}$ consisting of nm rectangles:

$$\{[t_i,t_{i+1}) \times [z_j,z_{j+1})\}_{i=1}^{n}{}_{j=1}^{m}$$

(Figure 3.4). This generates an augmented partition $\hat{\Pi} = \{(t_i,z_j)\}_{i=1}^{n+7}{}_{j=1}^{m+7}$ consisting of $(n+6)(m+6)$ subrectangles (Figure E.3).

Then as a basis of $S(\Pi)$ (the space of all piecewise bicubic splines on Π), we choose the set of $(n+3)(m+3)$ functions: $\{N_i(t)\cdot N_j(z)\}_{i=1}^{n+3}{}_{j=1}^{m+3}$. Letting

$$Z_k(t,z) = N_i(t)\cdot N_j(z) \quad i=1,2,\ldots,n+3, \quad j=1,2,\ldots,m+3$$
$$k=1,2,\ldots,p \qquad (E.9.1)$$

where

$$k = (j-1)(n+3) + i \qquad (E.9.2)$$

and

$$p = (n+3)(m+3) \qquad (E.9.3)$$

any linear combination

$$\sum_{k=1}^{p} \alpha_k Z_k(t,z)$$

will result in a piecewise bicubic spline in the domain with partition Π. Notice that for any k, $Z_k(t,z)$ is nonzero in only 16 subrectangles. Similarly the localness of $Z_k(t,z)$ implies that for any $(t,z) \in [t_1,t_{i+1}) \times [z_j,z_{j+1})$ there will be at most 16 $Z_k(t,z)$ which are nonzero at this point:

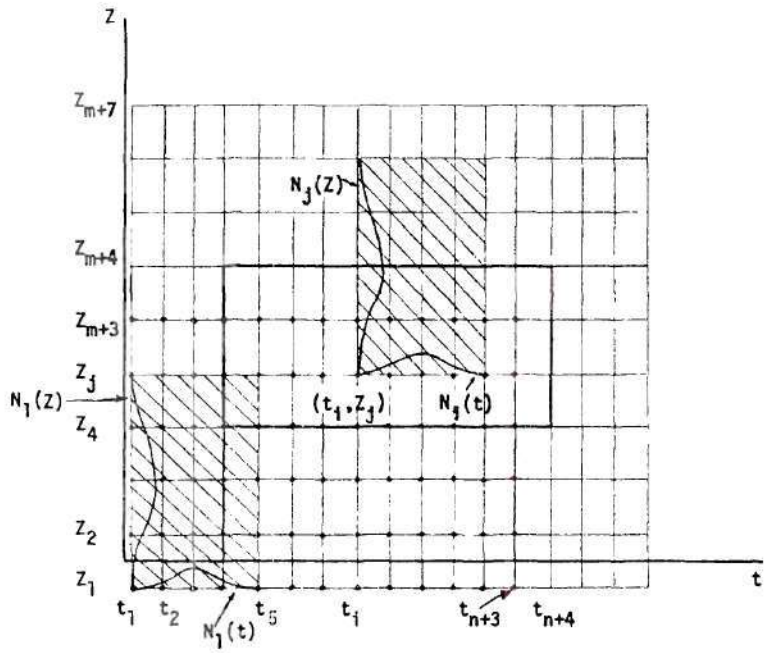

Figure E.3. The Augmented Partition: $\hat{\Pi} = \{(t_i,z_j)\}_{i=1\ j=1}^{n+7\ m+7}$, is Formed by Extending the Uniform Partitions of $[t_o,t_f)$ and $[z_o,z_f)$ by 3 Points on Each Side. The Temporal and Vertical Coordinates are Indexed in Increasing Order as Shown. On this Extended Partition there Exist $(n+3)(m+3)$ B-Spline Functions Given by $N_i(t)\cdot N_j(z)$ $i = 1,2,\ldots,n+3$, $j = 1,2,\ldots,m+3$. These form a Basis for the Space of Spline Functions: $S(\Pi)$ on the Partition Π of the Rectangle $[t_o,t_f) \times [z_o,z_f)$.

$$\begin{cases} Z_k(t,z) & (j-1)(n+3)+(i-3) \le k \le (j-1)(n+3)+i \\ Z_k(t,z) & (j-2)(n+3)+(i-3) \le k \le (j-2)(n+3)+i \\ Z_k(t,z) & (j-3)(n+3)+(i-3) \le k \le (j-3)(n+3)+i \\ Z_k(t,z) & (j-4)(n+3)+(i-3) \le k \le (j-4)(n+3)+i \end{cases} \tag{E.10}$$

Returning to the Least Squares Problem, we now choose as our set of approximating functions this basis set of $p = (n+3)(m+3)$ functions on $S(\Pi)$, i.e., $\{Z_j(t,z)\}_{j=1}^{p}$. We may then construct the

matrix Z whose jth column vector consists of the jth basis function $Z_j(t,z)$ evaluated at the N points (t_μ, z_μ). Equivalently the μth row will consist of the p basis functions evaluated at the point (t_μ, z_μ) - there will be at most only 16 nonzero entries given by (E.10). Having Z we may construct $\hat{Z}$ given by (E.5.2) and then proceed to solve the normal equations (E.6). The solution of (E.6) then yields approximates for $v_k(t,z)$ which as previously discussed are piecewise bicubic polynomials over subrectangles of the partition Π and which are such that the error in the line of sight observations is minimized. The normal equations are particularly well suited for numerical solution in that the resulting coefficient matrix, $Z^t\hat{Z}$, is symmetric positive definite. This implies a greater degree of stability for large systems.

REFERENCES

Aldridge, K. D. (1972), Axisymmetric inertial oscillations of a fluid rotating in a spherical shell, Mathematika, 19, 163-168.

Bath, M. (1974), Spectral Analysis in Geophysics, Developments in solid earth Geophysics, Vol. 7, Elsevier, Amsterdam.

Bitsadze, A. V. (1968), Boundary Value Problems for Second Order Elliptic Equations, N. Holland Pub. Co., Amsterdam.

Boville, B. W. (1966), Planetary waves in the stratosphere and their upward propagation, Space Research, Vol. 7, 20-29.

Bretherton, F. P. and Garret, C. I. R. (1969), Wavetrains in inhomogeneous moving media, Proc. Roy. Soc., A30?, 529.

Brillouin, M. (1932), In French, Les latitudes critiques, Compt. Rend. Acad. Sci. Paris, 194, 801-804.

Burpee, R. W. (1976), Some features of global scale 4-5 day waves, J. Atm. Sci. 33, 2292-2299.

C. D. C. Math Science Library (1971), RKINIT.

Charney, J. G. and Drazin, P. G. (1961), Propagation of planetary-scale disturbances from the lower into the upper atmosphere, J. Geophys. Res., 66, 83.

Charney, J. G. (1970), Planetary fluid dynamics, Dynamic Meteorology, P. Morel ed., Reidel, Dordrecht.

Clark, J. H. E. (1972), The vertical propagation of forced atmospheric planetary waves, J. Atm. Sci. 29, 1430.

Clark, R. R. (1976), Meteor measurements at Durham New Hampshire (43°N, 71°W), J. Atm. Sci., 32, 1689-1693.

Courent, R. and Hilbert, D. (1953), Methods of Mathematical Physics, Vol. I, II, Interscience, N.Y.

Craig, R. A. (1945), A solution of the nonlinear vorticity equation for atmospheric motion, J. Meteorology, 2, 175-178.

DeBoor, C. (1972), On calculating with B-Splines, J. Approx. Theory, 6, 50-61.

Deland, R. J. (1970), The vertical structure of planetary-scale Rossby waves, Quart. J. Roy. Meteorol. Soc., 96, 756.

_____ and Johnson, K. W. (1968), A statistical study of the vertical structure of travelling planetary-scale waves, Mon. Wea. Rev., 96, 12.

_____ and Friedman, R. M. (1972), Correlation of fluctuations of ionospheric absorption and atmospheric planetary-scale waves, J. Atm. Terr. Physics, 34, 295-304.

Dickinson, R. E. (1968 a), On the exact and approximate linear theory of vertically propagating planetary Rossby waves forced at a spherical lower boundary, Mon. Wea. Rev., 96, 405-415.

_____ (1968 b), On planetary Rossby waves propagating vertically through west westerly wind wave guides, J. Atm. Sci. 25, 984-1001.

_____ (1968 c), A note on geostrophic scale analysis of planetary waves, Tellus, 20, 548-550.

_____ (1969), Vertical propagation of planetary Rossby waves through an atmosphere with Newtonian cooling, J. Geophys. Res., 74, 929-938.

Dikii, L. A. (1961), Natural oscillations of a baroclinic atmosphere about a spherical earth, Izv. Akad. Nauk. SSSR, Geophys. Ser., 756-765.

_____ (1965), The terrestrial atmosphere as an oscillating system, Izv. Atmospheric and Oceanic Phys. Ser., 1, 469-489.

_____ (1966), On the asymptotic solutions of Laplace's tidal equation, Dokl. Akad. Nauk. SSSR, 170, 67-69.

Duffy, D. G. (1975), The baroclinic instability of Rossby wave motion: a reexamination, J. Atm. Sci., 32, 1271-1277.

Dutton, J. A. (1976), The Ceaseless Wind, McGraw Hill, N. Y.

Echart, C. (1960), Hydrodynamics of Oceans and Atmospheres, Pergamon Press, N. Y.

Finger, F. G., Woolf, H. M., Anderson, C. E. (1966), Synoptic analysis of the 5, 2, and .4 millibar surfaces for the IQSY period, Mon. Wea. Rev., 94, 651-661

Flattery, T. W. (1967), Hough Functions, Technical Report No. 21, Dept. of Geophysical Sciences, U. of Chicago.

Franklin, J. N. (1972), Axisymmetric inertial oscillations of a rotating fluid, J. Math. Anal. Appl., 39, 742-760.

Fultz, D. and Murty, T. S. (1968), Effects of the radial law of depth on the instability of inertia oscillations in rotating fluids, J. Atm. Sci., 25, 779-787.

Geisler, J. E. and Dickinson, R. E. (1975), External Rossby modes on a β-plane with realistic vertical wind sheer, J. Atm. Sci., 32, 2082-2093.

_____ (1976), The five-day wave on a sphere with realistic zonal winds, J. Atm. Sci. 33, 632-641.

Golitsyn, G. S., and Dikii, L. A. (1966), Oscillations of planetary atmospheres as a function of the rotational speed of the planet, Izv. Atm. and Oceanic Phys., 2, 225-235.

Gossard, E. E. and Hooke, W. H. (1975), Waves in the Atmosphere, Developments in Atmospheric Science, Vol. 2, Elsevier, Amsterdam.

Greenspan, H. P. (1968), The Theory of Rotating Fluids, Cambridge University Press, Cambridge.

Groves, G. V. (1959), A theory for determining upper-atmospheric winds from wind observations on meteor trails, J. Atm. Terr. Phys., 16 344-356.

_____ (1971), Atmospheric Structure and its Variations in the Region from 25 to 120 km, report AFCRL, AD-737 794.

Haurwitz, B. (1940 a), The motion of atmospheric disturbances, J. Mar. Res., 3, 35-50.

_____ (1940 b), The motion of atmospheric disturbances on the spherical earth, J. Mar. Res., 3, 254-267.

Hirato, I. and Sato, Y. (1969), Periodic variation of the winter stratospheric circulation and intermittent vertical propagation of planetary waves, J. Met. Soc. Japan, 47, 390-402.

Holton, J. R. (1976), A semi-spectral numerical model for wave-mean flow interactions in the stratosphere: applications to sudden stratospheric warmings, J. Atm. Sci., 33, 1639-1640.

Hough, S. S. (1897), On the application of harmonic analysis to the dynamical theory of the tides I, Phil. Trans. Roy. Soc., A189, 201-257.

_____ (1898), On the application of harmonic analysis to the dynamical theory of the tides II, Phil. Trans. Roy. Soc., A191, 139-185.

IMSL, International Mathematics and Statistics Library, (1975), FTFFTI.

Jacchia, L. G. and Kopal, Z. (1952), Atmospheric oscillations and the temperature profile of the upper atmosphere, J. Meteorol. 9, 13-23.

Kasahara, A. (1977), Numerical integration of the global barotropic primitive equations with Hough Harmonic functions, J. Atm. Sci., 34, 687-701.

Lamb, Sir Horace (1932), Hydrodynamics, Dover, N. Y.

Laplace, P. S. (later Marquis De La Place) (1775, 1776), In French, Oeuvres Complétes, IX 88, 187.

Lindzen, R. S. (1966), On the theory of the diurnal tide, Mon. Wea. Rev., 94, 295-301.

_____ (1967), Planetary waves on a beta-plane, Mon. Wea. Rev., 95, 441.

_____ and Chapman, S. (1969), Atmospheric Tides, Space Science Reviews, 10, Reidel, Dordrecht.

_____ (1971), Equitorial planetary waves in shear: I, J. Atm. Sci., 28, 609-622.

_____ (1972), Equitorial planetary waves in shear: II, J. Atm. Sci., 29, 1452-1463.

Longuet-Higgens, M. S. (1964), Planetary waves on a rotating sphere, Proc. Roy. Soc., A279, 446.

_____ (1968), The eigenfunctions of Laplace's Tidal Equation over a sphere, Phil. Trans. Roy. Soc., A262, 511.

Love, A. E. H. (1913), Notes on the dynamical theory of the tides, Proc. London Math. Soc., 12, 309-314.

Madden, R. A., and Julian, P. A. (1972), Further evidence of global-scale 5-day pressure waves, J. Atm. Sci. 29, 1464-1469.

Margules, M. (1893) In German, Luftbewegungen in einer rotierenden Spharoidschale, Sber. Akad. Wiss. Wien, 102, 11-56.

Matsuno, T. (1970), Vertical propagation of stationary planetary waves in the winter northern hemisphere, J. Atm. Sci., 27, 871-883.

_____ (1971), A dynamical model of the stratospheric sudden warming, J. Atm. Sci., 28, 1479-1494.

McNulty, R. P. (1976), Vertical energy flux in planetary-scale waves: observational results, J. Atm. Sci., 33, 1171-1183.

Morse, P. M. and Feshbach, H. (1953), Methods of Theoretical Physics, McGraw-Hill, N. Y.

Moura, A. D. (1976), The eigensolutions of the linearized balance equations over a sphere, J. Atm. Sci., 33. 877-907.

Muench, H. S. (1968), Large scale disturbances in the summertime stratosphere, J. Atm. Sci., 25, 1108-1115.

Nayfeh, A. H. (1973), Perturbation Methods, Wiley, N. Y.

Neamtan, S. M. (1946), The motion of harmonic waves in the atmosphere, J. Meteorol., 3, 53-56.

Paulin, G. (1970), A study of the energetics of January 1959, Mon. Wea. Rev., 98, 795-804.

Phillips, N. A. (1963), Geostrophic motion, Rev. Geophys., 1, 121-173.

_____ (1966), The equations of motion for a shallow rotating atmosphere and the "Traditional Approximation," J. Atm. Sci., 23, 626-628.

_____ (1968), Reply: Comments on Phillips' Proposed simplification of the equations of motion for a shallow rotating atmosphere, J. Atm. Sci., 25, 1155-1157.

Poincoré, H. (1910) In French, Sur la precession des Corps deformables, Bull. Astronomique, 27, 321-356.

Rao, S. T. and Ketchum, C. B. (1976), Spectral properties of baroclinic waves in an annulus with a rigid upper surface, J. Atm. Sci., 33, 1067-1072.

Rektorys, K. (1969), Survey of Applicable Mathematics, MIT Press, Cambridge.

Rodgers, C. D. (1976), Evidence for the five-day wave in the upper stratosphere, J. Atm. Sci., 33, 710-711.

Roper, R. G. (1972), Radio meteor winds in the southern hemisphere, Thermospheric Circulation, ed. Webb, W. L., Progress in Astronautics and Aeronautics, Vol. 27, MIT Press, 181-201.

Rossby, C. G. (1939), Relations between variations in the intensity of the zonal circulation of the atmosphere and the displacements of the semi-permanent centers of action. J. Mar. Res., 2, 38-55.

Schoeberl, M. R. and Geller, M. A. (1977), A calculation of the structure of stationary planetary waves in winter, J. Atm. Sci., 34, 1235-1255.

Schultz, M. H. (1972), Spline Analysis, Prentice Hall.

Siebert, M. (1961), Atmospheric tides, Advances in Geophysics, Vol. 7, Academic Press, N. Y.

Simmons, A. J. (1974 a), Planetary-scale disturbances in the polar winter stratosphere, Quar. J. Roy. Met. Soc., 100, 76-108.

_____ (1974 b), Baroclinic instability at the winter stratopause, Quart. J. Roy. Soc., 100, 531-540.

_____ and Hoskins, B. J. (1976), Baroclinic instability on the spheres: normal modes of the primitive and quasi-geostrophic equations, J. Atm. Sci., 33, 1454-1477.

Spizzichino, A. (1972), Meteor trail radar winds over Europe, Thermospheric Circulation, ed. Webb, W. G., Progress in Astronautics and Aeronautics, Vol. 27, MIT Press, 117-177.

Stewartson, K. (1971), On trapped oscillations of a rotating fluid in a thin spherical shell, Tellus, 23, 506-510.

_____ and Rickard, J. A. (1969), Pathological oscillations of a rotating fluid, J. Fluid Mech., 35, 759-773.

_____ and Walton, I. C. (1976), On waves in a thin shell of stratified rotating fluid, Proc. Roy. Soc., A349, 141-156.

Taylor, G. I. (1936), The oscillations of the atmosphere, Proc. Roy. Soc., A156, 318-326.

Theon, J. S., Nordberg, W., Katchen, L. B. and Horvath, J. J. (1967), Some observations on the behavior of the mesosphere, J. Atm. Sci., 24, 428-438.

Thompson, Sir W. (later Lord Kelvin) (1875), Note on the "Oscillations of the First Species," in Laplace's theory of the tides, Phil. Mag., 4, 279.

Tsay, C. Y. (1974), Analysis of large-scale wave disturbances in the tropics simulated by an NCAR general circulation model, J. Atm. Sci., 31, 330-339.

U. S. Standard Atmosphere (1976), NOAA.

Veronis, G. (1968), Comments on Phillips' proposed simplification of the equations of motion for a shallow rotating atmosphere, J. Atm. Sci., 25, 1154-1155.

Vinnichenko (1970), Kinetic energy spectra in the free atmosphere, Tellus, 20, 158-166.

Warn, H., Baroclinically unstable modes of a two-layer model on the sphere, J. Atm. Sci., 33, 1478-1498.

Wilkes, M. V. (1949), Oscillations of the Earth's Atmosphere, Cambridge at the University Press, London.

Yanowitch, M. (1967 a), Effect of viscosity on gravity waves and the upper boundary condition, J. Fluid Mech., 29, 209-201.

_____ (1967 b), Effect of viscosity on vertical oscillations of an isothermal atmosphere. Can. J. Phys., 45, 2003-2008.

_____ and Meyers, R. M. (1971), Small oscillation of a viscous isothermal atmosphere, J. Comput. Phys., 8, 241-257.

VITA

Murry Salby was born on March 26, 1951 in Atlanta, Georgia. After attending primary and high schools in Atlanta, he entered Georgia Tech as an undergraduate student in 1969. He received a BAE in 1973. In the following year he entered the graduate school where he served as a Graduate Research Assistant from 1974 to 1978 and a Teaching Assistant from 1976 to 1978.